



**Universität für Bodenkultur Wien**  
University of Natural Resources  
and Life Sciences, Vienna

# Master Thesis

## **Experimental Stormwater Runoff Modelling to Simulate the Reduction Potential of Pollutant Loads Through Land De-Sealing Measures**

Submitted by

**Cornelia FÜRNKRANZ, BSc**

in the framework of the Master programme

**Civil Engineering and Water Management**

in partial fulfilment of the requirements for the academic degree

**Diplom-Ingenieur**

Vienna, March 2023

Supervisor:

Univ.Prof. DI Dr.nat.techn. Thomas Ertl

Institute of Sanitary Engineering and Water Pollution Control

Department of Water, Atmosphere and Environment

This Master Thesis was written within the research team  
**Hydrologie et Hydraulique Urbaine**  
at the Research Unit  
**HydroSciences Montpellier, France**

Supervised by

**Univ.Prof. DI Dr.nat.techn. Thomas Ertl**  
**Institute of Sanitary Engineering and Water Pollution Control**  
**Department of Water, Atmosphere and Environment**  
at the  
**University of Natural Resources and Life Sciences, Vienna**

And co-supervised by

**Christian Salles, Maître de Conférences HDR**  
**Research Unit HydroSciences Montpellier (HSM)**  
**University of Montpellier**

Student number 01540669

## **Affidavit**

I hereby declare that I have authored this master thesis independently, and that I have not used any assistance other than that which is permitted. The work contained herein is my own except where explicitly stated otherwise. All ideas taken in wording or in basic content from unpublished sources or from published literature are duly identified and cited, and the precise references included.

I further declare that this master thesis has not been submitted, in whole or in part, in the same or a similar form, to any other educational institution as part of the requirements for an academic degree.

I hereby confirm that I am familiar with the standards of Scientific Integrity and with the guidelines of Good Scientific Practice, and that this work fully complies with these standards and guidelines.

Vienna, 21.03.2023

Cornelia FÜRNKRANZ (*manu propria*)

## Preface

This work was funded by “Centre National de la Recherche Scientifique” (CNRS) in the framework of a traineeship at the Research Unit HydroSciences Montpellier (HSM) from October 2022 to February 2023. A financial support was provided by the EU ERASMUS+ Traineeship programme, which facilitates a student mobility in professional contexts.

The master thesis was supervised “on-site” by Maître de Conference Christian Salles, Head of the research team “Urban Hydrology and Hydraulics” at HSM within the umbrella organisation Université de Montpellier. The present research was realised within the framework of the transversal theme “Water in the city”. The programme was announced under the research title: *“Reducing the imperviousness of urban soils for the protection of the quality of watercourses and the downstream coastal zone of the Gulf of Aigues Mortes: effectiveness, levers and obstacles. DESIMP'2022”*.

## Acknowledgements

This master thesis was carried out with the support of my supervisors Univ.Prof. Dipl.-Ing. Dr.nat.techn. Thomas Ertl, head of the Institute of Sanitary Engineering and Water Pollution Control (SIG) at the University of Natural Resources and Life Sciences (BOKU) and Christian Salles, Maître de Conférences HDR at the University of Montpellier, head of the research team Urban Hydrology and Hydraulics at the research unit HydroSciences Montpellier (HSM). I would like to thank them both for their guidance and feedback throughout the progression of my Master thesis and their critical suggestions. I also want to thank Pierre Marchand for the supply of the gauging station data and for conducting the topographic survey together as well as Junior Muyumba Munganga for the provision of the rainfall data.

My former colleagues at HSM, among all Nesrine, Pape, Syrine and Abderrahmane contributed to the accomplishment of my work through all our discussions. A special thanks goes to Batoul with whom I enjoyed working every day and for our great exchanges.

Finishing my studies, I would like to thank my fellow students for the great cooperation in all those years in the sense of the Boku-spirit. In particular, a big thank you to Sarah and Matthias for tackling all the projects and milestones together and on whom I could always count.

I would like to thank my friends, especially Anna, Claudia, Fanny, Lou and Philipp for the constant support, throughout the years of my studies and to Jules for always keeping up the good spirits and for encouraging me.

My biggest thank you goes to my family, in particular my parents and my sister for the continuous support of all kinds and their guidance. Euch ein großes Dankeschön!

# Table of contents

<b>Affidavit</b>	<b>I</b>
<b>Preface</b>	<b>II</b>
<b>Acknowledgements</b>	<b>III</b>
<b>Table of contents</b>	<b>IV</b>
<b>Abstract</b>	<b>VI</b>
<b>Kurzfassung</b>	<b>VII</b>
<b>1. Introduction</b>	<b>1</b>
<b>2. Objectives</b>	<b>2</b>
<b>3. Fundamentals</b>	<b>3</b>
3.1 Urban Rainwater Management	3
3.2 Legislative Framework	3
3.3 Green/ Blue Infrastructure	5
3.4 Runoff Modelling	6
3.4.1 Stormwater modelling with SWMM	6
3.4.2 Pollutant Build-up	7
3.4.3 Pollutant Wash-off	7
3.4.4 Representation of Catchment Surfaces	7
3.4.5 Modelling Data Accuracy	8
3.4.6 Model Optimisation	8
3.4.7 Best-Fit Criteria	9
3.4.8 Representation of the Runoff Water Quality by TSS	10
3.4.9 Relation between TSS and Turbidity	10
<b>4. Material and methods</b>	<b>12</b>
4.1 Study Site	13
4.2 Data acquisition	14
4.2.1 Rainfall data	14
4.2.2 Runoff data	15
4.2.3 Correlation Analysis	17
4.2.4 Event selection	18
4.3 Initial SWMM Model	18
4.4 SWMM Modelling	20
4.4.1 Sensitivity Analysis	20
4.4.2 Hydrological calibration of the model	21
4.4.3 Water Quality Calibration of the Model	22
4.4.4 Verification	23
4.4.5 De-sealing Modelling	23

<b>5. Results and discussion</b>	<b>26</b>
5.1 Analysis of Rainfall Data	26
5.2 Analysis of Observed Runoff Data	28
5.3 Simulations with the Initial Model	31
5.4 Sensitivity Analysis	33
5.4.1 Sensitivity Analysis of Hydrological Parameters	33
5.4.2 Sensitivity Analysis of Water Quality Parameters	33
5.5 Model Calibration	34
5.5.1 Hydrological Calibration	34
5.5.2 Water Quality Calibration	39
5.5.3 Verification of the Hydrological Calibration	47
5.5.4 Verification of Water Quality Calibration	48
5.6 De-Sealing Modelling	53
<b>6. Interpretation</b>	<b>57</b>
<b>7. Conclusion and outlook</b>	<b>59</b>
<b>8. Summary</b>	<b>62</b>
<b>9. Literature and References</b>	<b>64</b>
<b>10. List of abbreviations</b>	<b>71</b>
<b>11. List of Tables and Figures</b>	<b>72</b>
11.1 Tables	72
11.2 Figures	74
<b>12. Appendix</b>	<b>76</b>

## Abstract

When rainwater runs off urban surfaces it gets charged with pollutants and since its discharge into receiving waters leads to a deterioration of the water quality, decision makers need to be informed about possible countermeasures to comply with the Water Framework Directive. Rio (2020) created a model with SWMM to simulate the potential of Green/Blue Infrastructures (GBI) implemented in cities to reduce pollutant loads. In this work the model was further investigated by incorporating continuously observed runoff and turbidity data of a microscale catchment in Montpellier, France. Hydrographs and wash-off processes of total suspended solids (TSS) were simulated. A sensitivity analysis, a calibration and a verification were carried out for the hydrological and the water quality module of the model using the criteria Nash-Sutcliffe Efficiency, King-Gupta Efficiency, and Percentage Difference Error. De-sealing scenarios were simulated with the uncalibrated and the calibrated model and their reduction potentials of runoff, TSS concentration and TSS load were compared. In contrast to the hydrological calibration, the water quality calibration was not successful since the model showed a high sensitivity towards the tested parameters and a correlation between observed turbidity and simulated TSS was not successful. The magnitudes of the reduction potentials of both models were similar but results of the calibrated model were more reliable. The uncalibrated model returned partially unrealistic results and a standard deviation which was 35% to 36% higher than the one of the calibrated model. The investigations of the model prove its sensitivity and present the effect of a calibration on simulated reduction potentials. The outcomes contribute to research about the quality of urban rainwater runoff, its simulation with SWMM and its improvement through the implementation of GBI.

## Kurzfassung

Da sich Regenwasser beim Abfluss über urbane Oberflächen mit Schadstoffen anreichert und es durch die Einleitung in Vorfluter zu einer Verschlechterung der Gewässerqualität kommt, müssen Entscheidungsträger informiert werden, welche Gegenmaßnahmen ergriffen werden können, um die Wasserrahmenrichtlinie einzuhalten. Rio (2020) erstellte mittels SWMM ein Modell, mit welchem in einem Stadtgebiet das Schadstoff-Rückhaltepotenzial von Grün/Blauen Infrastrukturen (GBI) simuliert werden kann. In der vorliegenden Arbeit wurde dieses Modell unter Einbeziehung von kontinuierlich beobachteten Abfluss- und Trübungsdaten eines Micro-Einzugsgebiets in Montpellier, Frankreich, weiter untersucht. Es wurden Abfluss- und Schwebstoff-Auswaschungsprozesse simuliert sowie eine Sensitivitätsanalyse, eine Kalibrierung und eine Validierung unter Verwendung der Kriterien Nash-Sutcliffe-, Kling-Gupta-Effizienz sowie dem Prozentualen Differenz Fehler durchgeführt. Entsiegelungsszenarien wurden mit dem unkalibrierten und dem kalibrierten Modell simuliert und ihr Potenzial Abfluss, Schwebstoffkonzentration und -fracht zu reduzieren wurde verglichen. Im Vergleich zur hydrologischen Kalibrierung war die Wasserqualitätskalibrierung nicht erfolgreich, da sich das Modell hinsichtlich der getesteten Parameter als sensitiv herausstellte und keine Korrelation zwischen beobachteter Trübung und simulierten Schwebstoffen hergestellt werden konnte. Die Reduktionsausmaße waren bei beiden Modellen ähnlich, aber die Ergebnisse des kalibrierten Modells waren zuverlässiger. Das nicht- kalibrierte Modell lieferte vereinzelt unrealistische Werte und die Standardabweichung war um 35% bis 36% höher als jene des kalibrierten Modells. Diese Arbeit zeigt die Empfindlichkeit des Modells sowie die Auswirkung einer Kalibrierung auf simulierte Reduktionspotentiale auf. Die Ergebnisse tragen zur Forschung über die Regenwasserabflussqualität, ihre Modellierung mit SWMM und ihre Verbesserung durch Implementierung von GBI bei.

# 1. Introduction

A negative aspect of urbanisation is the sealing of large areas. Natural surfaces which previously allowed water to pass into the underlying soil get replaced by surfaces which are no longer able to infiltrate rainwater. Consequently, rainwater surface runoff is generated or increased. In urbanised areas runoff is usually evacuated and in the further course depending on the drainage system, separate rainwater sewers discharge into receiving waters. The increase in runoff poses a flood risk but, in addition, it also causes pollutants, which got accumulated on surfaces, to be washed off and carried away with it. Stormwater runoff which drains into receiving waters is thus charged with pollutants. Produced by human activities pollutants, for example polycyclic aromatic hydrocarbons (PAHs) deposited through motorised traffic, are hazardous to the ecosystem (Gasperi et al., 2022). To counteract the deterioration of the ecosystem a variety of green/blue infrastructures (GBI) for example pervious pavements (PP) or rain gardens can be implemented. This approach addresses the origin of the problem by reducing surface runoff and, along with it, pollutant loads.

In the framework of the present research project a first evaluation of the reduction potential of runoff and total suspended solids (TSS) through GBI was carried out within the doctoral thesis of Rio (2020). The study area, the city of Montpellier, is a rapidly growing metropolis and therefore the implementation of a sustainable urban development is needed. Additionally, the urban rivers of the area discharge into the ecologically and touristically valuable Gulf of Aigues-Mortes, highlighting the importance of implementing conservation measures. Rio developed a model for large urban areas with the U.S. Environmental Protection Agency's programme SWMM (Storm Water Management Model) which simulates hydrographs and pollutographs. The structure of the model facilitates the implementation of GBI to assess their reduction potential of contaminants. The developed tool can provide knowledge for public decision makers about the beneficial effects of GBI scenarios on both the surface runoff and the runoff quality. As a bigger aim this tool can be implemented in urban spatial development evaluations.

In the work of Rio (2020) the simulations of TSS loads which are an indicator for total pollution in surface runoff were not verified since no observed TSS data was available. Simulation results are hence obtained with parameter values from literature and are presented as a function of the input parameter, wash-off coefficient  $K_w$ . In this empirical master thesis, the model approach of Rio is applied on a small catchment in the same study area. Runoff observations including discharge and turbidity data which were collected over a period of 14 months from November 2021 to January 2023 are used for a model calibration. Within consecutive simulations of de-sealing scenarios, it is expected to gain a better understanding of the interrelations of model parameters and to obtain deeper insights into the reduction potential of pollutant loads.

Raising awareness about the relationship between rainfall runoff and the contamination in urban rivers, this thesis supports the development of a modelling tool which can support the preservation of the quality of surface waterbodies and protect the water ecology as required by the EU Water Framework Directive (WTF, DIRECTIVE 2000/60/EC).

## 2. Objectives

The aim of this master thesis is to set up a model with the open-source program EPA SWMM which is able to simulate de-sealing scenarios for a monitored study site. The results are expected to provide new insights into parameter calibration to assess priorities for data acquisition and model generation for future de-sealing modelling.

To accomplish this goal the following tasks and questions are targeted:

### 1) Data Analysis:

How representative is the available data for the research objective? Can enough data be acquired to accomplish the objectives? How reliable and error-prone are the individual data sources?

To respond to these questions a data analysis of the available rainfall and runoff data is conducted. Within the subsequent calibration process and de-sealing modelling additional findings are acquired.

### 2) Model Set-up:

How can the model be set up for the given study site implementing the model approach of Rio et al. (2020)? What simplifications must be carried out?

A topographic survey is conducted to obtain the dimensions of the whole study site and of individual subcatchments. The surfaces of the monitored study site are represented in the model by water quality response units and further settings and parameters are chosen to correspond with the approach of Rio et al. (2020).

### 3) Model Optimisation and Simulations:

How can the model be calibrated and evaluated? Is the model able to reproduce the observations? What runoff and pollutant reductions can be obtained by de-sealing scenarios?

A sensitivity analysis, a calibration of hydrological and water quality parameters as well as model verifications are conducted. In a next step de-sealing scenarios are simulated.

### 4) Conclusion of calibration effects:

Does the de-sealing model benefit from a prior model calibration? What should future modelling focus on?

For this final analysis findings from the de-sealing simulations are further evaluated.

### 3. Fundamentals

#### 3.1 Urban Rainwater Management

Most urbanised areas are covered with impervious surfaces. Consequently, rainwater cannot infiltrate into the soil and increased surface runoff is generated. Surface runoff simultaneously washes particles off surface covers and transports them with it. When rainwater is not collected by a combined sewer system, it commonly discharges through a stormwater network into natural receiving waters. The impacts of stormwater events in urbanised areas on the water quality of rivers is a broad subject of research. Rio et al. (2017) presented within their study negative consequences of urban runoff on the ecosystem of rivers and on the subsequent sea estuary by analysing Fecal Indicator Bacteria loadings in waterbodies in the same region as this master thesis. Brudler et al. (2019) presented a correlation between stormwater discharges and ecotoxicity levels, causing environmental damages. However, the deterioration of the surface water quality by urban runoff is not a new finding. Already in 1983 the U.S. Environmental Protection Agency (1983) identified urban runoff as a source of diffuse pollution of water bodies and on this basis, they highlighted the importance for better stormwater pollution control.

The substances in surface runoff affecting the water quality are various and their occurrence depends on environmental conditions and human activities. For example, are surfaces used by motorised traffic such as roads or car parks principal sources of polycyclic aromatic hydrocarbons and trace metals in runoff, due to leakages from vehicles and abrasion of tyre particles (Egodawatta et al., 2007).

An integrated rainwater management is of twofold interest for decision makers. In hydrological terms, a surface runoff reduction is crucial for flood prevention, avoiding physical and economical damage. It further impedes sewer overflows of wastewater treatment plants which discharge their effluents into the rivers endangering the aquatic ecosystem (Rio et al., 2017). Regarding water quality, standards for achieving an ecological good status of water bodies must be accomplished as legally specified.

#### 3.2 Legislative Framework

**At EU-scale** the following instruments provide the legal framework within the content of this master thesis. The directives are required to be implemented in national law within each member state, the strategies have a non-binding character.

- **DIRECTIVE 2000/60/EC:** the Water Framework Directive (WFD) standardises the legal framework for the water policy of the European Union and aims at shaping water utilisation in a sustainable and environmentally compatible way. It has as main objective to achieve a good ecological status of all water bodies and implements a prohibition of deterioration.
- **DIRECTIVE 2006/7/EC:** With the Bathing Water Directive quality standards of bathing water were established specifying management and surveillance methods as well as information provisions for the public about water quality.
- **DIRECTIVE 2006/11/EC:** The Dangerous Substances Directive regulates pollution caused by certain dangerous substances discharged into the aquatic environment.

- DIRECTIVE 2008/56/EC: The Marine Strategy Framework Directive (MSFD) has as objective to protect the marine ecosystem and biodiversity.
- DIRECTIVE 2008/105/EC: The Environmental Quality Standards Directive (EQS) set limits on maximum and annual average concentrations of each group of “priority” and “hazardous priority” substances in water bodies to not be exceeded.
- DIRECTIVE 2009/90/EC: The Commission Directive on technical specifications for chemical analysis and monitoring of water status establishes minimum performance criteria for monitoring methods and analysis.
- DIRECTIVE 2013/39/EU: The Priority Substances Directive amended the EQS for concerns and implemented new substances to be monitored.
- COMMUNICATION 2011/0244 final: In the EU Biodiversity Strategy to 2020 one target is to incorporate green infrastructure in spatial planning to restore at least 15% of degraded ecosystems.
- COMMUNICATION 2013/0249 final: The objective of the EU Green Infrastructure Strategy is the preservation and the enhancement of green infrastructure.
- COMMUNICATION 2020/380 final: Part of the European Green Deal the envisaged EU 2030 Biodiversity Strategy plans to enhance Urban Greening Planning in cities with more than 20 000 inhabitants.
- COMMUNICATION 2022/304 final: With the recently proposed Regulation on Nature Restoration the EU plans to bind targets which include an increase of total area covered by green urban space and securing natural functions naming flood protection and water cleaning.

**In France**, the Water Act of 3 January 1992 (L. n° 92-3) was the law in force before the implementation of the WFD. The Act of 21 April 2002 (L. n° 2004-338) prepared the transposition of the WFD by reorganising the national policy framework for the field of water. The transposition of the WFD was accomplished by the national Law on Water and Aquatic Resources 2006 (L. n° 2006-1772, LEMA).

According to Article 8 of the WFD, programmes for monitoring the status of waters must be established. The WFD demands a management on the scale of large river basins or districts and targets surface water bodies (rivers, water bodies, transitional waters, coastal waters) and groundwater bodies. In Austria this requirement is accomplished by the Gewässerzustandsüberwachungsverordnung (GZÜV) (BGBl. II Nr. 479/2006) as established in chapter 7 of the Austrian Water Act (WRG, 1959). In France “water status monitoring programmes” are established through the national Decree of 25 January 2010 (A. 25 janvier 2010). Monitoring programmes are defined through a “Schéma Directeur d'Aménagement et de Gestion des Eaux” (SDAGE), which are the main policy instruments. An SDAGE is established for each of the 7 continental river basin districts in France and is revised every 6 years.

To prevent and reduce water pollution, concentrations in water bodies are compared to Environmental Quality Standards (EQS), which numerically define concentration limits. Introduced by DIRECTIVE 2008/105/EC and DIRECTIVE 2013/39/EU, EQS were set on a national scope in France through the fundamental Decree of 25 January 2010 on the “methods and criteria for assessing the ecological status, chemical status and ecological potential of surface waters” and within modifications through Decree of 8 July 2010, Decree of 28 July 2011, Decree of 27 July 2015, Decree of du 27 July 2018. In Austria EQS are defined within the Qualitätszielverordnung Chemie Oberflächengewässer (QZV Chemie OG) (BGBl. II Nr. 96/2006) and Qualitätszielverordnung Ökologie Oberflächengewässer (QZV Ökologie OG) (BGBl. II Nr. 99/2010) with threshold values defined in their appendixes.

The guide “Guide technique Relatif à l'évaluation de l'état des eaux de surface continentales” aims to provide necessary information for a consistent application of the rules defined by the Decree of 25 January 2010 (Ministère de l'Environnement, de l'Énergie et de la Mer, 2016). Further information is provided in the guide “Guide relatif aux règles d'évaluation de l'état des eaux littorales dans le cadre de la DCE” including coastal and transitional waters (Bureau des milieux marins, et al., 2018). In addition, the French Micropollutant Plan 2016 – 2021 is dedicated to reduce micropollutant emissions to preserve water quality and biodiversity on a national scope (Ministère de l'Environnement, de l'Énergie et de la Mer, 2020). The objective of the plan is to meet a good water status set by the WFD and the MSFD by limiting the input of pollutants via waterways to the marine environment.

**At local scale** schemes on water management (Schéma d'Aménagement et de Gestion des Eaux, SAGE) are plans for sub-river basins or a group of river basins. At the level of the area of the present research project, the Syndicat du Bassin du Lez (which is a Public Territorial Federation of Catchment) is responsible for the local implementation of the SAGE and is also in charge of the flood prevention action programmes (Montpellier Méditerranée Métropole, 2022a). Since 2016 the metropolis of Montpellier is autonomously responsible for stormwater management and prepares zoning maps for stormwater draining, which are attached to the urban development plan. Part of the competences of the Metropolis of Montpellier is the “Schéma de Cohérence Territoriale” (SCoT) which defines the spatial planning guidelines and objectives for the territory of the Metropole Montpellier (Montpellier Méditerranée Métropole, 2022b). A council decision in force since the 1<sup>st</sup> of January 2023 brings the collective and non-collective sewage disposal under public management of the metropolis (Montpellier Méditerranée Métropole, 2022c).

### 3.3 Green/Blue Infrastructure

Green/Blue Infrastructure (GBI) is a collective term for the use of nature-oriented solutions for urban and land-use planning, which permit urban infrastructures in a sustainable framework. The beneficial natural functions are manifold and include water purification, flood control and temperature regulation, aiming for an adaptation of urban spaces to environmental conditions and climate change (COM/2013/0249 final). Being of emerging interest nowadays the multiple benefits of GBI are widely proved within research (Alves et al., 2019; Nassani et al., 2023; Stangl et al., 2022; Taghizadeh et al., 2021). Bioswales, green roofs, rainwater harvesting, and permeable pavements are common examples of GBI.

The shortage of space in urban areas can inhibit an implementation of GBI. Considering roads, pedestrian zones, and car parks pervious pavements (PP) can be an interesting alternative to conventional impervious surface covers. PP keep their original function and allow stormwater

infiltration through their surfaces at the same time, reducing stormwater runoff and improving runoff water quality. Permeable interlocking concrete pavement, pervious asphalt and permeable concrete are common examples. Summarising full-scale studies with different materials Marchioni and Becciu (2015) presented runoff coefficients from 0,00 to 0,45. In addition to high volume reductions other hydrological benefits are the reduction of runoff peaks, groundwater recharge and the enhancement of evapotranspiration. Considering the water quality, the synthesis of Marchioni and Becciu (2015) revealed the general function of PP as filter, enhancing the removal of several tested contaminants and suspended solids.

### 3.4 Runoff Modelling

#### 3.4.1 Stormwater modelling with SWMM

A wide range of modelling tools are used for stormwater modelling. Among other programs EPA SWMM (U.S. Environmental Protection Agency – Storm Water Management Model) is an open-source program, which can simulate a variety of hydrological and hydraulic processes relying on a semi-distributed model. A model is set-up by defining different environmental compartments. Subcatchments represent a project's land surface. They are each characterised by geometric parameters including dimensions and slope, as well as the area ratio of their impervious and pervious surfaces. Precipitation is applied on subcatchments through the atmospheric compartment which can also include evaporation and pollutant deposition information. The land surface compartment interacts with the groundwater compartment by transmitting infiltration data and with the transport compartment by conveying surface runoff which can include pollutant loading information. Runoff propagation is computed through the transportation compartment which contains pipes, channels, and other conveyance elements and which transports the runoff to a catchment outlet. Within the land surface compartment, subcatchment properties define if and how rainwater infiltrates, evaporates, and turns into runoff. Infiltration occurs only on pervious surfaces. Runoff is generated when the capacity of initial losses is exceeded. The latter implies surface wetting, interception and surface ponding and is in SWMM globally defined as depression storage. (Rossman, 2015)

Surface runoff is computed in SWMM employing the empirical Manning equation, which defines the relationship between flow rate  $Q$ , cross-sectional area  $A$  ( $m^2$ ), hydraulic radius  $R$  (m) and stream slope/ hydraulic gradient  $I$  (-) by introducing the Manning coefficient  $n$ , which is expressed in  $\left(\frac{s}{m^3}\right)$ .

$$Q = \frac{1}{n} * A * R^{\frac{2}{3}} * I^{\frac{1}{2}}$$

Within SWMM infiltration can be computed through 5 different methods. One of them is the SCS Curve Number (CN) introduced by the U. S. Department of Agriculture (1986). SCS Runoff Curve Number values are chosen depending on the land-use and on the best fitting soil group. The soil groups (A to D) are classified through soil texture and the saturated conductivity. The higher the assigned value the lower is the infiltration capacity with numbers approaching 100 which are considered as almost impervious.

Within runoff simulations SWMM can implement water quality data associated with this runoff. Water quality modelling is based on build-up and wash-off processes of pollutants. Their properties can individually be defined for different self-chosen pollutants and are implemented in the model through land-use categories. Within each category build-up and wash-off properties

can be specified. The different land-use categories are assigned individually to each subcatchment through percentages of its area.

### 3.4.2 Pollutant Build-up

The build-up process is an enrichment of non-point source pollutants on surfaces. The pollutant accumulation takes place on dry weather days and ends with a rainfall event. Among other formulas the process can be expressed in SWMM by an exponential growth which approaches asymptotically a pre-defined maximum build-up value using the following formula (Rossman, 2015):

$$b(t) = K_b * (1 - e^{-E_b * t})$$

with  $b(t)$  defining the build-up pollutant mass on a sub-catchment area  $\left(\frac{kg}{ha}\right)$  as a function of time ( $t$ ) which refers to the antecedent dry weather days, the coefficient  $K_b$  represents the maximal possible build-up  $\left(\frac{kg}{ha}\right)$  on the sub-catchment,  $E_b$  is the constant build-up rate expressed in  $\left(\frac{1}{days}\right)$ .

### 3.4.3 Pollutant Wash-off

Wash-off is the reduction process of pollutants from surfaces which get mobilised by rainfall and subsequent runoff. The quality of rainwater runoff therefore depends strongly on the wash-off behaviour of pollutants. According to Egodawatta et al. (2007) the key influences of wash-off are rainfall intensity and rainfall duration. They further stated that only a fraction of the available pollutants gets removed within a rainfall event. In SWMM an approach to compute wash-off processes is through the widely used exponential equation (Rossman, 2015):

$$w(t) = K_w * q(t)^{E_w} * m_{bi}(t)$$

where  $w(t)$  expresses the wash-off rate  $\left(\frac{kg}{h}\right)$  as a function of time ( $t$ ),  $K_w$  implicates the wash-off coefficient  $\left(\frac{h}{mm^{-2}}\right)$ ,  $q(t)$  is the runoff rate of a sub-catchment  $\left(\frac{mm}{h^{-1}}\right)$  at time  $t$ ,  $E_w$  is the wash-off exponent ( ) and  $m_{bi}(t)$  is the built-up mass remaining on the surface ( $kg$ ) at time  $t$ . Derived from the general formula of kinetic energy, an exponent  $E_w = 2$  leads to a representation of the erosive drag force of the runoff. The presented formula is easy to implement for runoff simulations as it comprises a few variables, yet it has its limitations as wash-off processes are difficult to generalise for heterogenous subcatchments (Bonhomme and Petrucci, 2017).

### 3.4.4 Representation of Catchment Surfaces

A common approach for considering different surface occupations of a catchment in runoff models is to combine areas, which are assumed to respond similarly to rainfall and therefore have a similar hydrological runoff behaviour. Combined areas of this kind are referred to as Hydrological Response Units. In common water quality models catchments are divided into subcatchments using land-use maps, which distinguish for example residential, commercial or industrial zoning. Within the structure of SWMM, build-up and wash-off behaviours of pollutants are specified for land-use categories. Within each land-use category build-up and wash-off processes can only be described homogeneously. Liu et al. (2012) criticise this form of distinction, pointing out the inconsistency between the behaviours of surface pollution and land-use zoning. For instance, two areas which are both assigned to the same land-use type (for example an industrial zone) can have a different compositions and proportions of surface types. Recent studies confirm this matter, Charters et al. (2022) analysed washed-off zinc loads with different surface modelling

approaches and concluded that an aggregation into land-use categories cannot properly simulate wash-off processes, since the main source of zinc is roof covers which are represented in all land-use categories. Contrarily, Soltaninia et al. (2022) who tested heavy metal concentration approved a classification through land-use classes, indicating their primary source in industrial areas. The conclusion can be drawn that achieving representative results by dividing a catchment using land-use categories depends on the analysed pollutant and its main source. It is considered that for an analysis of ubiquitous pollutants or sum indicators for example TSS a different surface representation is more adequate.

Investigating TSS concentrations Rio et al. (2020) combined those surfaces to one subcatchment which are assumed to have similar pollutant build-up and wash-off processes. The so-called Water Quality Response Units (WQRU) distinguish on one hand between surfaces regarding the nature of the released contaminants. A distinction was made for example between roads and pedestrian zones, whose surfaces contain different pollutants. On the other hand, WQRU also take into account factors which impact quantitative runoff generation. For example, a distinction was made between flat and sloped roofs, which have not only different surface cover materials but also different inclinations and initial losses, leading to different hydrological responses. According to Rio et al. (2020) WQRU are flexible to a calibration of wash-off parameters and additionally improve hydrological outputs. Similar conclusions were already made by Petrucci and Bonhomme (2014) who obtained a better model performance with a model which was discretised into homogenous units of land cover.

For their model set-up Rio et al. (2020) assumed that an urban subcatchment which is assigned to a WQRU is drained into a sewer system through a rain channel at its outlet. For model simplifications they left a further hydraulic propagation of the runoff out of consideration. With this basis their model approach combined all subcatchments of the same WQRUs forming one subcatchment in SWMM. All different WQRUs in the model discharge into one common outlet being directly connected with the outfall without the use of nodes or links.

### 3.4.5 Modelling Data Accuracy

The acquisition of reliable data is considered as most crucial not only for modelling purposes but for scientific research in all fields. It is important to know the influences of the data on research work in order to collect data with the appropriate accuracy. For this purpose, the margin of errors of collected data must be tested and their significance on results must be evaluated. This supports efficiency in data acquisition and model set-ups, allowing data with little influence on the outcome to be collected with less accuracy and thus less focus on acquisition. In exchange, the focus is directed to those data that significantly influence the outcome of the research objective.

### 3.4.6 Model Optimisation

Once set-up, runoff models are usually further developed through a sensitivity analysis, a calibration and a validation of the calibration. Being determined separately from each other in SWMM the hydrological and the water quality properties can be evaluated separately within each of the beforehand named processes. The hydrological response is computed independently from water quality characteristics. In contrast, the wash-off process is a function of the runoff so that quality simulations do not only rely on water quality parameters but also on beforehand defined hydrological parameters. The sensitivity analysis, the calibration and the verification can hence be carried out first for the hydrological response and in a second step using the already calibrated hydrological model as default setting for a consequent analysis of water quality parameters.

A sensitivity analysis investigates interrelations of model parameters and their effect on the model results. It should be carried out before the calibration of the model to select parameters for a further calibration. Testing how sensitive a model is regarding specific parameters prevents an over-parameterisation of a model and enhances a prioritisation of data acquisition for a model calibration. (Fraga et al., 2016)

A model calibration has as objective to approach the simulated results to the observed values. This can be achieved by testing a series of input values and combinations of selected parameters in a defined range. A hydrological calibration aims to find those hydrological parameter values leading to the best result. Considering the water quality, the calibration of the stormwater model has as objective to minimise the deviation between observed and simulated pollutographs.

Within runoff modelling sensitivity analysis and calibrations are carried out for preselected events or periods. Once optimised parameters are found within the calibration process it is evaluated if this parameter set achieves globally improved results. This is carried out by using the obtained parameter set for simulating runoff processes within additional events. Through this process, the so-called verification, the calibration and therefore the model can be approved or rejected.

### 3.4.7 Best-Fit Criteria

Best-fit Criteria (BFC) evaluate the performance ability of a model. They are used for the sensitivity analysis, calibration and validation of a model comparing simulation results to observations.

The percentage difference error (PD) is often considered for analysing hydrological responses. Absolute values for example peak discharges  $Q_{\max}$  or total runoff volumes  $V_{\text{tot}}$  can be compared. The lower the result the better is the model performance. PD for a specific value  $x$  is calculated by the following equation with  $x_o$  representing the observed value and  $x_s$  is the simulated value:

$$PD\ x = \left( \frac{x_o - x_s}{x_o} \right) * 100$$

The relative percentage difference RPD analyses a variable in the same way but expresses the results differently with 1,0 as the highest value representing a good fit and  $-\infty$  as bottom limit. Is is calculated in the following way:

$$RPD\ x = 1 - \frac{x_o - x_s}{x_o}$$

The widely used Nash-Sutcliffe Efficiency (NSE) presents its results due to a normalisation on a general interpretable scale from  $-\infty$  to 1,0, where 1,0 indicates a perfect fit. In the following formula  $N$  stands for the entire simulation period,  $x_{o:s}(t)$  are the observed:simulated values at the time step  $t$  and  $\mu_o$  is the mean of the observed values.

$$NSE\ x = 1 - \frac{\sum_{t=1}^N (x_o(t) - x_s(t))^2}{\sum_{t=1}^N (x_o(t) - \mu_o)^2}$$

Another established BFC is the Kling–Gupta Efficiency (KGE) which has the same scale as the NSE but involves multiple functions: the linear correlation between observations and simulations ( $r$ ), the ratio of standard deviations  $\left( \frac{\sigma_s}{\sigma_o} \right)$  which divides the simulated by the observed standard deviation and the ratio of means, dividing the simulated by the observed mean  $\left( \frac{\mu_s}{\mu_o} \right)$ .

$$KGE\ x = 1 - \sqrt{(r - 1)^2 + \left(\frac{\sigma_s}{\sigma_o} - 1\right)^2 + \left(\frac{\mu_s}{\mu_o} - 1\right)^2}$$

Comparing NSE and KGE both are informal metrics. Often considered as more reliable due to the implication of 3 instead of 1 comparative function, KGE was lately criticised by Vrugt and de Oliveira (2022) claiming that it prohibits an objective characterization of parameter confidence. In most literature where runoff and its pollution was simulated with SWMM authors employed multiple BFC in order to represent different objective functions.

### 3.4.8 Representation of the Runoff Water Quality by TSS

Substances which affect water quality are not all present in dissolved form. Trace substances predominantly adsorb on suspended solids, including heavy metals, polychlorinated biphenyls (PCBs) and polycyclic aromatic hydrocarbons (PAHs). Considering suspended solids in urban runoff Gasperi et al. (2022) and Li et al. (2020) studied their relation to PAH, Hengren et al. (2005) and Jeong et al. (2020) to heavy metals and Urbaniak et al. (2010) to PCBs. In addition, compounds of microorganisms are accumulated leading to an enrichment of suspended solids with biomass.

Total suspended solids are particles of small size, whose density is approximately similar to their environment liquid, which prevents their fall by gravity. TSS represent undissolved matter kept in suspension in the liquid by turbulences. The term TSS covers all particles between 0,2 and 0,7 mm of different shapes and includes all forms of sediment, organic matter, or other materials (Habersack et al., 2017). The determination of TSS contents in water comprises direct sampling and a laboratory analysis, where the water sample is filtered and subsequently the gained solids get dried. The TSS concentration can be obtained by weighting the filtered, dried mass and then setting it in relation to the volume of the sampled water. (EN 872:2005)

Since EQS imply testing suspended solids to detect accumulated pollution, Rüdél et al. (2007) identified 55 substances or groups of substances which are potentially bioaccumulating and/or sorb to suspended solids. In addition, suspended matter can cause immediate damage to fish population in watercourses as a result of turbidity, as well as long-term damage due to the deposition of turbid matter (Schmutz, 2009). Inoue et al. (2009) found that TSS concentrations were associated with chemical oxygen demand (COD) and total phosphorous concentrations and concluded that a SS removal improves the quality of water. For this reason, TSS concentration is often used as a primary indicator pollutant. Even though a general valid correlation between TSS concentrations and other contaminants cannot be established, it can be concluded that a reduction of TSS in runoff is linked to the reduction of emissions of other pollutants.

### 3.4.9 Relation between TSS and Turbidity

TSS analyses determine concentration results of the specific time of the sample extraction. When it is requested to continuously monitor suspended solids in a water body over a longer time, a direct determination through punctual sampling is time-consuming and costly. A parameter which is easy to obtain for long-term monitoring and has a high resolution in time to capture non-stationary conditions of water quality is the turbidity. Turbidity is the effect of transparency reduction due to the presence of suspended matter and colloids in water. It can be determined by optical measurement methods which quantify the reduction of emitted light rays passing through water. Turbidimeters can be installed at characteristic points of water bodies, sewer networks or other points of interest. Once calibrated and installed they can continuously register turbidity

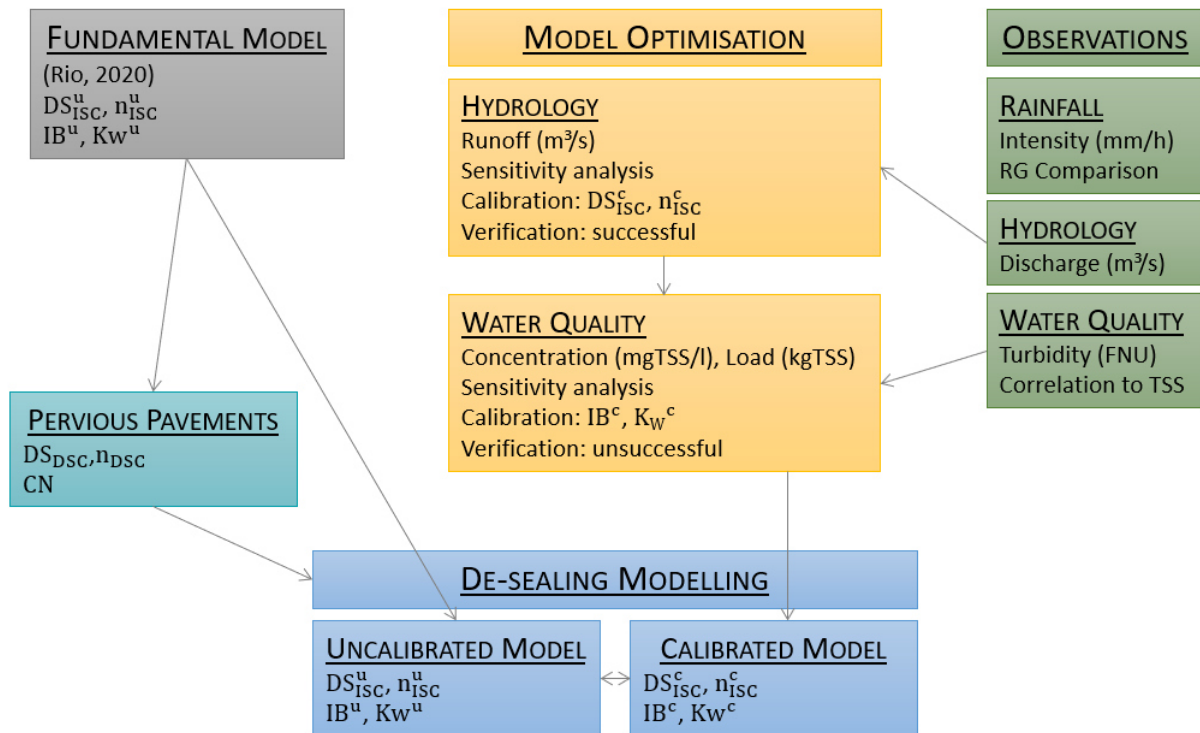
## Fundamentals

---

values within small time steps. This allows a long-term monitoring of the runoff quality with a reduced input of financial resources and time.

Turbidity and TSS concentration have a linear relationship if a liquid is considered which comprises only homogeneous particles with same properties (size, shape, etc.). This correlation is not constant when considering runoff, since runoff has a heterogeneous character regarding the composition of the water, the nature of particles, etc. and varies in time (Hannouche et al., 2011). This complexity makes it impossible to generally draw a connection between turbidity and TSS. Nevertheless, a relationship can be created for a specific catchment and the sampler in use. The correlation should be made in respect of the application objective of the obtained values. Nowadays turbidity measurements are broadly used to obtain a derivation to TSS. Correlations can be established by a linear regression following the guidelines of Habersack et al. (2017) or Versini et al. (2015). Based on long-term observations Bertrand-Krajewski et al. (2010) summarised how to establish representative relationships. Correlation curves should be established carefully due to many complex interactions (Bilotta and Brazier, 2008). However Lacour et al. (2010) concluded that a significantly better representation of dynamics of runoff phenomena is achieved with continuous turbidity data than with direct punctual measurement methods.

## 4. Material and methods



DS ...initial losses                      u ...uncalibrated Parameter                      ISC ...impervious sub-catchment  
 n ...Manning Coefficient                      c ...calibrated Parameter                      DSC ...de-sealed sub-catchment  
 IB ...initial built-up of TSS                      RG ...Rain Gauge                      PSC ...pervious sub-catchment  
 Kw ...Wash-off Coefficient

Figure 1: The methodology followed in this work.

The objectives of this master thesis are approached by the methodology presented in Figure 1. The fundamental de-sealing model of Rio (2020) in SWMM and the same parameter values are applied on an observed catchment. This model is referred to as “uncalibrated model”. The aim is to further develop this model. To accomplish this, model parameters are optimised with observation data. The model optimisation is carried out within 3 steps: a sensitivity analysis, a parameter calibration, and a verification of the calibration. To conduct these processes the hydrology module and the water quality module are examined separately from each other. Being independent from water quality elements, the hydrological response is the first to be calibrated which is conducted by using continuous discharge measurements. For assessing the water quality, TSS are simulated which are correlated to observed turbidity. Within calibration processes those parameter values were identified which reproduce observations the best. The objective of a consecutive verification is to review these input values on other observed events. The “calibrated model” is then set up with the optimised parameter values. With the calibrated and the uncalibrated model de-sealing simulations are carried out. This was conducted by replacing impervious surfaces with pervious pavements as proposed by Rio. Comparing the results of the two models provides information to evaluate the impact of a model calibration on de-sealing results.

## 4.1 Study Site

The study area is the metropolis of Montpellier with a population of 491 417 inhabitants in 2019 and its capital, the city of Montpellier, which counted a population of 295 542 in 2019 (Insee, 2022a). With an increase of 1,4% per year the city of Montpellier has the strongest national demographic growth among cities with a population over 100 000 inhabitants (Insee, 2022b). Hence urban development and corresponding development concepts play a major role. Characteristic for a semi-arid Mediterranean climate, most precipitation occurs in autumn with a high inter-annual variability marked by extreme events in summer months. Given that the leaching of pollutants from urban surfaces is among others also dependent on the rainfall intensity, the area with high precipitation intensities in summer and long antecedent dry periods is particularly affected by pollutant emission through rainfall runoff.

The study site of this work is situated on the modelling area of Rio et al. (2021). The observed catchment is at the Campus Triolet of the Faculty of Sciences of the University of Montpellier with a runoff gauging station installed in September 2021. Situated on a pedestrian area in front of the building “Polytech”, a rain channel drains the rainwater running off the catchment and discharges into the installed sampler. The gauging station registers continuously turbidity, water depth, conductivity, and temperature of the runoff. A topographic survey was conducted with an electrical theodolite, more precisely with the Tacheometry LEICA TCA1105, on the 07/12/2022 to measure the total area which contributes to the surface runoff collected by the sampler. The study site comprises a surface of 315,78 m<sup>2</sup> and is presented in Figure 2.



Figure 2: Study site “Polytech”, pervious surfaces are hatched in green, impervious surfaces are hatched in red.

The area comprises an impervious concrete surface of 217,73 m<sup>2</sup>, forming 69% of the total area. The pervious surfaces cover 31% with 95,05m<sup>2</sup>. With various slope inclinations at the upper boundaries of the catchment, defining precise boundaries of the catchment was complicated. Since a catchment is characterised by having only one outlet, it was decided to rather underestimate the catchment size. Therefore, it can be assured that the rain falling on the defined

catchment surface will be discharged by the installed gauging station. However, underestimating the catchment surface leads to a supplement run-on onto the catchment, which can hardly be measured. Being part of the university campus, a general maintenance of the pathway and the park is conducted regularly including the removal of plant residues, etc. Mostly frequented by students and staff and with no known construction work or other interferences at the observed catchment, no impacts on the measurements of on-site activities are expected. Unknown single manipulations in this area could affect observed runoff interpretations.

## 4.2 Data acquisition

### 4.2.1 Rainfall data

HydroSciences Montpellier (HSM) has several rain gauges in the study area. The nearest to the observed catchment and therefore most crucial for this work is the rain gauge (RG) “Polytech”. It is located on the roof of the building “Polytech”. Due to their proximity the rainfall measured at “Polytech” is expected to correlate well with the runoff measurements. The RG “UM35” was also partly used for specific observed runoff events when there was no data registered at Polytech. With a linear distance of 168 m from Polytech to the west, RG UM35 is also close to the observation site and therefore it is supposed to correlate well with the observed runoff. Figure 3 indicates the positions of the used rain gauges and the monitored catchment.



Figure 3: Overview of the exact positions of the rain gauges and the runoff gauging station.

Used as input data for the runoff modelling the pluviometry data was accessed via the website [istSOS<sup>2</sup>](https://www.istSOS2.org/) (IstSOS2, 2022). IstSOS<sup>2</sup> takes part in the Open Geospatial Consortium and provides hydro-meteorological data. HSM uses this data management tool to provide continuously collected rainfall data from their RGs for scientific use. The considered RGs, which are both 6463-M AeroCone Davis rain collectors measure the rain accumulation with a 0.2 mm tipping bucket. The obtained data consists of the measured rain accumulation per minute. Operated by HSM, both RG are subjected to the same calibration methods and maintenance.

Due to the proximity of RG Polytech to the observed catchment, it is expected that the registered rainfall represents well the rainfall onto the observed catchment. Considering that RG UM35 is located further from the catchment, it is anticipated that the representation of the actual rainfall with the registered one is less precise. Within the modelling part of this work, no analysis nor a

further distinction will be drawn between the two rain gauges. For this reason, a comparison of them is necessary to be aware of a possible effect of the spatial distribution of the rain gauges. Scatter plots were plotted for different scales to depict all registered rain data of the observation period from 01.10.2021 to 07.01.2023. A further statistical analysis of the two rain gauges was carried out for further clarity. A 5-minute intensity as well as the rainfall sum over different durations were calculated with the obtained raw data for further simulation purposes.

### 4.2.2 Runoff data



Figure 4: Outfall of the observation catchment through a rain channel covered by a trench drain grate and draining into a catchpit.

At the outfall of the observation catchment a gauging station is installed. Rainwater drains through a rain channel which transversely crosses the pathway and is covered by a trench drain grate (Figure 4) into a catchpit where a fixed sampling bucket with a weir outfall is installed (Figure 5 and Figure 6). The discharge drains into the bucket where the water level raises until the height of the bucket's weir outfall (at a height of 56mm) is reached. Surpassing this height, the gauging station starts to discharge into the sewer system and in this work the start of the runoff is defined at this moment. The bucket contains 3 sensors of the brand IJINUS (Figure 6): a water level sensor, a turbidity meter and a sensor measuring the conductivity and the temperature.

The water level measurement method is based on hydrostatic pressure recorded on a stand-alone device with the serial number CNR0002-A2-05 (CNR-IJINUS). The system works with a vented (relative) pressure sensor which compensates barometric pressure changes. Long-term drifts were registered for the water level observations. They commonly occur and reflect differences of measured values for the same water level. An automatic drift-correction as proposed by Chowdhury et al. (2021) and Kajikawa & Kobata (2019) was not carried out, however a manual data analysis as explained in chapter 4.2.4 achieved a correction. For observing the turbidity, a NTU – Nephelometric Turbidity Sensor (NTU-IJINUS) is installed. Analysed with a wavelength of 860nm of radiation the scattered light is measured at an angle of 90° (according to ISO 7027-1:2016) and expressed in the unit FNU (Formazine Nephelometric Unit). Before installing this probe, a comparison of 3 different turbidity sensors was conducted in former works in order to find the most appropriate to the given circumstances (El Gaouzi, 2021). Within the work of El Gaouzi the chosen turbidity sensor was furthermore calibrated. Additionally, regarding the water level probe, a rating curve was created for the gauging bucket based on discharge

## Material and methods

---

experiments. This rating curve was used in the present work for a deviation from the measured water level to runoff.

A C4E Conductivity/Salinity Sensor (C4E-IJINUS) measures the conductivity and the temperature. The 3 installed probes work independently from each other, and measured data is registered with time steps of 5 minutes on a IJINUS LOG09V3 which is a stand-alone recorder with an integrated battery.



Figure 5: Surface runoff gauging station, covered with a protection rake.



Figure 6: Surface runoff gauging station consisting of a sampling bucket with 3 sensors.

The observation period started mid-November where the gauging station was temporally installed for specific rainfall events occurring on 22-26/11/2021 and 10-24/03/2022. Since 19.04.2022 the gauging station was fix installed to avoid missing out on recording unforeseen events. In times when the gauging station was not installed, no runoff data is available. Once obtained a first check was conducted by correlating the runoff data with rainfall data. As an example, when rainfall occurred but no runoff was recorded an error was identified. Several possible sources of measurement errors were determined:

To keep out of litter and other big materials a mechanical rake was installed above the gauging bucket. Figure 5 shows the protection rake covered by litter after a rain event. A high maintenance of the monitoring station is requested during and after runoff events to keep the rake free from litter and to make sure that the runoff does neither get blocked nor filtered by the materials stuck on the rake. This phenomenon could have an influence on the runoff quality as well as quantity. It could also occur, that bigger particles succeed to pass the rake and enter the bucket. They could block the turbidity sensor and distort the measured data leading to very high recorded false turbidity values. An accumulation of particles at the bottom of the bucket as well as drain blockages due to trapped particles at the outflow of the bucket could furthermore falsify the measured water level. A regular as well as an event-based maintenance would therefore be

mandatory to secure data quality. This includes the removal of big particles blocked by the rake and emptying the sampling bucket.

In addition, a supervision of activities happening in the catchment would be necessary. Construction works, the cleaning of instruments and other actions are important to report in order to avoid wrong data interpretation due to perturbations.

Due to the Mediterranean climate snow fall did not occur during the observation period, however hail occurs during rainfall events in summer. There is a lack of knowledge how the sensors measure hail grains. A further investigation would have been beyond the scope of this work but would be interesting to investigate.

The only outlet of the gauging bucket is on the height of the weir overflow. This means that after a rainfall event rainwater runoff remains in the bucket. This runoff contains particles which start to sediment when turbulences are poor. When circumstances are given the remaining water can evaporate, leaving the particles in the bucket. The particles could lead to an overestimation of turbidity during subsequent events. At the beginning of the next runoff event the remaining residues could lead to a strong raise of turbidity which might easily be confused with first flush phenomena. For this reason, a consideration of first flush effects was not reasonable.

The gauging station was well maintained for temporal installations between November 2021 and April 2022 since before a rainfall event the gauging station was every time newly installed. A lower maintenance was carried out after the gauging station was constantly installed onsite. Between mid of June 2022 and beginning of September 2022 no maintenance was conducted due to university vacations. Therefore, events which were observed during this period must critically be evaluated before a further data processing.

### 4.2.3 Correlation Analysis

Water quality simulations are generated in SWMM as a concentration of a pollutant in mg/l. Turbidity curves cannot be reproduced directly as they are expressed through different units (FNU, NTU or FAU). For this reason, a correlation between observed turbidity and TSS concentrations is necessary. It was envisaged in this work to use the long-term observations of turbidity of the surface runoff to derivate TSS concentrations, which can then be compared to the TSS simulations of SWMM. A correlation curve can be set up by manually analysing runoff samples on their concentration of TSS and to correlate the measurements with the recorded turbidity. In order to obtain a reliable correlation function multiple representative measurements are necessary. Due to lacking rainfall during the observation period, a relation between turbidity and TSS was not possible to be established in a representative way as suggested by Bertrand - Krajewski et al. (2010). Accurate water quality values can therefore not be reproduced in this study. Nevertheless, turbidity can be used to draw conclusions about runoff contamination.

An understanding of correlations between turbidity and TSS concentrations was provided by literature. Bertrand-Krajewski (2004) established reliable linear correlations with gradients of 1.71 and 1.64 for a combined sewer system during wet weather flow. Hannouche et al. (2011) assigned values of 0.6 and 1.4 mg/l to 1 FAU for combined sewer systems during rain events. Correlating TSS to turbidity for a waste water treatment plant Azeez et al. (2012) found a factor of 0.94 as significant. Rügner et al. (2013) presented an overview of TSS-turbidity correlation results from literature analysing river discharge. They summarised that in natural rivers a linear relationship of NTU and TSS with slopes of 1.0 to 2.5 is commonly established. In their own study they created a general relation of 1 mgTSS/l equals  $1.86 \times$  NTU-turbidity for fall and winter months from

October to January. The work of Leutnant et al. (2016) was specifically interesting for this master thesis since they analysed urban surface runoff on microscales which depend on land use and surface cover. For the linear equation  $TSS = f(\text{turbidity}) = a + b * \text{turbidity}$  they found b-values of 1.89, 3.69, 0.84 and 0.97 depending on the catchment.

For this study it was decided to rather rely on a theoretical correlation than to establish an unrepresentative one derived from sparse values. Considering values obtained in other studies an approximate linear correlation of  $1 \text{ mgTSS/l} = 1 \text{ FNU-turbidity}$  was chosen. Using this direct relation to raw turbidity data could facilitate future interpretations of this study's results when more data for a correlation is obtained. With regard to the present study, this simplification has as consequence that TSS concentrations which were correlated from observed turbidity could be higher or lower than real TSS concentrations of the analysed runoff.

### 4.2.4 Event selection

The rainfall data is expressed by the rainfall sum (in mm) registered at the end of every minute. It was computed to the rainfall sum at the end of every 5 minutes to correlate precipitation to runoff which was observed within a 5-minutes interval. This temporal resolution leaves it unclear when exactly raindrops were registered within the 5 minutes. The beginning of a rainfall event was defined with the first reaction of the RG. In this study runoff starts when the first runoff was registered by a recorded change of the water level in the gauging bucket. In theory it already starts earlier depending on the shape of the catchment (considering the runoff distance to the gauging station) and initial losses defined by the lag time. As already stated, long-term drifts complicate the definition of the end of the runoff event. The height of the weir outfall which was at a height of 56 mm was assigned by the water level sensor with lower values descending over the observation period. In this work the runoff therefore ends when no change of registered water level was recorded. The distinction was conducted carefully to assure to represent the whole event but to not confuse runoff with evaporation reducing the water level after a runoff event. When the runoff process is not completely finished and a new rainfall occurs, this series of rainfall events is considered as one runoff event, where two hydrographs superimpose each other. A runoff event was selected for further modelling purposes when the precipitation surpassed a total rainfall height  $\geq 3,0 \text{ mm}$ . Rainfall events below this limit were considered to lead to unclear results due to initial losses reducing the final runoff at the catchment outlet and to measurement inaccuracies. Similar limits were set within comparable studies, as an example Leutnant et al. (2016) defined a minimum rainfall depth  $> 2,0 \text{ mm}$ . Comparing the total runoff volume  $V_{\text{tot}}$  to the total rainfall height applied over the catchment surface, a runoff coefficient was obtained for every event. Leaving unreasonable runoff coefficients out to consideration the limits for runoff-coefficients were between 0,1 and 2,0. Runoff-coefficients over 1,0 are theoretically not possible. In this case the study site has a supplement run-on from the catchment above, whose quantitative and temporal contribution to the total runoff of the observed catchment cannot specifically be defined. Therefore, this run-on is not considered in the model. However, a possible maximum contribution of this catchment was evaluated by accounting the dimensions of the catchment above.

## 4.3 Initial SWMM Model

The objective of the model is to realise hydrograph and pollutograph simulations. Within simulations two units were used to visualise with pollutographs. Water quality responses are expressed in SWMM through concentrations of TSS in mg/l at a certain moment of the runoff

## Material and methods

process. TSS loads are obtained by multiplying TSS concentrations and the time-integrated discharge resulting in a washed-off mass in mg within time steps of 5 minutes. For de-sealing simulations the total washed-off mass in kg integrated over the whole event duration was computed.

An EPA SWMM model was set up with two subcatchments which were defined regarding their land-use and surface cover, as it was introduced by Rio et al. (2020). The impervious subcatchment (ISC) is fully covered by an impervious surface and is completely used as a pedestrian zone with one pathway connecting university buildings and a terrace with a ramp at the entrance of the building “Polytech”. The pervious subcatchment (PSC) comprises mostly gravel surfaces and a small part is covered with grass and bush vegetation. Table 1 gives an overview of all fundamental parameter values of the subcatchments and on what basis the values were obtained. The geometrical parameters area, width and slope were obtained within the topographic survey. Since the objective of this work is to apply the model approach of Rio et al. (2020) on an observed study site, several input parameter values which were chosen by Rio were adopted for this work in order to maintain the same assumptions. These pre-defined values facilitate to compare the results of this work with the ones of Rio. The PSC has its outfall theoretically in the middle of the catchment discharging onto the the downstream area of the ISC. To keep the model simplifications of Rio et al. (2020) each subcatchment was modelled to discharge directly into one common outlet. With less runoff flowing over the ISC an underestimation of the wash-off effect is expected from this simplification.

Table 1: Input Parameter values of the initial model

	Input Parameters	Sourcing-Method/ Approach	Impervious Sub- catchment	Pervious Sub- catchment
Geometry	Area (m <sup>2</sup> )	Survey	217.73	98.05
	Width (m)	Survey (length-width ratio of catchment)	6.98	4.68
	Slope (%)	Survey (average slope of catchment)	2.51	
Hydrology	Depression storage (mm)	Defined by Rio 2020	0.5	8
	Manning coefficient		0.025	0.05
	Curve number	Based on modelling site	/	76
Water Quality	Initial Build-up (kg/ha)		10	
	Wash-off Function	Defined by Rio 2020	Exponential	
	Wash-off Exponent		2	
	Wash-off Coefficient (h/mm <sup>2</sup> )	Literature	0.01	

Rio et al. (2020) applied a universal CN value of 50 for pervious areas of the whole modelled site. For a more precise representation of infiltration processes the CN was adapted to site specific conditions. Most of the PSC is covered with gravel with a loose top layer of 1,0 to 1,5 cm and gravel packed bags underneath. Therefore, soil group A was chosen, being defined with more than 90 percent of sand or gravel. Consulting table 2-2a of U. S. Department of Agriculture (1986) which defines CN values for the land use description “gravel” a value of 76 was chosen.

Focusing on the wash-off behaviour pollution was applied on the catchment’s surfaces through a fixed initial built-up (IB) in kg/ha. This mass of pollution was newly available at the beginning of each simulated event, not considering the time which had passed since the last rainfall event as proposed by an initial built-up function. Even though built-up processes are left out of consideration the rain frequencies are very low during most time of the year regarding the arid

Mediterranean climate. Since specific rainfall events were simulated, a necessary drying time was not considered either.

## 4.4 SWMM Modelling

### 4.4.1 Sensitivity Analysis

The sensitivity analysis was executed in two parts. The first one was only focused on the hydrological response of the model. The second part analysed the sensitivity of the water quality parameters and was conducted with the calibrated hydrological parameter values since the pollution load propagation depends on the hydrological behaviour of the catchment. The event RG\_6-9-12h was chosen for a sensitivity analysis due to its reasonable runoff coefficients and high intensities representing well runoff extreme behaviours during summer months. To evaluate the model performance during the sensitivity analysis the best fit criterion NSE was chosen. NSE is suitable for this comparison since it returns normalised value ranges. The response of the hydrograph analysed the discharge Q with the NSE-Q. The pollutograph was assessed through concentration C with the NSE-C.

A first simulation was carried out with the initial model with the values indicated in Table 1. For all further simulations only one parameter was modified at the same time as indicated by step 1 and 2 (Table 2 and Table 3). The alteration values of the hydrological parameters are presented in Table 2. Regarding the alteration of the hydrological parameters, simulations were conducted separately for the impervious and the pervious catchment, assuring that the results of all parameter modifications are individually recorded. The changed values for steps 1 and 2 were defined by an alteration of -50% (step 1) and +50% (step 2) of the initial value (Table 1). For some parameters a 50% alteration was not suitable. Simulations of all observed events indicated a contribution of the PSC only during three events: the episode defined as RG\_11-3-17h, when a continuous rainfall lasted more than 1,5 days, RG\_7-9-2h and RG\_14-11-9h when very high intensities and runoff volumes were reached. In all other cases the rainfall on the PSC did not contribute to the total surface runoff. This is why a change to a lower CN would not lead to different BFC results for the chosen event RG\_6-9-12h. Lower CN values enhance an infiltration even more, which would not make a difference since already all rainwater infiltrated on the PSC. Therefore, the maximum CN of 99.9 (< 100 is the maximum) was chosen for step 2 and to maintain equal distances a value of 88 was assigned to step 1.

Table 2: Parameter values for the sensitivity analysis of hydrological parameters.

	Impervious Subcatchment			Pervious Subcatchment		
	Initial values	Step 1	Step 2	Initial values	Step 1	Step 2
Depression storage (mm)	0.5	0.25	0.75	8.0	4	12
Manning coefficient	0.025	0.0125	0.0375	0.05	0.025	0.075
Curve number		/		76	88	99.9

As stated above the sensitivity analysis of the water quality module was conducted with the calibrated hydrological input parameter values: Depression storage of 0.75 mm and Manning Coefficient of 0.001. The alteration values of the water quality parameters are presented in Table 3. For comparing the results of the sensitivity analysis, the difference between NSE results of step 1 and step 2 were computed for each parameter while all other parameters were kept unchanged.

Table 3: Parameter values for the sensitivity analysis of water quality parameters.

	Initial Model	Step 1	Step 2
Initial Build-up (kg/ha)	10	5	15
Wash-off Function	Exponential		
Wash-off Exponent	2	1	3
Wash-off Coefficient (h/mm <sup>2</sup> )	0.01	0.005	0.015

#### 4.4.2 Hydrological calibration of the model

The hydrological model calibration was conducted by testing different input values for the parameters depression storage DS and Manning coefficient  $n$  of the ISC. Within the sensitivity analysis, the variables appeared the most interesting for a more precise definition. The calibration was realised by carrying out runoff simulations with various parameter values. For the variation of DS and  $n$  maximum and minimum values were defined by physical parameter limits and in accordance with widely adopted literature. A lower boundary of 0,01 was chosen for  $n$ . Rossman (2015) suggested this value for smooth asphalt and Chow (1959) assigned smooth metal and glass to this value. Considering already very smooth surfaces it is expected that a modelling with even lower values would not lead to useful results from a physical point of view. An upper boundary of 0,025 was chosen since Chow assigned this value to corrugated metal surfaces, gravel, and barren soil coinciding with Rossman (2015). The presented examples of surfaces seem rougher than the impervious surface of the study site so that a consideration of higher values is not expected to improve the model performance. The value 0,0125, which is -50% of the initial value achieved a good NSE result through the sensitivity analysis so that it was decided to add this value. For the parameter DS a bottom limit of 0 with no initial losses was set which is physically not possible. Butler and Davies (2004) indicate typical DS values for impervious areas other than flat roofs between 0.5 and 2.0 mm. According to Rammal and Berthier (2020) who analysed a collection of urban catchments in Europe, adequate values for urban drainage modelling adopted by computer software range from 0.5 to 2.5 mm with an average of 0.58 mm. Testing upper boundaries of 2,0 and 1,5 mm DS for the calibrated event led to significant lower NSE. For this reason and considering the present surface slope of 2,5%, the upper boundary of 1.25 mm was chosen. The value variations of the two parameters were plotted in a 6x3-matrix, where 6 and 3 represent different input values for DS and  $n$ . The matrix visually facilitates the computation of every parameter combination and is below referred to as parameter set.

5 of 17 exploitable events were chosen randomly for model calibrations. Table 4 summarises essential event properties for all calibration events. 4 events were recorded in autumn, 2 with a low and 2 with high rainfall intensity and 1 stormwater event occurred in summer which is characterised by a high intensity, a short duration, and a long period without precipitation before. The runoff coefficient of the observed events varies strongly in contrast to the calculated runoff coefficient of model. The mean runoff coefficient of the model was 0.68.

Table 4: List of events chosen for calibration.

	Rainfall sum (mm)	max. rainfall intensity (mm/h)	Rain gauge	max. turbidity observed (FNU)	Runoff coefficient observed	Runoff coefficient simulated
RG_24-11-23h	7.4	7.2	UM35	131	0.72	0.60
RG_6-9-12h	22.6	63.6	Polytech	407	0.80	0.69
RG_24-9-1h	27.7	28.8	Polytech	245	1.26	0.67
RG_14-11-9h	57.3	67.2	Polytech	118	0.51	0.77
RG_4-12-9h	3.4	12	Polytech	76	0.42	0.67
						0.68

4 best-fit-criteria were identified to compare the results obtained with the altered parameter values: NSE, KGE as well as RPD of maximum discharge  $Q_{max}$  and the total discharged Volume  $V_{tot}$ . The latter, the relative deviation of absolute values (RPD) was interesting for the further water quality modelling, since  $Q_{max}$  and  $V_{tot}$  impact the wash-off process. For all 5 calibration events runoff simulations were conducted with all parameter sets. NSE Q, KGE Q, RPD  $Q_{max}$  and RPD  $V_{tot}$  were calculated for every simulation. The results of each criterion were separately plotted in a matrix. As a result, 4 matrices (one for each BFC) were obtained for each of the 5 events. With the purpose of obtaining a general optimal parameter-combination median values were calculated for all events combined, resulting in 4 matrices (one for each BFC). A final matrix combining all 4 BFC indicates a global optimal parameter set. The use of several BFC at the same time is supposed to enhance the performance, due to a multiple representation of objective functions. The median was chosen as statistical value to allow a combination of the results of all events, which is more robust than for example the mean regarding statistical outliers. In order to better understand the distribution of the BFC results, mean and median, 1st and 3<sup>rd</sup> quartile, minimum and maximum values as well as whiskers were computed and presented in box-plots.

#### 4.4.3 Water Quality Calibration of the Model

The calibration of water quality parameters was conducted with the already calibrated hydrological parameters:  $n=0.01$  and  $DS=0.75$  mm. The same events used for the hydrological calibration were used for calibrating the water quality, see Table 4. The parameters initial built-up IB and wash-off coefficient KC turned out during the sensitivity analysis to be the most useful to be further developed. For choosing a useful range of parameter values maximum and minimum boundaries were defined for IB and  $K_w$ . An initial built-up of 10kg/ha was considered as minimum. This is the only variable applying pollutants on the surface. Consequently, when the IB is too low the disposable pollution is not sufficient. 10 kg/ha corresponds to the input value in the study of Rio et al. (2020). In terms of defining an upper boundary a wider range of maximum build-up values was found in literature. While Borris et al. (2014) used a maximum build-up 35 kg of TSS/ha, Lehtinen (2014) indicated optimized maximum build-up values ranging between 20.3 and 286 kg/ha. After first tests with higher values a limit of 200 kg/ha was chosen as maximum IB in this study. A higher IB seems not reasonable since the observed surface is used as pedestrian zone at a university campus. Therefore, no bigger pollution is expected. Concerning the  $K_w$  Rio et al. (2020) varied between  $10^{-6}$  and  $10^{-1}$  and additionally  $5 \cdot 10^{-1}$  in an interval of the power of ten. In her paper almost no reaction of the pollutographs was produced for  $10^{-6}$  and  $10^{-5}$  and therefore these values were excluded in this work with the lowest  $K_w$  value of  $10^{-4}$ .  $10^{-2}$

was chosen as upper boundary since an even higher  $K_w$  led to a complete wash-off at the very beginning of an event.

In a next step the intervals within the maximum and minimum values of IB and  $K_w$  were densified. This was realised by testing intervals with different spacings on the event RG\_6-9-12h which was used for the sensitivity analysis. Regarding the  $K_w$  an alteration of half a power of ten was defined. As a result, the following 4  $K_w$  values serve as input values within the calibration: 0.0001; 0.0005; 0.001; 0.005. For the IB an interval of 25kg/ha seemed necessary to well reproduce an impact of the parameter variation, leading to the following input values: 10, 30, 50, 75, 100, 125, 150, 175, 200). Between 10 and 50 a value of 30 kg/ha was chosen for keeping the same spacing between the lower boundary and the regular interval.

The final input values for the calibration were plotted in a 9x4-matrix to visualise all parameter combinations. Simulations were conducted for all possible parameter combinations. From the resulting pollutographs best-fit criteria were calculated to compare the simulated to the observed water quality. As best fit criteria NSE and KGE was chosen. The beforehand used RPD is not reasonable for the water quality calibration since this criterion only analyses absolute value accuracy. The objective of the calibration of the water quality response is a qualitative accuracy. This means that simulated concentration curves are expected to react simultaneously with the observed curve but not with the same magnitudes. For each simulation NSE and KGE was calculated twice, to compare one time the simulated TSS concentration and the other time the simulated pollution load with the observed turbidity. For statistically analysing the results of the water quality responses and combining them for all events the same procedure with median results and box-plots was applied as it was carried out for the hydrological calibration.

### 4.4.4 Verification

The verification was conducted with all observed, exploitable 17 rainfall events. The objective of this process is to check if better best fit values can generally be achieved with the new input values, defined through calibration. Every event was simulated with SWMM first with the initial input values of the uncalibrated model and then with the parameter values, which were in the hydrological calibration identified as most favourable. For both simulations NSE and KGE were calculated. The obtained BFC values for the uncalibrated and the calibrated model were then compared through scatterplots. Additionally, a median of all events was calculated for both BFC of the initial and the calibrated model and the number of events where an improvement regarding the BFC was registered was counted.

Within the hydrological calibration a clear optimal parameter set was found. Consequently, the hydrological verification only involved the comparison of this specific parameter set with the initial model. Within the water quality calibration, 4 parameter sets were chosen for a more precise analysis. As a result, 4 comparisons were carried out for the verification of the water quality calibration, where the results of each set were compared to the results of the initial model.

### 4.4.5 De-sealing Modelling

As focus of this study de-sealing measures on the study site were simulated with the modelling approach of Rio et al. (2021). The implementation of GBI was modelled two times: once with the calibrated model and once with the initial (uncalibrated) model. A comparison of the results points out the sensitivity of the model parameters and their impact on land de-sealing modelling.

## Material and methods

Simulations of all observed events were conducted with the scenario of a de-sealing of 50% and 100% on the study site, replacing the present impervious pedestrian zone, which equals the total impervious surface of the catchment. In this case a permeable pavement is the most applicable GBI replacing the impervious surface in a way that the function of the surface is not impacted. According to Rio et al. (2021) PP can be modelled with a Manning coefficient of 0.04 and depression storage of 1.5 mm. To compare the de-sealing scenarios with the initial state without GBI simulations the uncalibrated and the calibrated model were used to simulate all events. The uncalibrated model was set up with the input values of Table 1. For the calibrated model there was a choice between 4 different parameter value sets which were discussed in chapter 4.4.3. Set 1 was chosen, since it is statistically more reliable than the mean and in comparison to the sets 3 and 4 it considers the concentration as much as the pollutant load. Two separate models were created in SWMM to simulate the de-sealing of 50% and 100%. The model with a 50% de-sealing consists of 3 subcatchments. The former ISC was divided into 2 separate ones, which cover each 50% of the area of the former one. The width did not change since the determining length-width ratio did not change. The new depression storage and Manning coefficient values of PP were applied on the de-sealed subcatchment (DSC), while for the pervious subcatchment the initial input values (8,0; 0,05) were kept. For the ISC the uncalibrated values (0,5; 0,025) and the calibrated values (set 1: 0,75; 0,01) were applied. The second model, to simulate the effect of de-sealing of 100% of the impervious area, only consists of two subcatchments which are both pervious. The PSC has the same properties as the model of a 50% de-sealing and the de-sealed subcatchment has the same dimensions as the model without GBI measures but with the beforehand named parameter values of the new applied pervious pavement. As in the model approach of Rio et al. (2021) the water quality parameters are the same for all subcatchments. A distinction was made between the initial and the calibrated model concerning the initial built-up and the wash-off coefficient, as indicated in Table 5 Table 6.

Table 5: Input parameter values of the SWMM model with a de-sealing of 50%. For parameters, where it was necessary to distinguish between the uncalibrated and the calibrated values a double crossbar ( // ) separates the uncalibrated (before the crossbars) from the calibrated value (after the crossbars).

Input Parameters		Impervious Subcatchment (ISC) 50%	De-Sealed Subcatchment (DSC) 50%	Pervious Subcatchment (PSC)
<i>Geometry</i>	Area (m <sup>2</sup> )	108.87	108.87	98.05
	Width (m)	6.98	6.98	4.68
	Slope (%)		2.51	
Hydrology	Depression storage (mm)	0.5 // 0.75	1.5	8.0
	Manning coefficient	0.025 // 0.01	0.04	0.05
	Curve number	/		76
	General Drying times (days)	/		11
Water Quality	Initial Build-up (kg/ha)		10 // 75	
	Wash-off Function		Exponential	
	Wash-off Exponent		2	
	Wash-off Koefficient (h/mm <sup>2</sup> )		0.01 // 0.001	

## Material and methods

Table 6: Input parameter values of the SWMM model with a de-sealing of 100%. For parameters, where it was necessary to distinguish between the uncalibrated and the calibrated values a double crossbar ( // ) separates the uncalibrated (before the crossbars) from the calibrated value (after the crossbars).

Input Parameters		De-Sealed Subcatchment (DSC) 100%	Pervious Subcatchment (PSC)
<i>Geometry</i>	Area (m <sup>2</sup> )	217.73	98.05
	Width (m)	6.98	4.68
	Slope (%)		2.51
Hydrology	Depression storage (mm)	1.5	8
	Manning coefficient	0.04	0.05
	Curve number		76
	General Drying times (days)		11
Water Quality	Initial Build-up (kg/ha)		10 // 75
	Wash-off Function		Exponential
	Wash-off Exponent		2
	Wash-off Koefficient (h/mm <sup>2</sup> )		0.01 // 0.001

After the simulations the following variables were computed for each simulation: the maximum Discharge  $Q_{max}$  during the event, the total runoff Volume  $V$  after the end of the runoff event, the maximum Concentration  $C_{max}$  during the event, the total pollutant load PL at the end of the runoff event and the event mean concentration EMC which was obtained by calculating the mean of the simulated TSS concentrations over the event duration. In a further step a relative difference was calculated for these variables between the model with no GBI measures and the model of a de-sealing scenario. The formation of these differences was conducted twice, once with the uncalibrated and once with the calibrated input values. Global values for the 5 presented variables were obtained by calculating the median of all events. Considering all simulation events, standard deviations were calculated separately for all 5 reduction indicators (PD of  $Q_{max}$ ,  $V_{tot}$ ,  $C_{max}$  and EMC). The two models (uncalibrated and calibrated) were distinguished as well as the two de-sealing scenarios, resulting in 20 standard deviation results. Combining all reduction indicators into one a normalised mean standard deviation was obtained for the uncalibrated and the calibrated model for a de-sealing scenario of 50% and 100%.

Based on these results, the following questions can be discussed: What is the impact of the applied GBI measures? What role had the calibration of the input parameters and what is its impact on the results? How important is a model calibration for this de-sealing model?

## 5. Results and discussion

### 5.1 Analysis of Rainfall Data

Figure 7 presents scatterplots of all observed rainfall data, which were recorded by at least one of the two rain gauges. The scatterplot on the left side (Figure 7a) opposes the rainfall intensities calculated for a 5 minutes time step. Punctual measurements served as input values for this figure, meaning that a rainfall event, which for example first occurs at RG Polytech and 5 minutes later at RG UM35, would not be well represented by this figure, since this time lag is not considered. Figure 7b on the right side considers the cumulative rainfall over 7 days. The sum of all registered rainfall data was calculated over a period of 7 days hence small lag times as explained before are considered through this comparison. Figure 7a suggests that intensities within rainfall events were higher at the site Polytech, Figure 7b indicates either more intensive or more rainfall events within the considered 7- days interval.

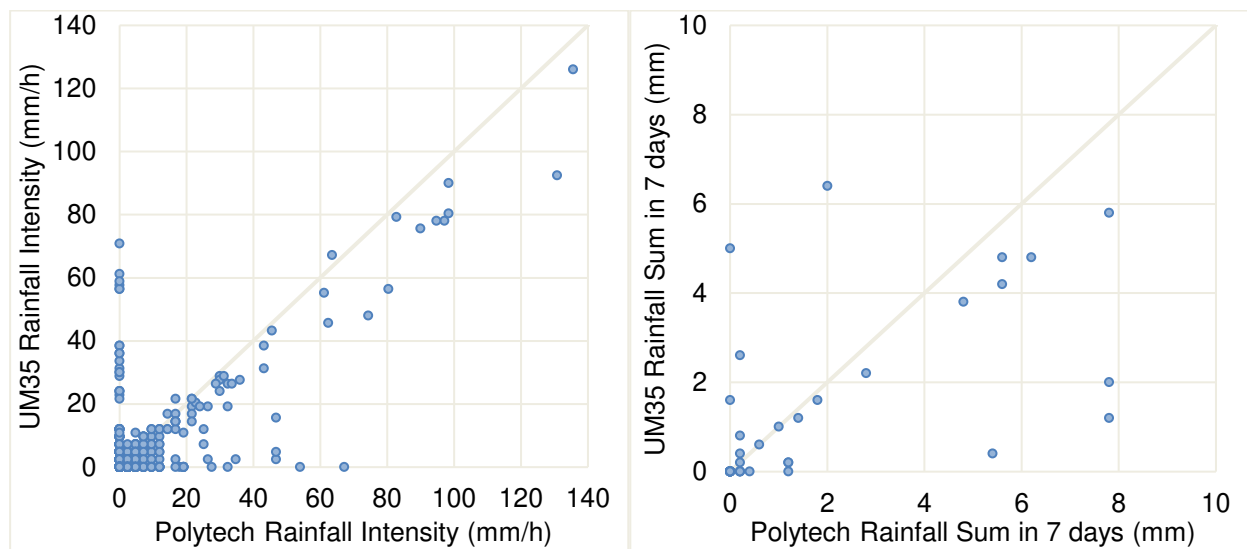


Figure 7a and b: Comparison of the rain gauges “Polytech” and “UM35” for the observation period from 01.11.2021 to 01.11.2022.

Table 7: Comparison of absolute rainfall values registered at RG Polytech and UM35.

	Polytech			UM35		
	Maximum	Mean	Median	Maximum	Mean	Median
Intensity (mm/h)	136	4.8	2.4	126	5.0	2.4
Sum in 1 hour (mm)	92	2.1	0.6	60	1.6	0.6
Sum in 1 day (mm)	112	6.6	1.5	93	6.2	1.4
Sum in 7 days (mm)	137	13.9	4.8	115	13.6	4.0
Cumulative Rainfall (mm)	542			515		

Table 7 presents a statistical analysis of the rainfall data. Polytech has higher cumulative values including a summation of fallen rain in 1 hour, 1 day and 1 week as well as an absolute higher cumulative result. Comparing the rainfall event with the maximum intensity, a higher value was recorded at RG Polytech. Considering the mean of the intensities, RG UM35 registered in average slightly higher intensities. This can be explained by the rainfall events with high intensities which occurred in August 2022 which were recorded only by RG UM35 and missed by RG Polytech. The fact that the median of the intensities of both RGs are the same, confirms this explanation since median values implicate outliers less.

## Results and discussion

The cumulative rainfall curves in Figure 8 point out the divergence of the two rainfall recordings. The plotted intensities on the second axis depict the applied method of exploiting the rainfall data of RG UM35 charted in yellow when no data was recorded by RG Polytech. Important data lacks occurred in autumn 2021 and in August 2022. The reliability of the RG UM35 data from October 2022 until January 2023, which coincides with the end of the observation period is questioned considering the growth of the cumulative curve of RG Polytech, while the slope of RG UM35 remains flat.

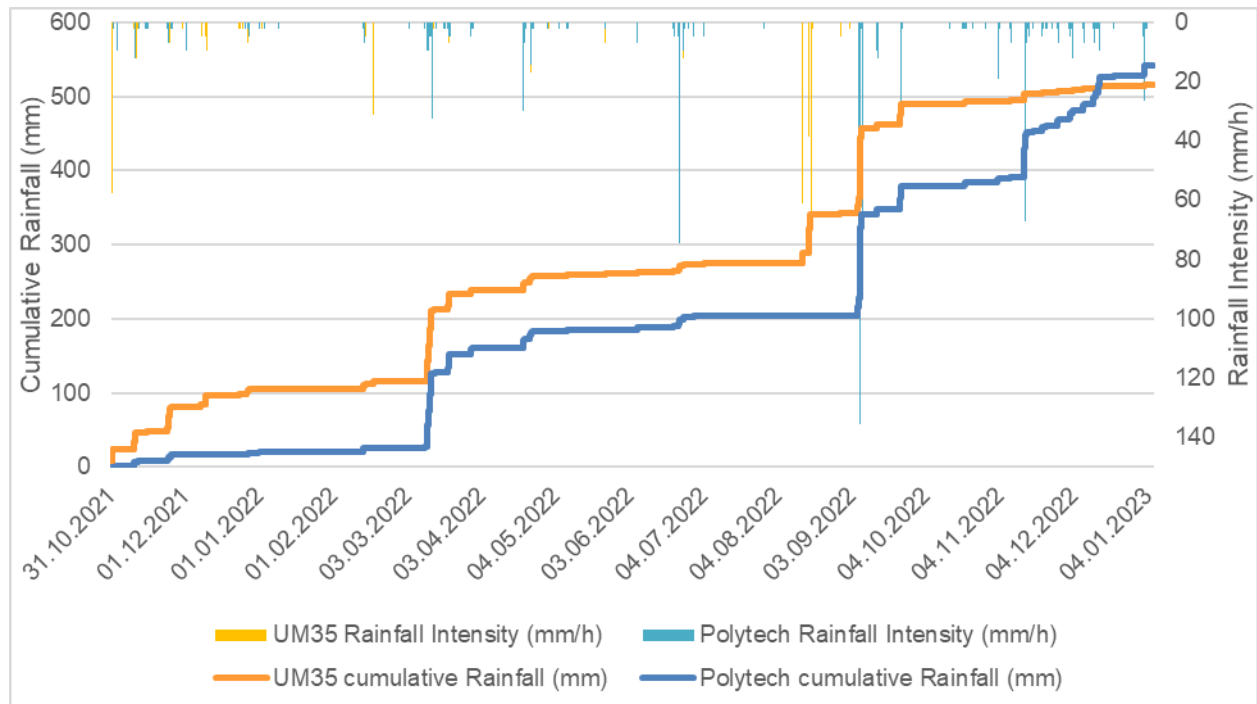


Figure 8: Combination of cumulative rainfall & rain intensity for both rain gauges (RG Polytech and RG UM35).

The reason for the variance in the results of the two RGs cannot specifically be found in their distance since they are only 168 m apart. Conversely, it can be concluded that local proximity does not assure the reliability of RGs. Analysing the positions of the RGs their exposition to wind is different. The main wind comes from north and UM35 is directly exposed to it since it is situated in a wind corridor which is created by the street next to it coming from north and without any obstacles. In contrast, RG Polytech is installed on a roof which is slightly lower than the roof north of it, which can act as a wind protection. Trees around the building act as surface roughness elements which also influences the wind but without creating wind shading since the trees are approximately as high as the building. Investigated within the studies of Blocken and Carmeliet (2006) and Hochedlinger et al. (2007), occurring wind reduces the collected rainfall since the catching surface of the RG gets reduced with the arrival angle of the rain. Therefore, the globally higher amount of rain collected by Polytech can be explained by the influence of the wind.

Processing the data of the whole observation period, 24 rainfall events surpassed the limit for the total cumulative rainfall height of 3,0 mm. The events are presented in Table 8 and were used for a further runoff analysis.

Table 8: Observed rainfall events with a total rainfall sum  $\geq 3,0\text{mm}$ .

Rainfall event	Rainfall						
	Event (RG_d-m-h)	total cumulative height (mm)	max. Rainfall sum during 1hour (mm)	max. Intensity (mm/h)	mean Intensity (mm/h)	total Volume (l)	Rainfall duration (h)
RG_24-11-4h	4.6	2.6	4.8	1.7	1453	2.75	UM35
RG_24-11-13h	15.6	4.4	7.2	2.3	4926	6.75	UM35
RG_24-11-22h	7.4	4.0	7.2	3.3	2337	2.25	UM35
RG_11-3-17h	71.2	4.2	9.6	2.0	22484	34.75	Polytech
RG_13-3-9h	29.3	12.9	32.4	3.8	9252	7.75	Polytech
RG_20-3-16h	13.8	3.8	4.8	2.0	4358	6.75	Polytech
RG_21-3-0h	5.4	4.0	4.8	1.4	1705	3.75	Polytech
RG_20-4-14h	6.1	4.5	30.0	2.4	1926	2.50	Polytech
RG_23-4-9h	4.6	4.4	14.4	4.6	1453	1.00	Polytech
RG_24-6-8h	6.8	6.8	74.4	27.2	9320	0.25	Polytech
RG_14-8-7h	14.7	13.7	61.2	11.8	4642	1.25	UM35
RG_16-8-21h	32.4	19.1	38.4	16.2	10231	2.00	UM35
RG_17-8-18h	19.5	19.5	70.8	39.0	6158	0.50	Polytech
RG_6-9-12h	22.6	11.9	63.6	5.5	7137	4.08	Polytech
RG_7-9-2h	92.4	70.5	135.6	52.8	29178	1.75	Polytech
RG_7-9-22h	17.3	17.3	80.4	69.2	5463	0.25	Polytech
RG_14-9-4h	4.0	3.4	9.6	2.3	1263	1.75	Polytech
RG_24-9-1h	27.7	18.0	28.8	10.1	8747	2.75	Polytech
RG_14-11-9h	57.3	50.5	67.2	10.0	18094	5.75	Polytech
RG_28-11-7h	5.0	2.8	7.2	1.3	1579	4.00	Polytech
RG_4-12-9h	3.4	3.2	12.0	3.4	1074	1.00	Polytech
RG_15-12-4h	21.0	4.6	9.6	2.6	6631	8.00	Polytech
RG_2-1-23h	12.2	9.0	26.4	3.8	3853	3.25	Polytech

## 5.2 Analysis of Observed Runoff Data

Figure 9 visualises all rainfall events and marks the observed periods with a black Frame. The frame with a grey background marks the period during summer vacations when no maintenance of the runoff gauging station was carried out due to summer vacations.

Table 9 links the presented rainfall events to the runoff observations. The presented runoff coefficients vary extremely. A rejection of runoff events with a runoff coefficient  $< 0,1$  and  $> 2,0$  was necessary. Reasons can be found in the unclear additional run-on from the catchment above. However, it is also expected that measurement errors cause these high variations. Additionally, the time resolution of the observed data is another source of inaccuracies. Measurements were recorded in a 5-minutes interval. The measurements are taken at a non-particular moment of the runoff behaviour. This moment might not be representative for the whole 5-minutes period. When an outlier is measured, it can distort the entire observed data series. A reproduction by model simulations can therefore become difficult or even impossible. Especially the turbidity sensor is error prone. Unrepresentatively high turbidity values can be registered due to big particles blocking the sensor and falsifying the measurements.

## Results and discussion

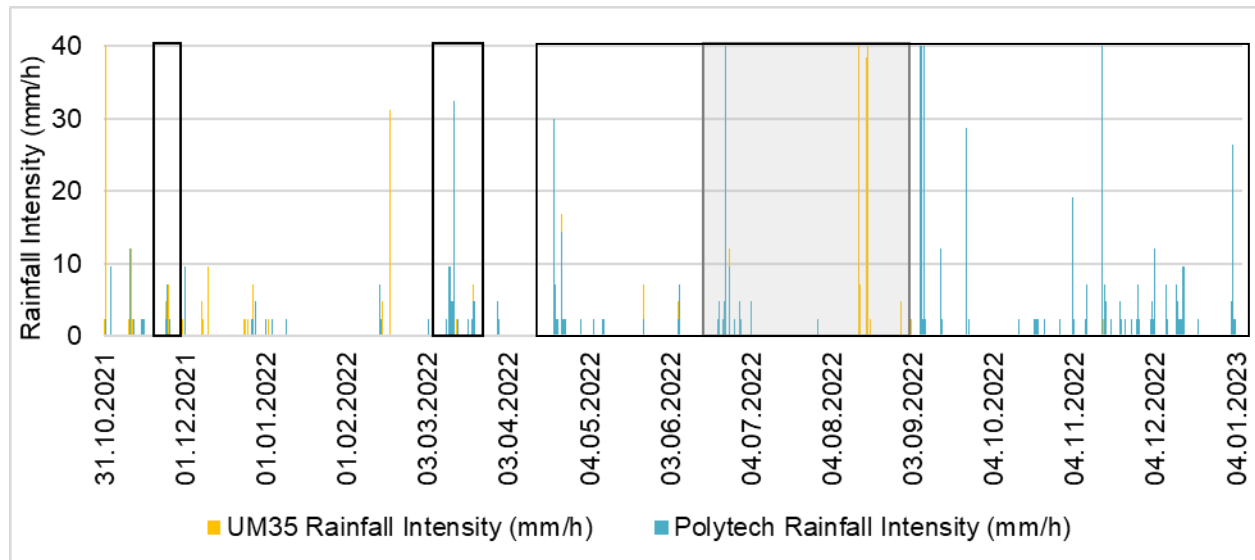


Figure 9: Runoff observation periods.

Table 9: Runoff events correlated with observed runoff.

Rainfall event	Rainfall			observed Runoff			Analysis
	total height (mm)	max. Intensity (mm/h)	total Volume (l)	max. Runoff (l/s)	total Volume (l)	max. Turbidity (FNU)	Runoff coefficient
RG_24-11-4h	4.6	4.8	1 453	0.37	2 268	96	1.56
RG_24-11-13h	15.6	7.2	4 926	0.34	2 890	417	0.59
RG_24-11-22h	7.4	7.2	2 337	0.56	1 676	131	0.72
RG_11-3-17h	71.2	9.6	22 484	0.80	27 010	147	1.20
RG_13-3-9h	29.3	32.4	9 252	2.57	8 673	88	0.94
RG_20-3-16h	13.8	4.8	4 358	0.20	1 499	73	0.34
RG_21-3-0h	5.4	4.8	1 705	0.10	371	1	0.22
RG_20-4-14h	6.1	30	1 926	0.18	327	890	0.17
RG_23-4-9h	4.6	14.4	1 453	0.10	114	48	0.08
RG_24-6-8h	6.8	74.4	9 320	6.48	2 081	1 329	0.97
RG_14-8-7h	14.7	61.2	4 642	20.11	14 466	1 011	3.12
RG_16-8-21h	32.4	38.4	10 231	4.89	22 495	89	2.20
RG_17-8-18h	19.5	70.8	6 158			53	
RG_6-9-12h	22.6	63.6	7 137	3.24	5 681	407	0.80
RG_7-9-2h	92.4	135.6	29 178	16.10	34 294	161	1.18
RG_7-9-22h	17.3	80.4	5 463	6.17	3 995	45	0.73
RG_14-9-4h	4	9.6	1 263	0.37	460	98	0.36
RG_24-9-1h	27.7	28.8	8 747	3.76	10 366	245	1.19
RG_14-11-9h	57.3	67.2	18 094	3.20	9 198	118	0.51
RG_28-11-7h	5	7.2	1 579	0.23	1 612	39	1.02
RG_4-12-9h	3.4	12	1 074	0.71	447	76	0.42
RG_15-12-4h	21	9.6	6 631	0.91	5 939	110	0.90
RG_2-1-23h	12.2	26.4	3 853	2.81	4 301	222	1.12

In Figure 10 two non-exploitable events are presented as examples for occurring errors. With a maximal intensity of 70.8 mm/s the event RG\_17-8-18h well represents extreme stormwater runoff in summer. However, the recorded gauging station reported negative water level values as

## Results and discussion

well as an unreliable turbidity curve which slightly raises at the beginning of the event to an unrepresentative low value and then suddenly drops. A lack of maintenance during summer vacation is considered to be the main reason for these errors. Since the water level sensor as well as the turbidity sensor which work independently from each other are affected there might have been a problem at the gauging station itself. Nonetheless, the shape and magnitude of the conductivity curve presents quite realistic values. The event on the 02/01/2023 seems to represent well a possible discharge curve trough the water level sensor. Contrarily, the turbidity sensor did not work correctly. The recorded turbidity at the beginning of the event which was constant over the days before was unrepresentatively high. Since no rainfall occurred before the event for two weeks no turbulences are expected in the gauging bucket keeping particles in suspension. The sensor might have been blocked by a bigger particle which stuck on the sensor, which does not explain the continuous slow raise of the turbidity during the previous dry period though.

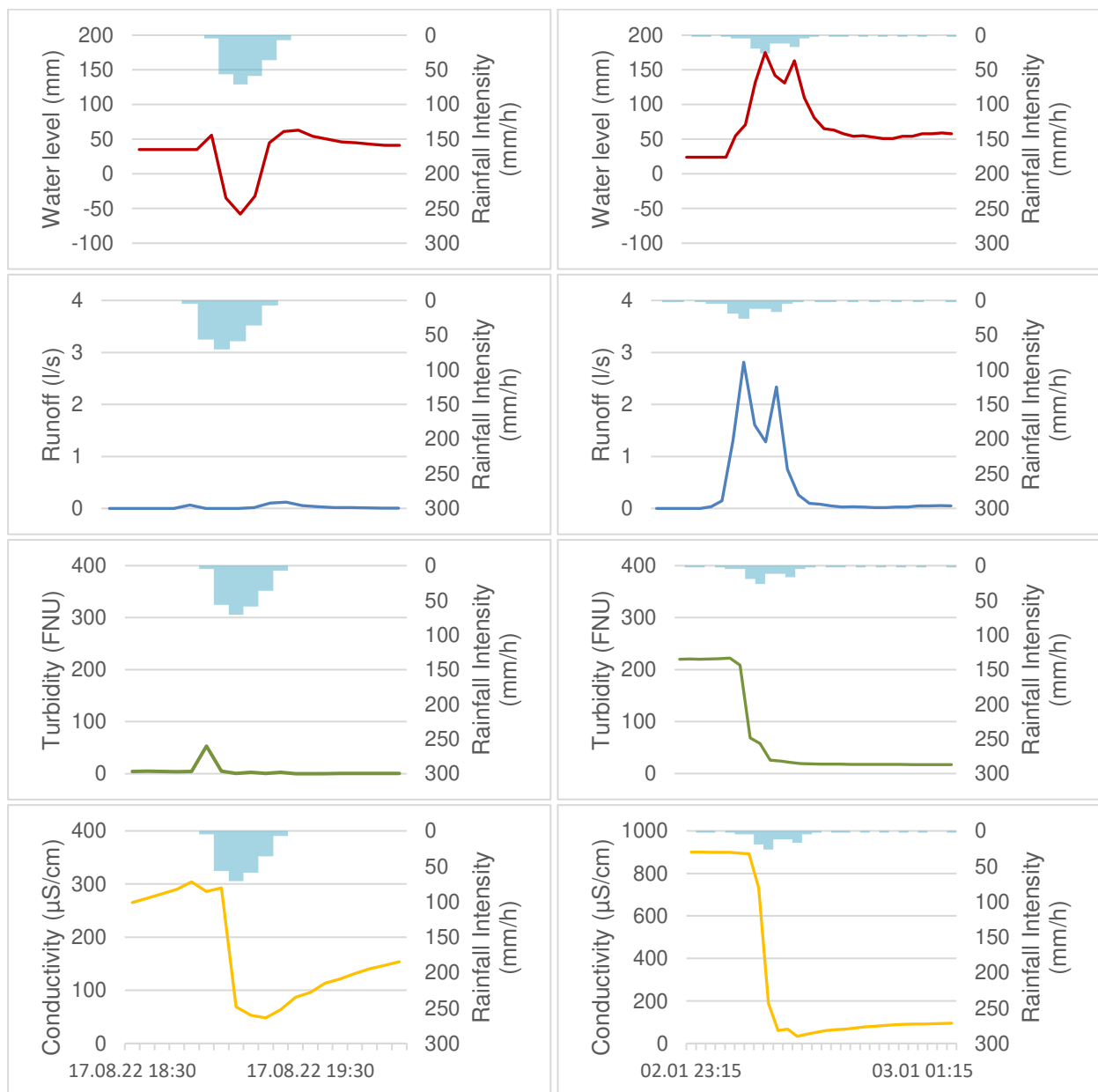


Figure 10: Results of two observed runoff events with sensor errors: 1) on the right side the event RG\_17-8-18h, 2) on the left side the event RG\_2-1-23h.

Further rejections of the events on the 21/03/2021, 20/04/2022 and 24/06/2022 due to turbidity sensor errors had to be undertaken.

### 5.3 Simulations with the Initial Model

17 events from the observation period from October 2021 until January 2023 were considered as exploitable for modelling purposes. An overview of these events is given by Table 10 which opposes observed and simulated runoff. The latter was computed with the uncalibrated model. The observed runoff coefficients vary in a high range in comparison to the simulated runoff coefficients ranging between 0.59 and 0.79. A contribution of the PSC was observed within 3 simulated events which correlates with the highest total runoff volume  $V_{tot}$ . According to Table 8 these events have the highest cumulative rainfall height with values from 57.3 mm to 92.4 mm.

Table 10: Simulation results of all runoff events, modelled with the uncalibrated model and opposed to the runoff observations.

Event (RG_d-m-h)	observed Runoff				simulated Runoff				
	$Q_{max}$ (l/s)	$V_{tot}$ (l)	$T_{max}$ (FNU)	Runoff Coeff.	$Q_{max}$ (l/s)	$V_{tot}$ (l)	$C_{max}$ (mg/l)	Runoff Coeff.	Surface Contri- bution
RG_24-11-4h	0.37	2 268	96	1.56	0.20	891	32	0.61	imp
RG_24-11-13h	0.34	2 890	417	0.59	0.33	3 285	46	0.67	imp
RG_24-11-23h	0.56	1 676	131	0.72	0.38	1 494	53	0.64	imp
RG_11-3-17h	0.80	27 010	147	1.20	0.38	16 071	38	0.71	imp + perv
RG_13-3-9h	2.57	8 673	88	0.94	1.55	6 297	72	0.68	imp
RG_20-3-16h	0.20	1 499	73	0.34	0.29	2 895	40	0.66	imp
RG_20-4-14h	0.18	327	890	0.17	0.97	1 215	183	0.63	imp
RG_24-6-8h	6.48	2 081	1329	0.97	2.19	1 560	576	0.73	imp
RG_6-9-12h	3.24	5 681	407	0.80	2.28	4 962	327	0.70	imp
RG_7-9-2h	16.1	34 294	161	1.18	8.21	21 765	176	0.75	imp + perv
RG_7-9-22h	6.17	3 995	45	0.73	4.07	3 759	354	0.69	imp
RG_14-9-4h	0.37	460	98	0.36	0.31	753	52	0.60	imp
RG_24-9-1h	3.76	10 366	245	1.19	1.56	5 928	129	0.68	imp
RG_14-11-9h	3.20	9 198	118	0.51	3.33	14 226	179	0.79	imp + perv
RG_28-11-7h	0.23	1 612	39	1.02	0.21	990	35	0.63	imp
RG_4-12-9h	0.71	447	76	0.42	0.44	630	76	0.59	imp
RG_15-12-4h	0.91	5 939	110	0.90	0.56	4 476	56	0.67	imp

For the sensitivity analysis the event RG\_6-9-12h was chosen which represents a series of extreme rainfall events of an arid Mediterranean climate during summer season with very high intensities during a short time span. The event consists of 3 separate rainfall peaks. Since the end of the runoff of the anterior rainfall was not reached until the next rainfall occurred, the 3 rainfall events were considered as one runoff event. Table 11 indicates the performance ability of the uncalibrated model through best-fit criteria by comparing simulated to observed results. With a value of 0.70 the NSE Q presents a quite satisfactory performance. The error of the total runoff volume (PD  $V_{tot}$ ) of 14 % is also rather low indicating a good hydrological model performance. In contrast a NSE C of 0.34 indicates a poor performance ability of the water quality simulations, which is confirmed by the difference of the total exported load between the observed (1.09 kg) and the simulated (0.32 kg) event resulting in PD PL of 71 %.

## Results and discussion

Table 11: Results of event chosen for sensitivity analysis simulated with initial model.

	Observed	Simulated
max. Runoff (l/s)	3.24	2.28
NSE Q		0.70
total volume (l)	5 681	4 962
PD - V (%)		14
max. Turbidity (FNU) // TSS (mg/l)	407	327
NSE C		0.34
total load (kg)	1.09	0.32
PD - PL (%)		71

Presenting the hydrographs and pollutographs of the observed and simulated event Figure 11 Figure 12 give deeper insights into the hydrological and water quality behaviour to better understand the obtained BFC vales. While the reproduction of the observed hydrograph was quite successful the simulated pollutograph does not seem suitable to represent observed processes. When the wash-off coefficient  $K_w$ , which controls the availability of pollutants, is too high, accumulated pollutants are washed-off too quickly. Consequently, no further pollution is available to be washed off for the rest of the event. Additionally, the initial built-up which controls the amount of applied pollution at the beginning an event, might have been too low so that not enough pollution is available.

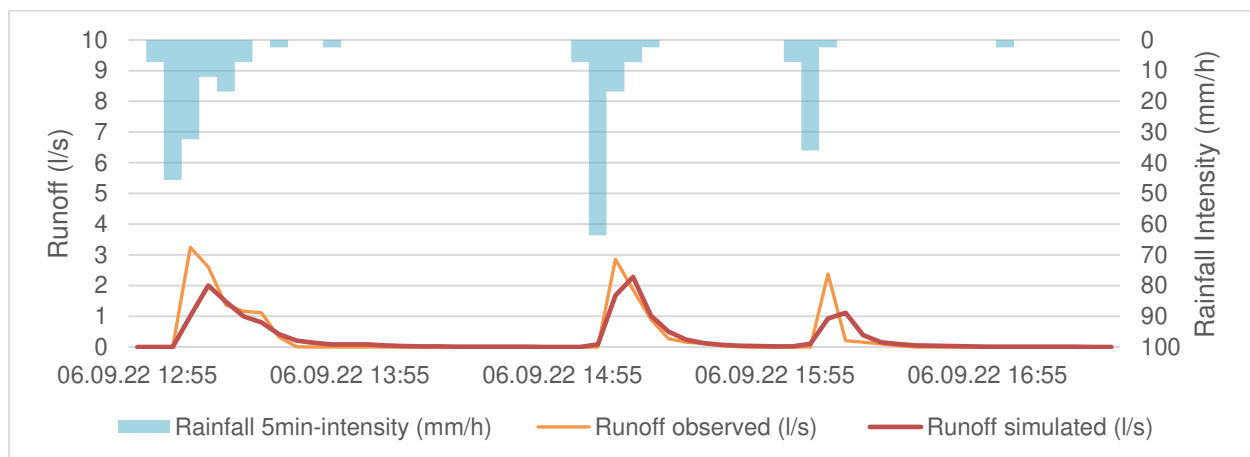


Figure 11: Comparison of observed and simulated hydrograph.

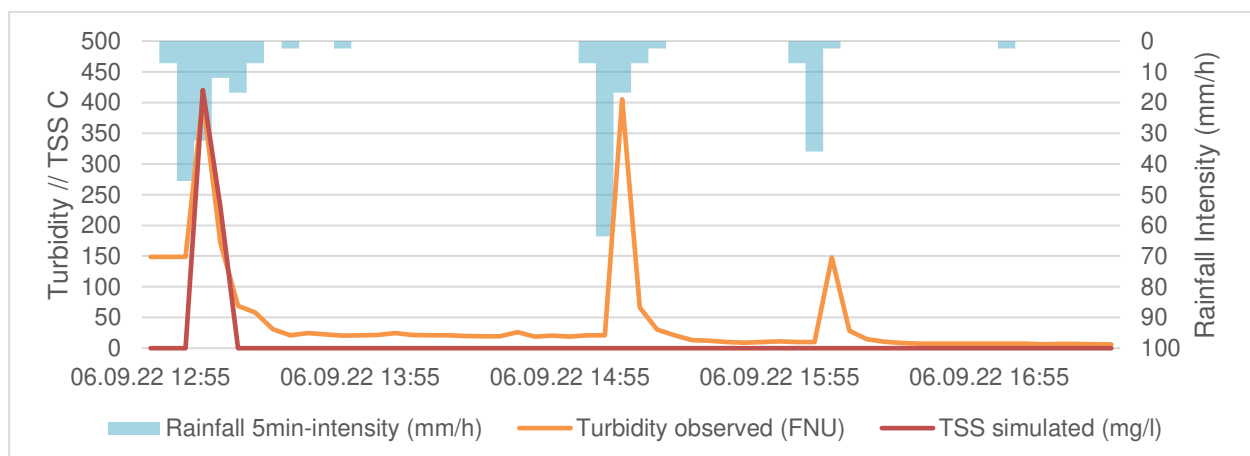


Figure 12: Comparison of observed and simulated pollutograph.

## 5.4 Sensitivity Analysis

### 5.4.1 Sensitivity Analysis of Hydrological Parameters

The sensitivity analysis revealed that a contribution of the pervious area to the surface runoff was not achieved within the first alteration step of the curve number (CN88) but within the second step (CN99.9). An alteration of the DS of the PSC additionally controls the runoff from the PSC. A lower DS would lead to a higher contribution of PSCs however a DS lower than 8 mm is not reasonable. A CN higher than 88 is also not plausible for the present catchment. Only stormwater events with a high total runoff volume contribute to the surface runoff with the initial parameters. Considering that this is only the case for 3 stormwater events a further focus on parameters of the PSC is not of specific interest for the calibration process. For this reason, the parameters Depression Storage and Manning coefficient are investigated within the calibration.

Table 12: Results of the sensitivity analysis of the hydrological input parameters.

Model Input Parameters		NSE Q		
uncalibrated Model		0.70		
Sensitivity Analysis		Step 1	Step 2	Difference
Impervious	Depression storage (mm)	0.71	0.69	0.02
	Manning coefficient	0.76	0.64	-0.12
Pervious	Curve number 88 // 99.9	0.70	0.65	-0.04
	Depression storage (mm)	0.65	0.67	-0.02
	Manning coefficient	0.66	0.66	0.00

### 5.4.2 Sensitivity Analysis of Water Quality Parameters

Table 13 and Figure 13 summarises the alteration of the input parameter values through step 1 and 2. Unsurprisingly the wash-off exponent varies extremely indicating that the model is very sensitive towards its alterations.

Table 13: NSE results of the sensitivity analysis of the water quality input parameters.

Model Input Parameters	NSE C (Correlated turbidity – TSS)			NSE PL (Correlated. turbidity – TSS)		
	-50	+50	Difference	-50	+50	Difference
uncalibrated Model	0.34			0.34		
Initial Build-up (kg/ha)	0.23	0.11	0.12	0.18	0.41	0.24
Wash-off Exponent	-0.14	-1189	1189	-0.04	-285	285
Wash-off Coefficient (h/mm <sup>2</sup> )	0.33	0.11	0.22	0.23	0.41	0.19

The ranges of the obtained NSE results are presented in Figure 13. Interestingly the alteration has different impacts depending on the evaluated variables TSS concentration and TSS load. A higher range was obtained for the  $K_w$  considering TCC C and a higher range of IB considering TSS PL. As explained in chapter 3.4.3 a wash-off exponent of 2 is broadly common for such wash-off simulations. Parameters the model is very sensitive to should be left out of calibration. For this reason, it was decided to not consider  $E_w$  for a calibration and to further investigate only IB and  $K_w$ .

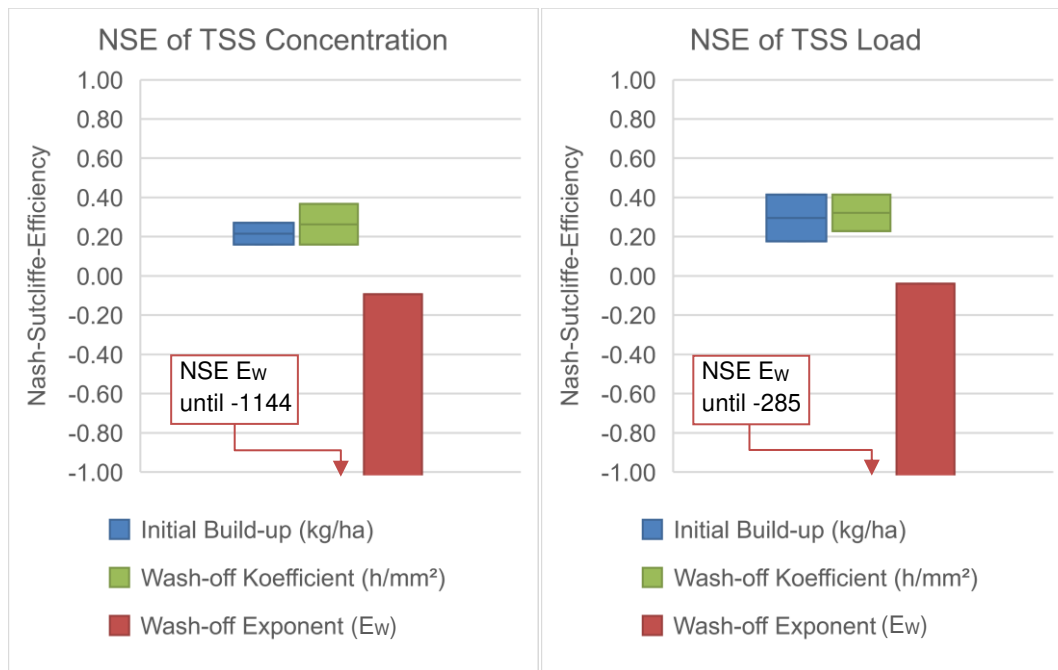


Figure 13: Range of Nash-Sutcliffe Efficiency regarding an alteration of parameter values.

## 5.5 Model Calibration

### 5.5.1 Hydrological Calibration

Calibration results for each event and each BFC were plotted in matrices with parameter combination and are added to the appendix 1.1 in Table 1 to Table 5. Figure 14 and Figure 15 present how the shape of the hydrograph changes within alternating one input parameter at a time while the other ones were fixed. Event RG\_04-12-9h was chosen for this demonstration, it gives a good overview of the hydrograph responses since the rainfall event has one clear peak. An alternation of DS in Figure 14 was conducted with a fixed  $n$  of 0,025. The peak discharge is reached earlier for higher initial losses with a delay of 5 minutes. A higher DS also leads to a reduced runoff volume and peak discharge. Additionally, the shape of the hydrograph changed with slopes of the graph. An alteration of  $n$  with a fixed DS of 0,5 produces a slight delay of the runoff by a small shift to the right. but no change of peak time (Figure 15). A higher  $n$  which represents a rougher surface flattens the hydrograph by transforming the peak into a plateau.

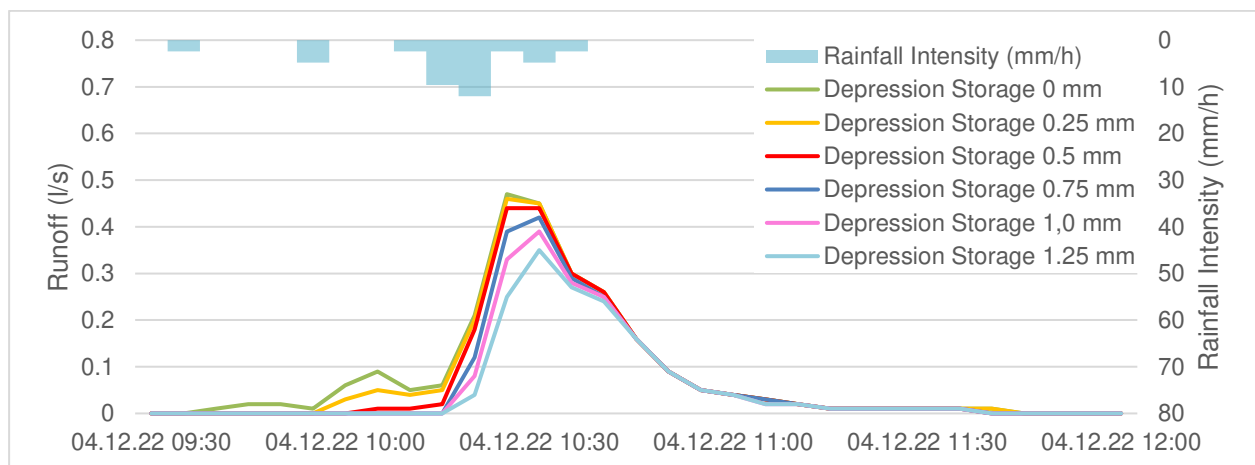


Figure 14: Hydrograph simulation with alterations of Depression Storage and fixed Manning Coefficient at 0.025.

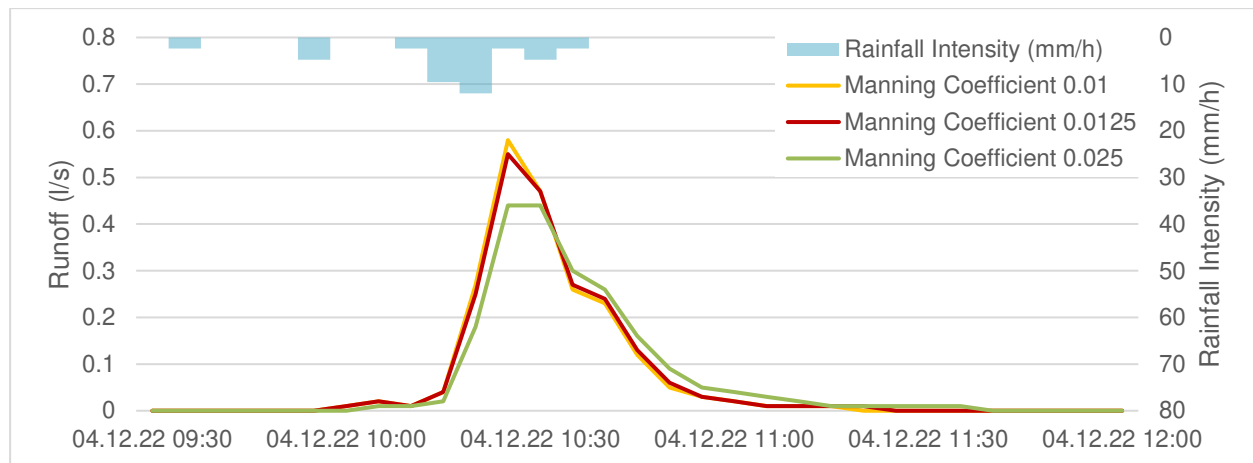


Figure 15: Hydrograph simulation with alterations of Manning coefficient and fixed Depression Storage at 0.5 mm.

Table 14 presents the calculated median values for every parameter combination in (DS x n)-matrices separately for every best fit criterion. These results were obtained by considering all 5 calibration events. BFC results in all cases vary from minus infinite to 1,0. The higher the obtained values, the better the result. The value, the closest to 1,0 is considered as best simulation. A colour spectrum of green- yellow- red indicates the performance ability of the parameter values, where a green background highlights the best obtained results, and a red background indicated the least favourable ones. The alteration of depression storage values DS (from 0 to 1,25, with an interval of 0,25) are plotted within the rows and Manning coefficient values n (0,01, 0,0125 and 0,025) are plotted vertically in the columns. Tendencies of the impact of parameter alterations on each BFC can be observed.

Table 14: Median values of each tested parameter combination calculated separately for all 4 best-fit criteria.

DS (horizontal)	n (vertical)	0	0.25	0.5	0.75	1	1.25
NSE Q							
	0.01	0.65	0.67	0.70	0.71	0.70	0.63
	0.0125	0.64	0.67	0.68	0.70	0.67	0.60
	0.025	0.61	0.62	0.62	0.60	0.55	0.54
KGE Q							
	0.01	0.40	0.42	0.54	0.65	0.69	0.69
	0.0125	0.55	0.43	0.54	0.66	0.68	0.67
	0.025	0.41	0.43	0.55	0.62	0.61	0.57
RPD Q <sub>max</sub>							
	0.01	0.72	0.72	0.72	0.72	0.72	0.72
	0.0125	0.71	0.71	0.71	0.70	0.70	0.70
	0.025	0.62	0.62	0.62	0.62	0.62	0.62
RPD V							
	0.01	0.50	0.56	0.57	0.57	0.58	0.58
	0.0125	0.50	0.57	0.57	0.57	0.58	0.58
	0.025	0.51	0.57	0.57	0.57	0.58	0.58

Each of the 4 criteria considers different variables (see chapter 3.4.7). For this reason, the results of NSE Q, KGE Q, RPD Q<sub>max</sub> and RPD V<sub>tot</sub> did not have the same tendency what parameter combinations are most favourable. From Table 14 can be concluded that the two analysed RPD

## Results and discussion

each depend on only one of the two investigated parameters. Considering  $Q_{\max}$ , the alteration of the depression storage had almost no influence in comparison to the Manning Coefficient, where a low  $n$  (on the top of the raster) lead to better results. On the contrary, considering RPD of  $V_{\text{tot}}$ ,  $n$  has a low influence on the model performance, while a DS alteration has a big impact on the results, indicated by higher values on the right side of the raster. In this case higher initial losses led to a better model performance, which implicates a reduction of  $V_{\text{tot}}$ . Comparing NSE  $Q$  and KGE  $Q$  the analysed variable  $Q$  is the same regarding the equations it is assessed differently, leading to a different tendency of parameter alterations. NSE  $Q$  takes peak accuracy stronger into account while KGE depends on 3 criteria. KGE  $Q$  depends stronger on the alteration of the depression storage while NSE  $Q$  is slightly more influenced by  $n$  alterations and rather influenced by both.

An emerging trend of general of global optima was noticed for a medium until high depression storage (in the middle to the right side of the raster) and a low Manning coefficient (on the top). A further statistical analysis was conducted by creating boxplots for every parameter combination. Figure 16 to Figure 18 allow to analyse outliers and deviations. Whiskers and quartiles do not indicate unconsidered dynamics, presenting rather robust results.



Figure 16: Boxplots which present the hydrological calibration results by combining all BFC efficiencies for different DS and a fixed  $n$  of 0.01.

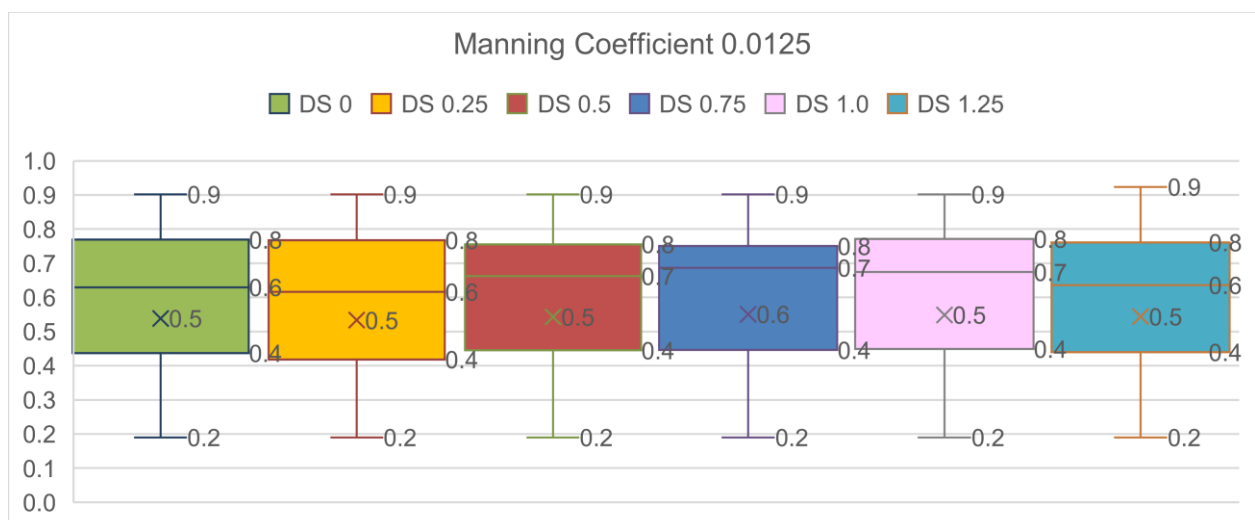


Figure 17: Boxplots which present the hydrological calibration results by combining all BFC efficiencies for different DS and a fixed  $n$  of 0.0125.

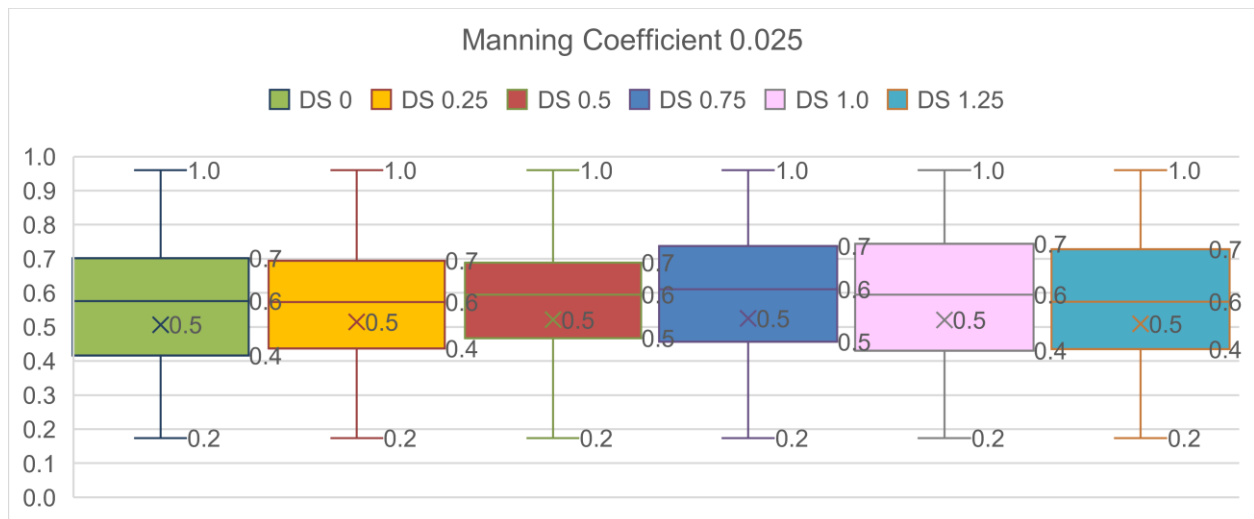


Figure 18: Boxplots which present the hydrological calibration results by combining all BFC efficiencies for different DS and a fixed n of 0.025.

Table 15: Median of all calculated events and all criteria combined for every parameter combination.

All BFC	n							
DS		0	0.25	0.5	0.75	1	1.25	
	0.01	0.61	0.62	0.67	<b>0.71</b>	0.70	0.66	
	0.0125	0.63	0.62	0.66	0.69	0.67	0.64	
	0.025	0.58	0.57	0.59	0.61	0.59	0.57	

Table 15 summarises the obtained median values combining all BFC and indicates the optimum result at 0,71 which was obtained by the parameter combination n= 0.01 and DS= 0,75 mm. Regarding every best-fit-criterion separately an improvement of 3 out of 4 BFC was obtained comparing the initial and the optimised parameter combination for the 5 calibration events (Table 16). Only the RPD  $Q_{max}$  was raised leading to a less accurate peak runoff.

Table 16: Comparison of median results of each best-fit criteria of uncalibrated and calibrated model

	Uncalibrated model DS=0.5; n=0.025	Calibrated model DS=0.75; n=0.01
NSE Q	0.65	0.71
KGE Q	0.54	0.65
RPD $Q_{max}$	0.59	0.72
RPD $V_{tot}$	0.31	0.57

Through the analysis of the BFC a combination of n = 0.01 and DS = 0.75 mm returns theoretically the most fitting outcome. An additional visual comparison between observed and simulated hydrographs was carried out.

Figure 19 and Figure 20 oppose the simulations with the initial model on the left side and the optimised model on the right side.

## Results and discussion

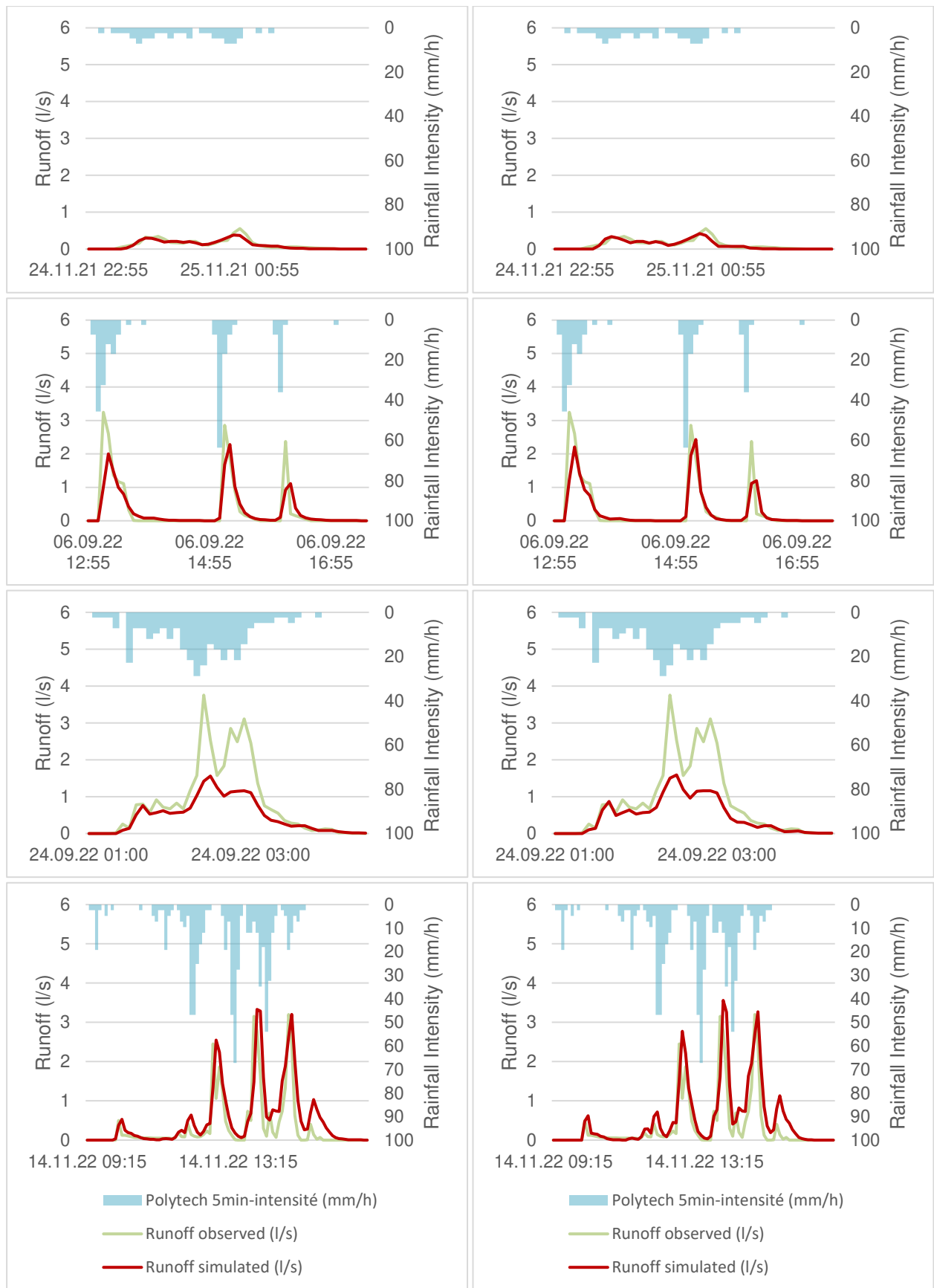


Figure 19: Comparison of the uncalibrated model on the left side and the hydrologically calibrated model on the right side with the events (from the top to the bottom): 1) RG\_24-11-23h, 2) RG\_6-9-12h, 3) RG\_24-09-1h and 4) RG\_14-11-9h.

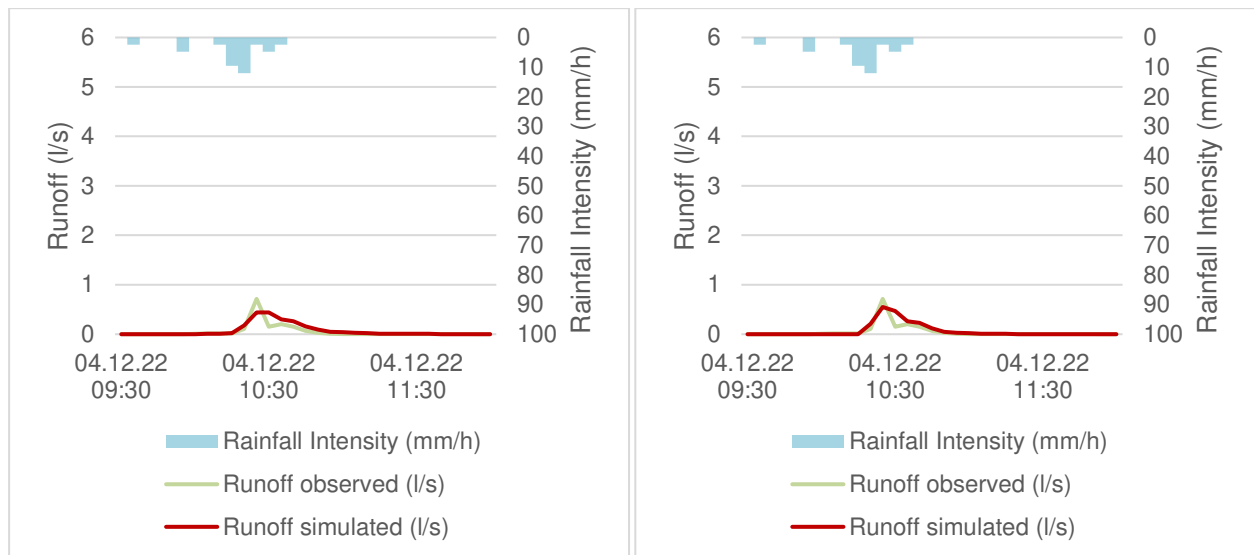


Figure 20: Comparison of the uncalibrated model on the left side and the hydrologically calibrated model on the right side with the event RG\_4-12-9h.

For all events the hydrographs of the calibrated model have higher peaks reducing the general underestimation of the runoff peaks within the uncalibrated model. Considering the event RG\_14-11-9h, the runoff peak was already well reproduced by the uncalibrated model. Therefore, the calibration led to lower BFC results since the calibration increased the peak even more.

### 5.5.2 Water Quality Calibration

Figure 21 and Figure 22 present different pollutograph responses when one parameter was modified while the other parameter was fixed at a medium value. The event RG-6-9-12h was chosen for this visualisation, since it has characteristic rainfall curves resulting in a clear response. Figure 21 presents pollutograph variations due to an alteration of IB and a fixed  $K_W$  of 0,001. The initial built-up has a direct impact on the magnitude of the response. The higher the IB the more pollution is washed-off resulting automatically in higher slopes of the graph.

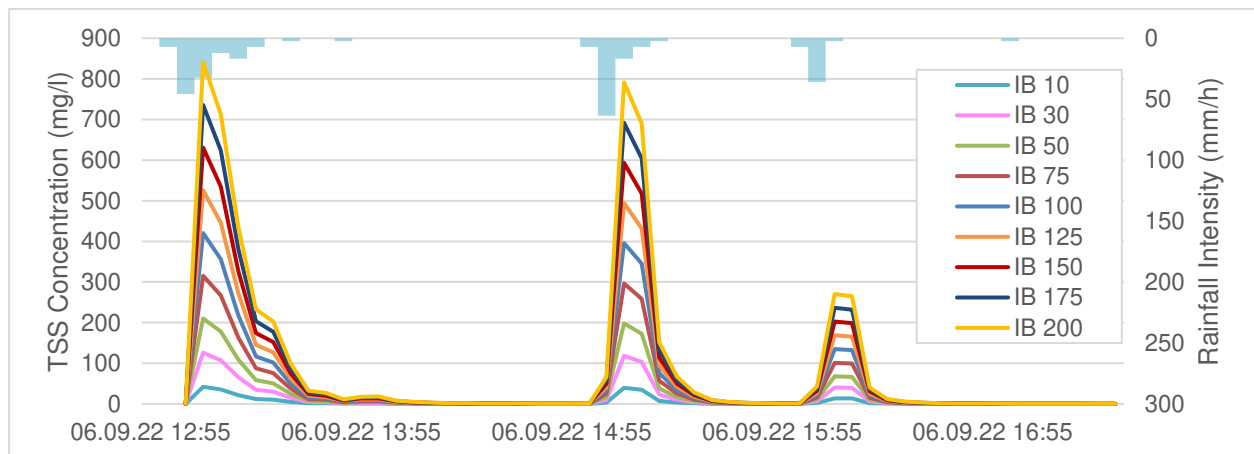


Figure 21: TSS Concentration for a Wash-off Coefficient of 0.001 and an alteration of the initial built-up between 10 and 200kg/ha.

Pollutographs with a variation of  $K_W$  and a fixed IB of 100 kg/ha are presented in Figure 22. A high wash-off coefficient ( $K_W$  of 0,01 and 0,005) produced a high peak at the start of the runoff. According to the course of  $K_W$  0,01 after the sharp peak at the beginning no more pollutants are available in the further phase of the event, as they have already been washed out at the beginning.

## Results and discussion

This behaviour was buffered with lower  $K_w$ , where values of 0,001, 0,0005 and 0,0001 reacted less to the first rainfall and within similar magnitudes as later runoff phases. A  $K_w$  of 0,0001 resulted in a very low response to the pollution runoff making the pollution less available to be washed-off.

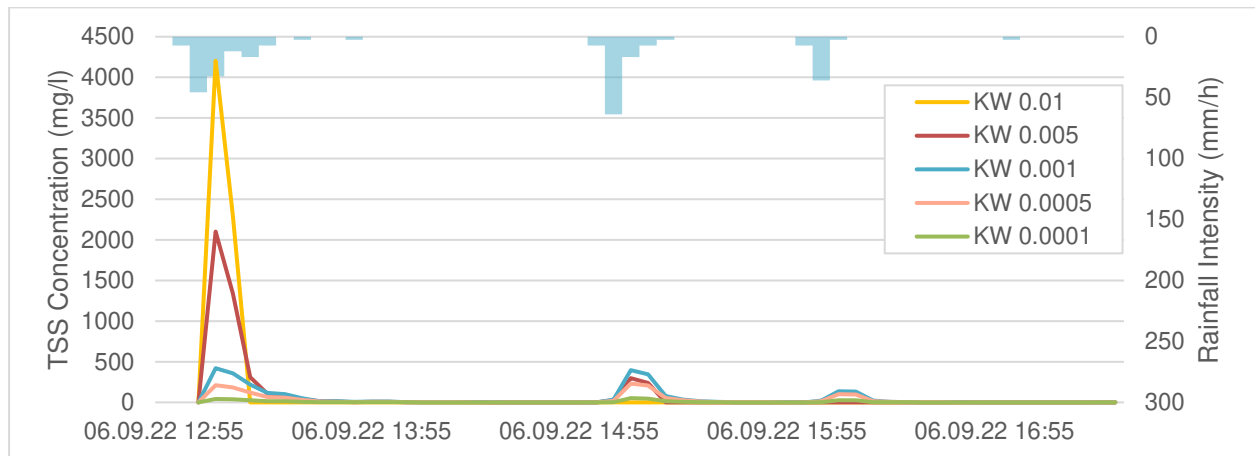


Figure 22: TSS Concentration for an initial built-up of 100 kg/ha and an alteration of the wash-off coefficient between 0.0001 and 0.01.

Results of the water quality calibration for each event and each BFC were plotted in matrices with parameter combination and are added to the appendix 1.2 in Table 6 to Table 10 in form of tables. Median BFC were calculated for all parameter combinations and all calibration events combines. The results are presented in Table 18. At the top on the left of each table it is indicated which BFC was tested. The alteration of initial built-up values (from 10 to 200 kg/ha) are plotted within rows and wash-off coefficient values are plotted vertically in columns. The same colour spectrum as already used for the hydrological calibration, with the highest values in green and the lowest in red, was applied.

## Results and discussion

Table 17: Median values of all parameter value combinations considering all 5 calibration events, tested for NSE-C, NSE-PL, KGE-C and KGE-PL.

NSE C	KW									
IB		10	30	50	75	100	125	150	175	200
NSE C	0.0001	-0.74	-0.69	-0.65	-0.56	-0.45	-0.43	-0.46	-0.41	-0.37
	0.0005	-0.65	-0.28	-0.28	-0.08	-0.08	-0.24	-0.50	-0.87	-1.35
	0.001	-0.50	-0.20	-0.01	-0.29	-0.93	-1.93	-3.28	-4.99	-7.05
	0.005	<b>0.07</b>	-0.38	-2.97	-9.22	-19	-32	-48	-68	-91
NSE PL										
IB		10	30	50	75	100	125	150	175	200
NSE PL	0.0001	-0.06	-0.03	0.00	0.04	-0.06	-0.14	-0.11	-0.07	-0.03
	0.0005	0.00	-0.11	0.04	0.18	0.32	0.44	0.51	0.50	0.46
	0.001	0.05	0.09	0.31	<b>0.52</b>	0.50	0.12	-0.46	-1.26	-2.26
	0.005	0.23	-0.39	-3.98	-12	-25	-42	-64	-89	-121
KGE C										
IB		10	30	50	75	100	125	150	175	200
KGE C	0.0001	-0.42	-0.37	-0.33	-0.27	-0.22	-0.17	-0.12	-0.07	-0.02
	0.0005	-0.33	-0.12	0.06	0.01	0.12	0.12	0.06	-0.10	-0.30
	0.001	-0.24	0.12	0.13	0.15	-0.12	-0.53	-1.00	-1.50	-2.01
	0.005	0.04	<b>0.28</b>	-0.79	-2.30	-3.84	-5.38	-6.93	-8.48	-10
KGE PL										
IB		10	30	50	75	100	125	150	175	200
KGE PL	0.0001	-0.41	-0.39	-0.36	-0.30	-0.24	-0.18	-0.20	-0.16	-0.12
	0.0005	-0.37	-0.13	-0.07	0.10	0.28	<b>0.44</b>	0.27	0.38	0.33
	0.001	-0.27	-0.05	0.20	0.37	0.33	-0.15	-0.64	-1.14	-1.64
	0.005	0.10	0.32	-0.83	-2.40	-3.98	-5.57	-7.16	-8.75	-10

As observed within the hydrological calibration, for every tested criterion a different parameter set was most favourable. However, a general tendency of optimal parameter combinations, which was consistent for all 4 BFC was noted: A high wash-off coefficient demands a low initial built-up value. The more the wash-off coefficient was reduced the higher was the demanded initial-built-up to counterbalance the amount of the released pollutants. Although NSE C and KGE C assess both the simulated concentration, the table indicates different parameter sets as most appropriate. The same dynamic was observed for NSE PL and KGE PL. NSE results are smaller than KGE results, since NSE considers more the peak accuracy. Higher PL results in comparison to C can be explained with the implication of Q which was calibrated before and proved to well replicate the observations. Considering the concentration criteria NSE C and KGE C, Table 17 shows the tendency that higher BFC values were obtained for low IB values, whereas for the PL criteria medium IB values were favourable.

Boxplots in Figure 23 give an overview of the magnitude of the variation of the BFC results for all parameter sets. Each boxplot presents all tested IB values for a specific fixed  $K_w$  value. Unsurprisingly in all cases small IB and  $K_w$  values led to lower magnitude ranges. The comparison of all median values suggests a maximum median value of 0,25 for the parameter combination IB=75 and  $K_w=0,001$ . The same parameter set was obtained when only considering NSE-PL as indicated in the 2<sup>nd</sup> section of Table 17.

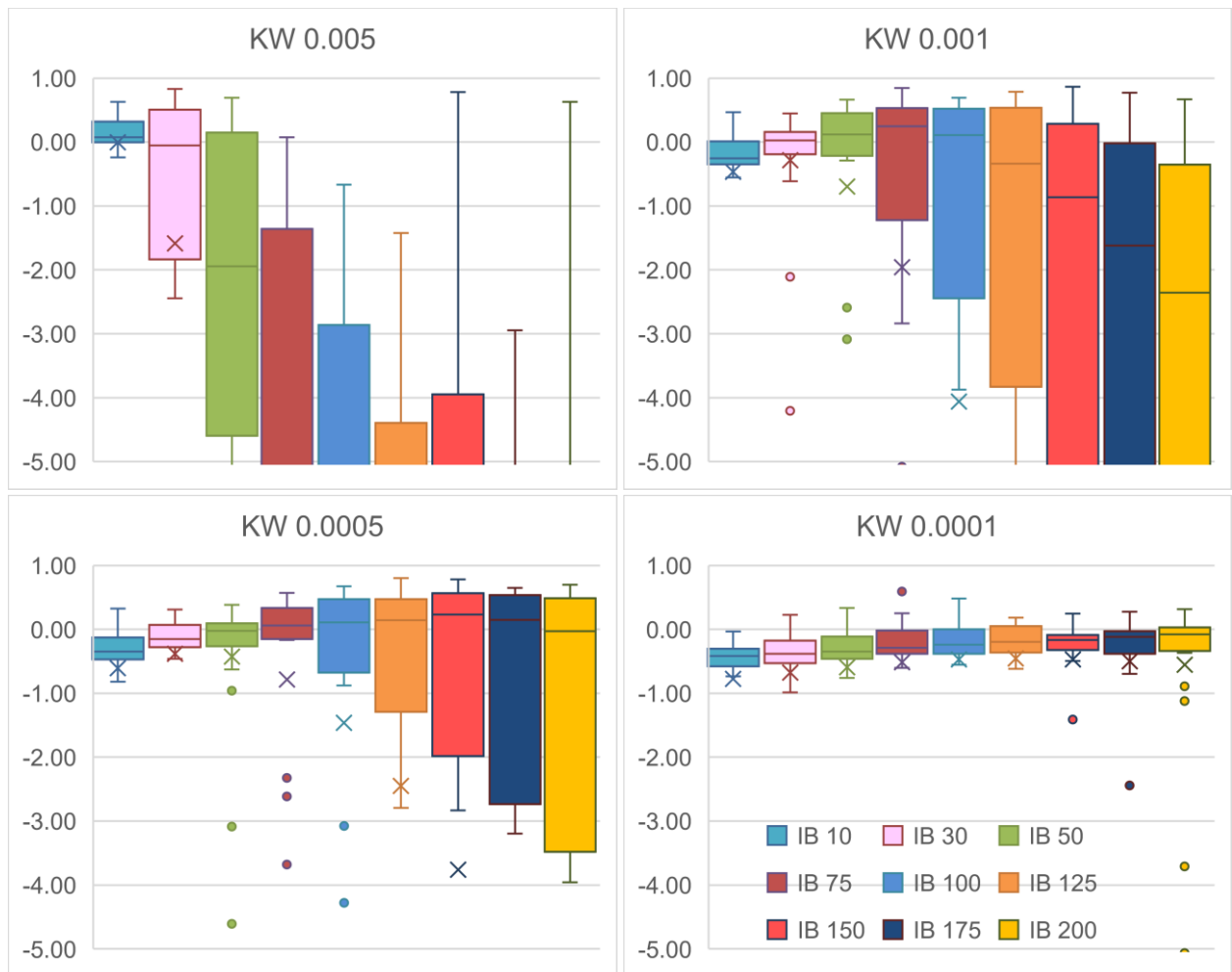


Figure 23: All BFC results presented with boxplots with all parameter value combinations.

Table 18: Median of all calculated events and all criteria combined for every parameter combination.

Median	KW	10	30	50	75	100	125	150	175	200
IB	0.0001	-0.42	-0.38	-0.35	-0.29	-0.23	-0.20	-0.17	-0.12	-0.08
	0.0005	-0.35	-0.15	-0.02	0.06	0.11	0.15	0.23	0.15	-0.03
	0.001	-0.26	0.02	0.12	<u>0.25</u>	0.11	-0.34	-0.86	-1.62	-2.35
	0.005	0.07	-0.05	-1.95	-5.30	-9.44	-14	-17	-22	-24

Table 18 summarises all computed median values for a better overview than as presented in Figure 23. In addition to analysing the median of all BFC of every parameter set also mean values were evaluated (Table 19). The parameter combination with the lowest  $K_W=0.005$  and the lowest  $IB=10$  resulted in the highest performance capacity. Since the mean value is very susceptible to statistical outliers and therefore the values were strongly evened out, parameter sets which show very low reactions suggested with this method. The median is considered as more robust and therefore more reliable for calibration since it is less affected by statistical irregularities.

## Results and discussion

Table 19: Mean difference of the combination of all best-fit criteria.

Mean	KW									
IB		10	30	50	75	100	125	150	175	200
	0.0001	-0.71	-0.62	-0.53	-0.45	-0.41	-0.40	-0.41	-0.44	-0.50
	0.0005	-0.55	-0.32	-0.37	-0.73	-1.40	-2.39	-3.70	-5.33	-7.26
	0.001	-0.41	-0.22	-0.64	-1.90	-4.00	-6.88	-10	-15	-20
	0.005	<b>0.05</b>	-1.53	-6.66	-18	-33	-54	-76	-110	-140

To find a parameter combination which is able to generally improve the model performance regarding water quality, the robustness of the combined median was assessed by considering the variables C and PL apart, see Table 20 Table 21.

Table 20: Median result considering only the variable concentration by coupling NSE-C and KGE-C.

only C considered	KW									
IB		10	30	50	75	100	125	150	175	200
	0.0001	-0.48	-0.41	-0.38	-0.34	-0.30	-0.27	-0.24	-0.21	-0.18
	0.0005	-0.38	-0.24	-0.12	-0.05	0.06	<b>0.11</b>	-0.03	-0.24	-0.49
	0.001	-0.31	-0.06	0.05	0.02	-0.40	-0.92	-1.48	-2.17	-3.15
	0.005	0.05	-0.05	-2.16	-6.57	-11	-15	-18	-29	-24

Table 21: Median result considering only the variable pollutant load by coupling NSE-PL and KGE-PL.

only PL considered	KW									
IB		10	30	50	75	100	125	150	175	200
	0.0001	-0.36	-0.32	-0.29	-0.25	-0.20	-0.18	-0.14	-0.08	-0.03
	0.0005	-0.29	-0.13	0.03	0.15	0.30	0.44	0.39	<b>0.44</b>	0.39
	0.001	-0.20	0.08	0.26	0.43	0.41	-0.01	-0.55	-1.20	-1.95
	0.005	0.16	-0.03	-1.69	-3.70	-6.08	-9.69	-14	-19	-23

This separation shows again different outcomes of a most favourable parameter set. When only considering the BFC analysing C, the best parameter set was  $K_W = 0.0005$ ,  $IB = 125$ ; a consideration of only PL analysing criteria indicated the parameter set  $K_W = 0.0005$ ,  $IB = 175$  as best fitting. Since the outcomes vary a lot depending on the considered best-fit and statistical criteria, the decision was taken to not only choose one best fitting parameter set to carry out a verification but 4 sets. These are for further simulations defined as the following:

- set 1 ( $IB = 75$  kg/ha,  $K_W = 0.001$ ): the parameter set which obtained the highest median of all BFC (Table 18),
- set 2 ( $IB = 10$  kg/ha,  $K_W = 0.005$ ): the parameter set which obtained the highest mean of all BFC (Table 19),
- set 3 ( $IB = 125$  kg/ha,  $K_W = 0.0005$ ): the parameter set which obtained the highest median with BCF considering only the concentration C (Table 20),
- set 4 ( $IB = 175$  kg/ha,  $K_W = 0.0005$ ): the parameter set which obtained the highest median with BCF considering only the pollution load PL (Table 21).

To not focus on one general parameter set allows to compare different analysis approaches. Table 22 opposes the results of the 4 BFC of the initial model and the ones of the parameter sets 1-4. In the box on the left side the median of all events was used to combine the results. This was necessary for the parameter sets 1, 3 and 4 since the led to the best parameter combinations considering the median. Assessing NSE-C and KGE-C all parameter sets led to lower median results than the initial model. Considering the median values of NSE-PL and KGE-PL, the values

## Results and discussion

obtained within the parameter sets 1, 3 and 4 were higher than the initial ones. The box on the right side opposes mean values of the initial model and the results of set 2. Comparing them reveals an improvement of NSE-C, NSE-PL and KGE-C, while the KGE-PL was decreased through the calibration.

Table 22: Comparison of the median and the mean best-fit criteria results of the initial and the best parameter sets.

Statistical variable Parameter combination	Set 1		Set 3	Set 4	Set 2	
	Before calibration median of all BFC	Highest median of all BFC	Highest median of BFC only considering C	Highest median of BFC only considering PL	Before wq- calibration mean of all BFC	Highest mean of all BFC
	Median				Mean	
	IB=10 kg/ha, KW=0.01	IB=75 kg/ha, KW=0.001	IB=125 kg/ha, KW=0.0005	IB=175 kg/ha, KW=0.0005	IB=10 kg/ha, KW=0.01	IB=10 kg/ha, KW=0.005
NSE C	0.09	-0.29	-0.24	-0.87	-0.68	-0.54
NSE PL	0.34	0.52	0.44	0.50	0.14	0.19
KGE C	0.23	0.15	0.12	-0.10	0.07	0.14
KGE PL	0.21	0.37	0.44	0.38	0.24	0.19

Comparing Table 16 and Table 22 it can generally be concluded that the performance ability of the water quality simulations was inferior to the one of the hydrological simulations. Considering NSE and KGE the highest values for the hydrological simulations were 0.71 for NSEQ and 0.69 for KGE Q, whereas 0.09, 0.53, 0.28 and 0.44 were obtained for the water quality simulations for NSE C, NSE PL, KGE C and KGE PL respectively. This means that the hydrological performance results in higher values and therefore stands for a better reproduction of the observed values. It must be noted that the range of all obtained median values is very high, meaning that the difference between the lowest and highest results of each BFC is 91, 121, 10 and 10 (respectively for NSEC, NSE PL, KGE C and KGE PL). In contrast the difference for the BFC obtained for the hydrological calibration is 0.17 for NSE Q and 0.29 for KGE Q. This finding is due to the chosen alteration magnitude of the different calibration parameters however, it points out the high sensitivity of the model regarding the water quality parameters.

As already done for the hydrological calibration it is important to graphically assess the outcome of the calibration. A comparison of pollutographs computed with the initial model and with the calibration parameter set 1 is visualised in Figure 24 to Figure 28. Each figure is composed of 4 graphics of one event. The graphics on the top present the results with initial model, and the ones on the bottom with the calibrated values. The graphics on the left side compare concentrations and on the right side pollution loads.

## Results and discussion

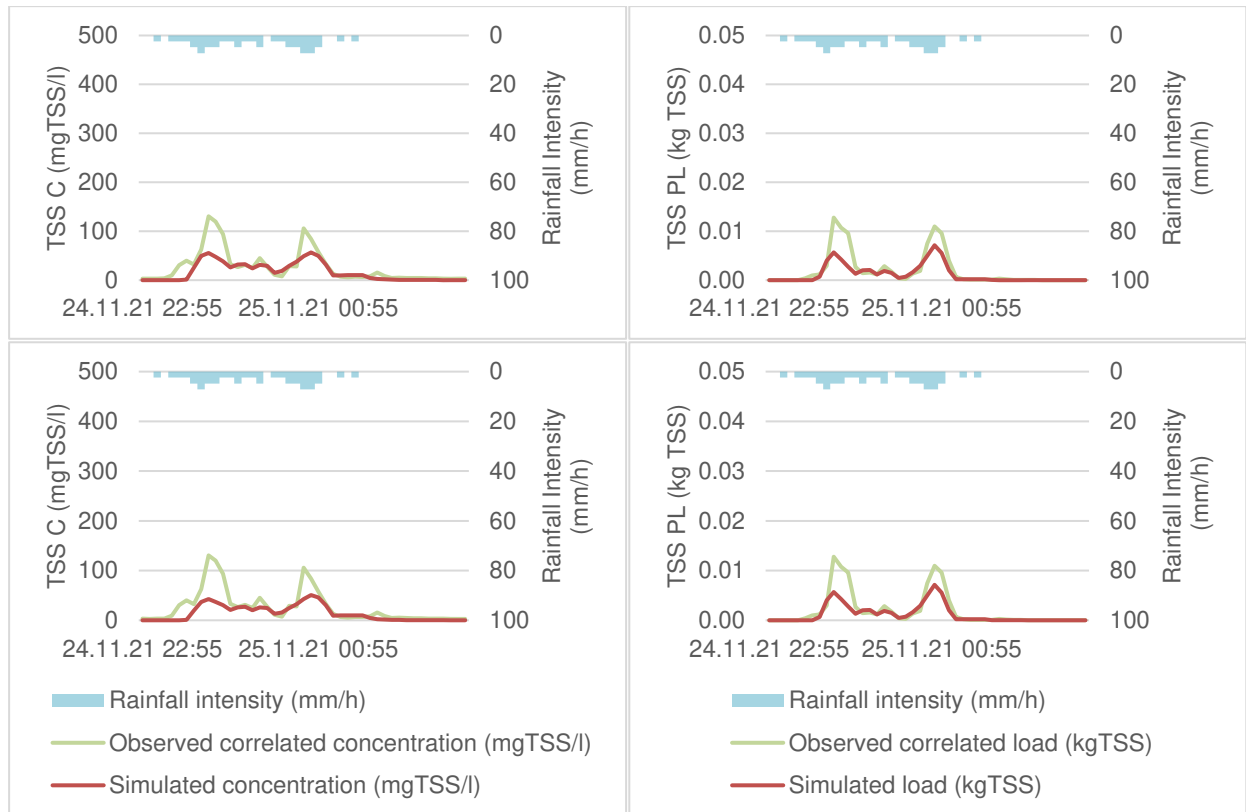


Figure 24: Event RG\_24-11-23h simulated with the initial model (on top) and the calibrated model (on the bottom) presented with pollutographs of the concentration (left) and of the pollution load (right).

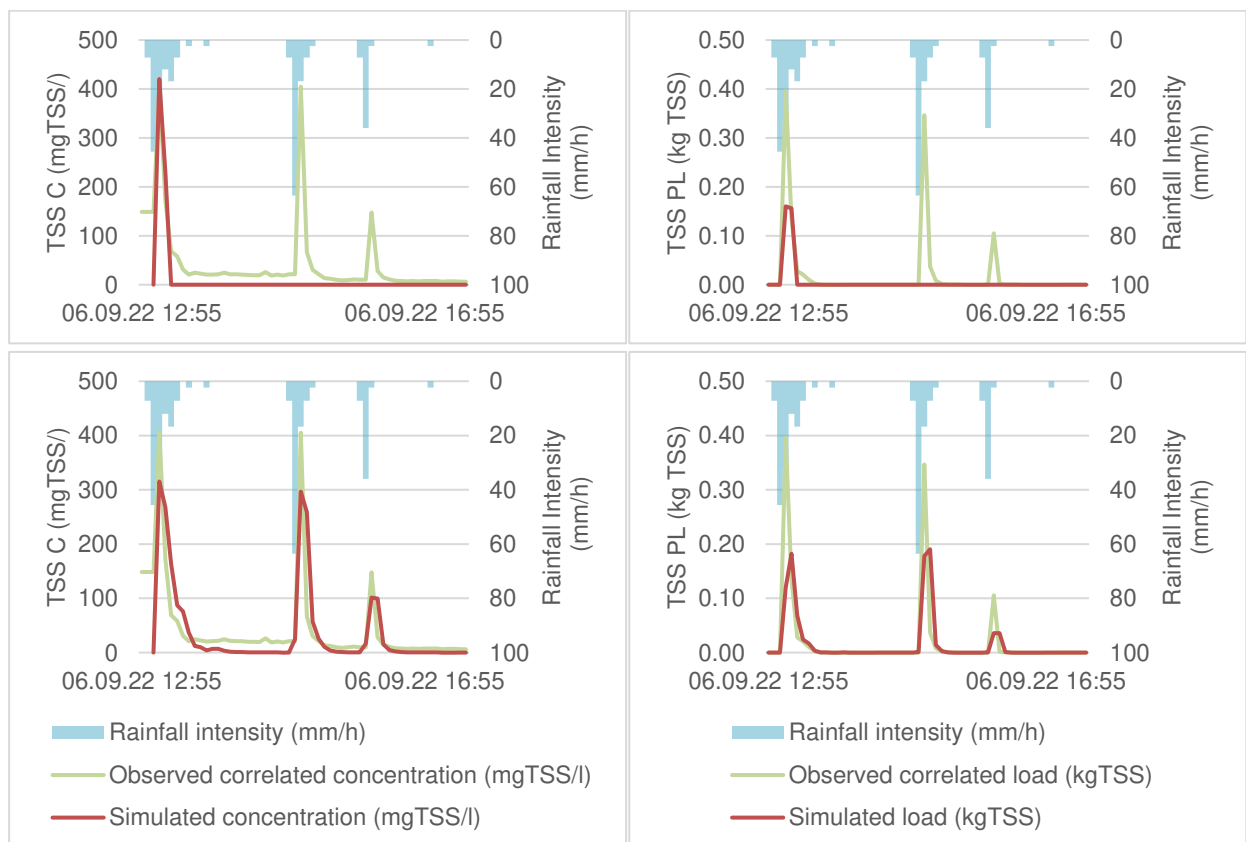


Figure 25: Event RG\_6-9-12h simulated with the initial model (on top) and the calibrated model (on the bottom) presented with pollutographs of the concentration (left) and of the pollution load (right).

## Results and discussion

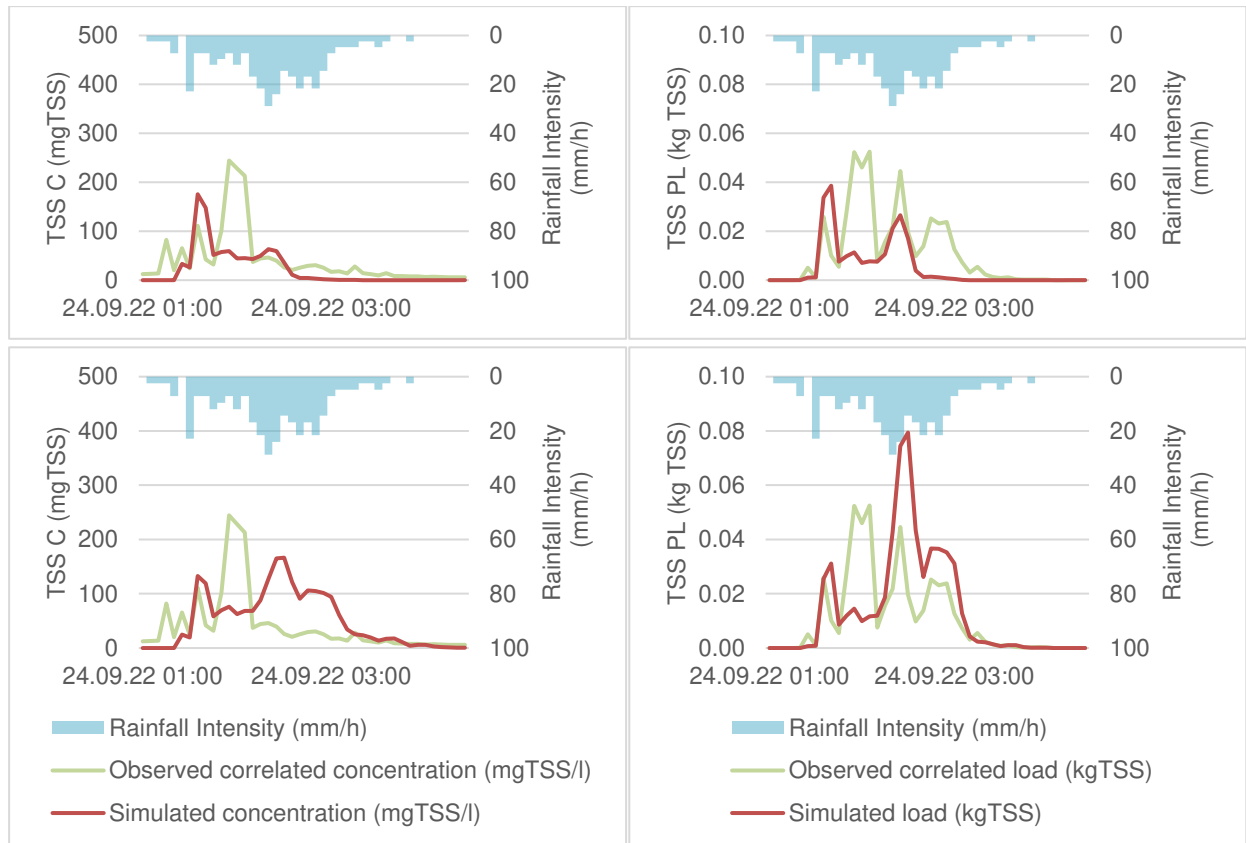


Figure 26: Event RG\_24-9-1h simulated with the initial model (on top) and the calibrated model (on the bottom) presented with pollutographs of the concentration (left) and of the pollution load (right).

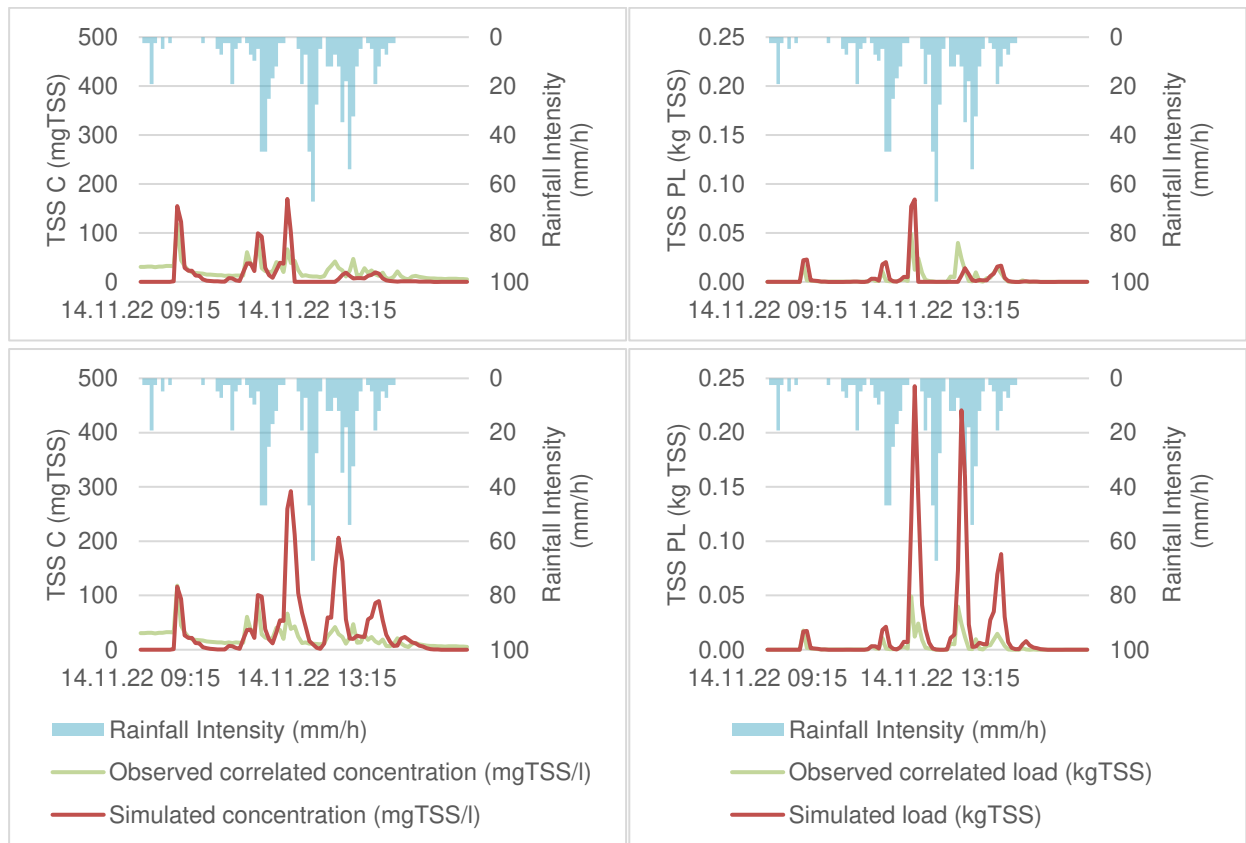


Figure 27: Event RG\_14-11-10h simulated with the initial model (on top) and the calibrated model (on the bottom) presented with pollutographs of the concentration (left) and of the pollution load (right).

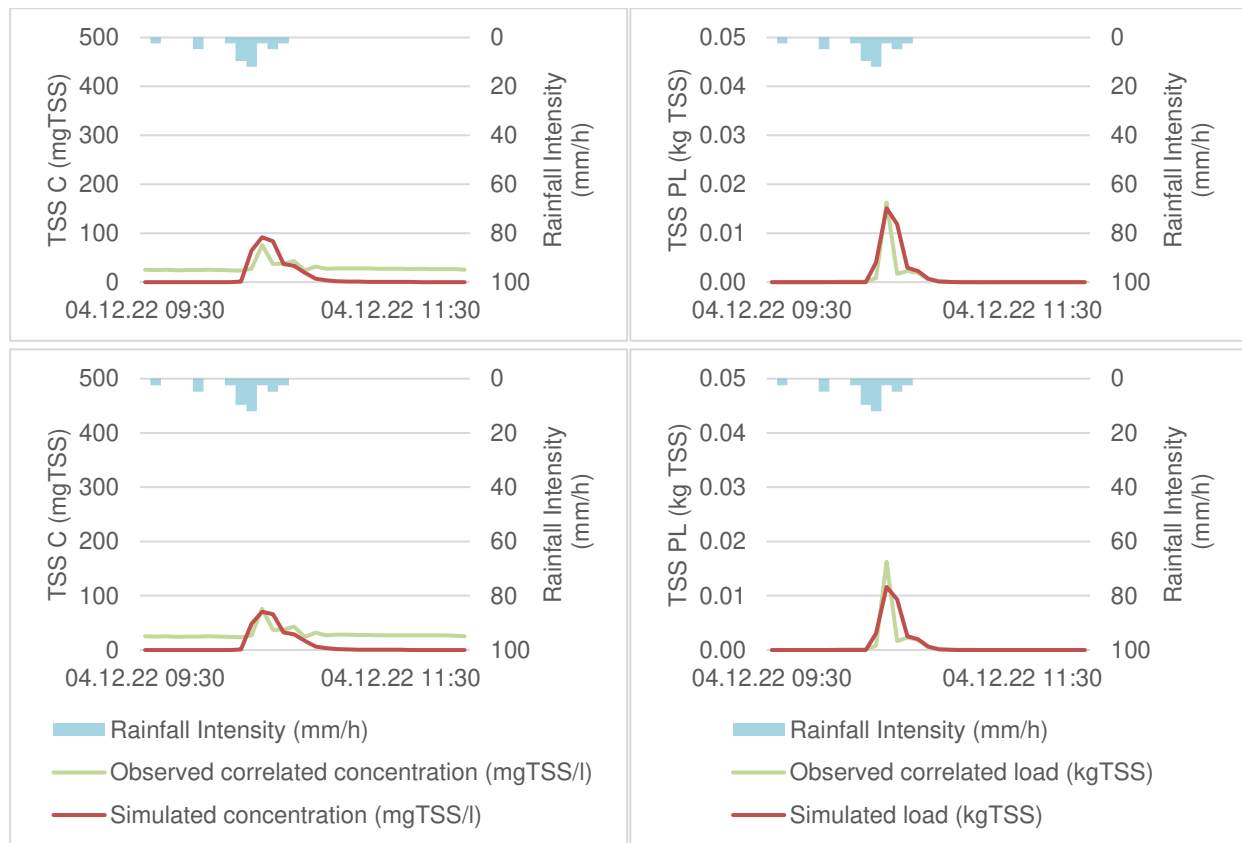


Figure 28: Event RG\_4-12-10h simulated with the initial model (on top) and the calibrated model (on the bottom) presented with pollutographs of the concentration (left) and of the pollution load (right).

By analysing Figure 24 to Figure 28 the effect of the calibration was assessed for every event separately. The only event where the calibration seemed to have a positive impact on the simulated pollutographs was RG\_6-9-12h where the observations were well reproduced with the calibrated model. For all other events C and PL values were overestimated and underestimated. However, simulating the correct magnitude of washed-off pollution is not of main interest in this work, since the correlation between turbidity and TSS concentration is missing.

### 5.5.3 Verification of the Hydrological Calibration

Results of NSE as well as KGE of the discharge of the initial and the calibrated model are presented in Table 23. On the bottom of the table median values of all rainfall events serve to globally represent the model correlation with the observed data. A positive difference between the median values suggests a general improvement of the model through the calibration process. With a difference of 0,01 (for NSE) and 0,04 (for KGE) of the medians, a slight improvement was obtained. Reviewing the model improvement for every event separately, a total of 8 and 13 out of 17 events led to higher NSE-Q and KGE-Q values respectively. The scatterplots in Figure 29 confirm the general improvement of the model through the hydrological calibration. The obtained NSE and KGE values are mostly located above the identity function.

## Results and discussion

Table 23: Comparison of NSE and KGE results of the uncalibrated (left) and the calibrated (right) model.

Events	initial model		calibrated model	
	NSE Q	KGE Q	NSE Q	KGE Q
RG_24-11-4h	0.01	0.18	-0.03	0.19
RG_24-11-13h	0.90	0.85	0.86	0.82
RG_24-11-22h	0.86	0.81	0.81	0.82
RG_11-3-17h	0.11	0.20	0.24	0.29
RG_13-3-9h	0.51	0.50	0.51	0.51
RG_20-3-16h	-0.33	-0.05	-0.36	-0.08
RG_20-4-14h	-17.40	-4.07	-22.96	-4.61
RG_24-6-8h	0.34	0.27	0.41	0.34
RG_6-9-all	0.70	0.63	0.77	0.70
RG_7-9-2h	0.61	0.47	0.67	0.58
RG_7-9-22h	0.59	0.59	0.66	0.64
RG_14-9-4h	0.22	0.28	0.21	0.35
RG_24-9-1h	0.52	0.31	0.53	0.32
RG_14-11-9h	0.64	0.78	0.56	0.71
RG_28-11-7h	0.28	0.34	0.29	0.41
RG_4-12-9h	0.62	0.55	0.71	0.65
RG_15-12-4h	0.80	0.66	0.78	0.69
median of best-fit-values	0.52	0.47	0.53	0.51
difference to original model			0.01	0.04

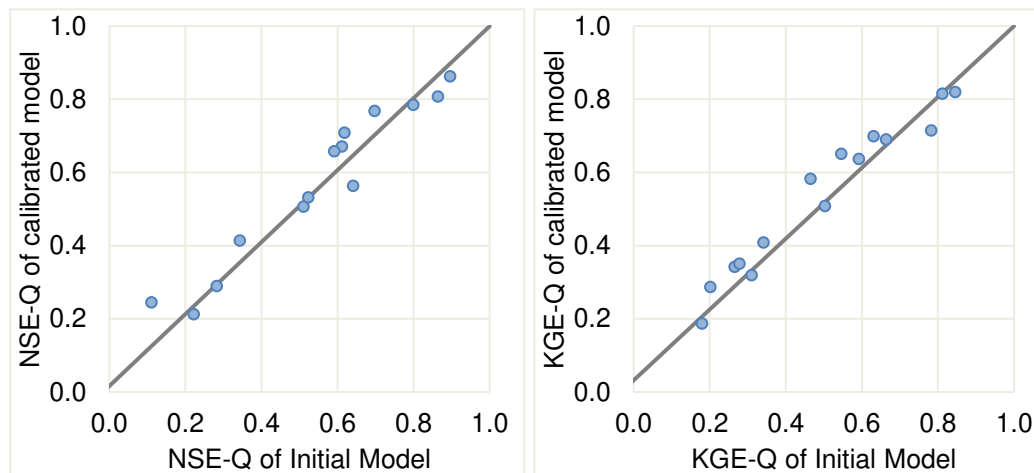


Figure 29: NSE-Q results (left side) and KGE-Q results (right side) of the initial model (horizontal axis) and the calibrated model (vertical axis).

### 5.5.4 Verification of Water Quality Calibration

To verify the water quality calibration the 4 previously defined parameter sets were tested. This was necessary since the tested parameters turned out to be very sensitive to their alteration and an the considered BFC. For this reason, the best fitting parameter combination depends on the best-fit and statistical criteria, which were chosen for the analysis of calibration. Table 24 and Table 25 summarise the tested BFC results of the initial model and the 4 parameter sets for all events.

## Results and discussion

Table 24: Comparison of NSE and KGE results of the uncalibrated model (on the left side) and the parameter sets 1 and 2 from calibrated model (on the right side).

Events	initial model				Set 1 median of all criteria (0.001; 75)				Set 2 mean of all criteria (0.005; 10)			
	NSE C	NSE PL	KGE C	KGE PL	NSE C	NSE PL	KGE C	KGE PL	NSE C	NSE PL	KGE C	KGE PL
RG_24-11-4h	-2.43	-1.05	-0.17	-0.18	-2.65	-1.14	-0.20	-0.22	-3.11	-1.34	-0.30	-0.30
RG_24-11-13h	0.07	0.27	-0.08	0.06	0.01	0.23	-0.15	0.02	-0.12	0.08	-0.27	-0.15
RG_24-11-22h	0.49	0.59	0.32	0.32	0.38	0.54	0.23	0.26	0.07	0.29	-0.01	0.01
RG_11-3-17h	0.24	0.23	0.19	0.08	0.22	0.43	0.20	0.30	0.07	0.36	0.06	0.25
RG_13-3-9h	-0.61	0.75	-0.03	0.64	-2.86	0.03	-1.18	-0.47	0.60	0.81	0.71	0.66
RG_20-3-16h	-0.81	-5.86	-0.24	-2.94	-0.50	-4.72	-0.14	-2.57	-0.28	-1.27	-0.26	-0.79
RG_20-4-14h	0.31	0.28	-0.06	0.13	0.29	-0.08	-0.06	-0.15	0.29	-0.08	-0.06	-0.15
RG_24-6-8h	0.59	0.14	0.34	-0.18	0.54	0.17	0.32	-0.15	0.38	0.09	0.06	-0.25
RG_6-9-all	0.35	0.23	0.12	-0.14	0.71	0.52	0.84	0.49	0.33	0.23	0.01	-0.14
RG_7-9-2h	-0.66	-0.27	0.26	-0.44	-10	-1.03	-1.71	0.04	0.01	-0.30	0.44	-0.52
RG_7-9-22h	-64	-22	-7.35	-4.99	-149	-105	-12	-13	-17	-6.44	-3.29	-2.23
RG_14-9-4h	-0.12	-0.60	0.20	0.18	-0.17	-0.63	0.20	0.26	-0.38	-0.07	-0.02	0.29
RG_24-9-1h	0.22	0.11	0.28	0.18	-0.29	-0.42	0.15	0.37	0.08	0.06	0.04	0.10
RG_14-11-9h	-0.63	-0.70	0.19	0.29	-8.40	-26	-1.49	-5.08	-0.03	-0.24	0.42	0.46
RG_28-11-7h	-113	-1.60	-1.01	0.04	-127	-1.73	-1.20	0.07	-149	-2.19	-0.67	-0.10
RG_4-12-9h	-2.40	0.57	-0.20	0.62	-2.84	0.67	-0.12	0.72	-3.16	0.63	0.22	0.51
RG_15-12-4h	-0.94	0.22	-0.11	0.10	-0.87	0.28	-0.02	0.25	-1.32	0.10	-0.26	-0.07
median of best-fit-values difference to original model	-0.61	0.14	-0.03	0.08	-0.50	-0.08	-0.12	0.04	-0.03	0.06	-0.01	-0.10
					0.10	-0.22	-0.09	-0.04	0.48	0.13	0.11	-0.14

Table 25: Comparison of NSE and KGE results of the uncalibrated model (on the left side) and the parameter sets 3 and 4 from calibrated model (on the right side).

Events	initial model				Set 3 median of criteria considering C (0.0005; 125)				Set 4 median of criteria considering PL (0.0005; 175)			
	NSE C	NSE PL	KGE C	KGE PL	NSE C	NSE PL	KGE C	KGE PL	NSE C	NSE PL	KGE C	KGE PL
RG_24-11-4h	-2.43	-1.05	-0.17	-0.18	-2.86	-1.23	-0.25	-0.26	-2.44	-1.04	-0.14	-0.18
RG_24-11-13h	0.07	0.27	-0.08	0.06	-0.04	0.17	-0.20	-0.05	0.06	0.29	-0.09	0.10
RG_24-11-22h	0.49	0.59	0.32	0.32	0.25	0.44	0.12	0.16	0.48	0.63	0.34	0.38
RG_11-3-17h	0.24	0.23	0.19	0.08	0.14	0.35	0.11	0.21	0.25	0.51	0.28	0.44
RG_13-3-9h	-0.61	0.75	-0.03	0.64	-1.63	0.35	-0.76	-0.15	-6.13	-1.09	-2.03	-1.17
RG_20-3-16h	-0.81	-5.86	-0.24	-2.94	-0.49	-3.10	-0.23	-1.75	-1.01	-7.17	-0.32	-3.29
RG_20-4-14h	0.31	0.28	-0.06	0.13	0.23	0.43	-0.12	0.27	0.36	-0.81	0.00	-0.58
RG_24-6-8h	0.59	0.14	0.34	-0.18	0.47	0.13	0.21	-0.20	0.60	0.20	0.45	-0.10
RG_6-9-all	0.35	0.23	0.12	-0.14	0.69	0.49	0.80	0.44	0.48	0.50	0.56	0.65
RG_7-9-2h	-0.66	-0.27	0.26	-0.44	-14	-2.73	-2.31	-0.62	-32	-6.48	-4.14	-1.68
RG_7-9-22h	-64	-22	-7.35	-4.99	-137	-100	-12	-13	-282	-204	-18	-19
RG_14-9-4h	-0.12	-0.60	0.20	0.18	-0.24	-0.30	0.10	0.34	-0.16	-1.09	0.28	0.08
RG_24-9-1h	0.22	0.11	0.28	0.18	-0.24	-0.26	0.13	0.44	-0.87	-1.41	-0.10	-0.04

## Results and discussion

RG_14-11-9h	-0.63	-0.70	0.19	0.29	-9.90	-34	-1.63	-5.94	-23	-71	-3.17	-9.28
RG_28-11-7h	-113	-1.60	-1.01	0.04	-137	-1.93	-0.90	-0.01	-117	-1.56	-1.55	0.13
RG_4-12-9h	-2.40	0.57	-0.20	0.62	-2.79	0.68	0.09	0.70	-3.20	0.61	-0.39	0.55
RG_15-12-4h	-0.94	0.22	-0.11	0.10	-0.97	0.27	-0.09	0.15	-0.75	0.25	0.07	0.36
median of best-fit-values	-0.61	0.14	-0.03	0.08	-0.49	0.13	-0.12	-0.01	-0.87	-1.04	-0.10	-0.04
difference to original model					0.11	-0.01	-0.09	-0.09	-0.27	-1.18	-0.07	-0.12

Unlike the hydrological calibration, a general improvement was not registered for the water quality calibration. In Table 24 and Table 25 the median of all events calculated for each BFC did not generally increase for the 4 tested parameter sets in comparison to the initial model. The parameter set 2 led to an improvement of NSE-C, NSE-PL and KGE-C. The parameter sets 1 and 3 led to an improvement only of the NSE-C, while a decrease of all BFC was registered for set 4. Comparing the BFC results of each event, an improvement was registered only in some cases. The number of improved events, obtained by comparing the BFC results of the parameter sets 1-4 to the initial model, is presented in Table 26. Since in total 17 events were analysed the presented numbers in Table 26 do not indicate an absolute improvement for none of the 4 sets. Considering only BFC which analyse the pollution load (NSE-PL and KGE-PL) higher numbers were achieved. This is not a surprising outcome since the analysed pollution load is a function of the runoff for which a model improvement was already registered within the hydrological verification.

Table 26: Number of improved events considering each tested BFC separately.

	NSE C	NSE PL	KGE C	KGE PL
Set 1	3	6	7	10
Set 2	2	7	5	8
Set 3	5	9	8	8
Set 4	5	7	7	6

The following Figure 30 to Figure 33 oppose the BFC results obtained with the initial parameter set and with each of the 4 calibration sets with scatterplots. The same conclusion can be drawn. With no parameter set a general improvement was registered. Only set 4 (Figure 33) returns a higher number of events surpassing the identity function.

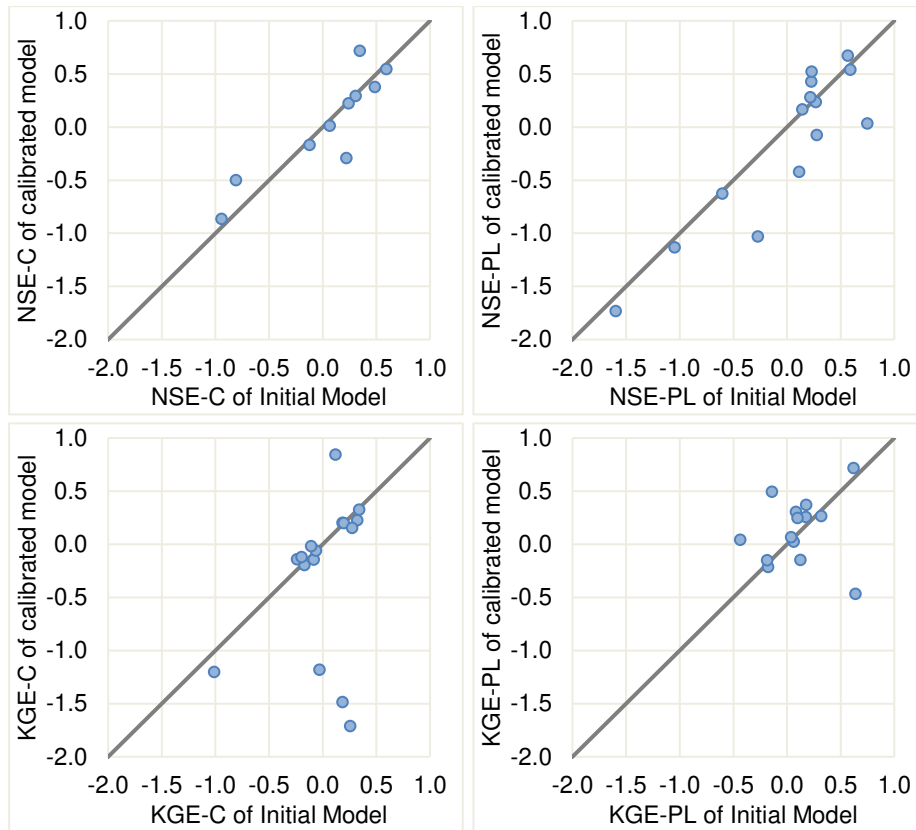


Figure 30: Scatterplots comparing BFC results of the initial model and the model with set 1 as input values.

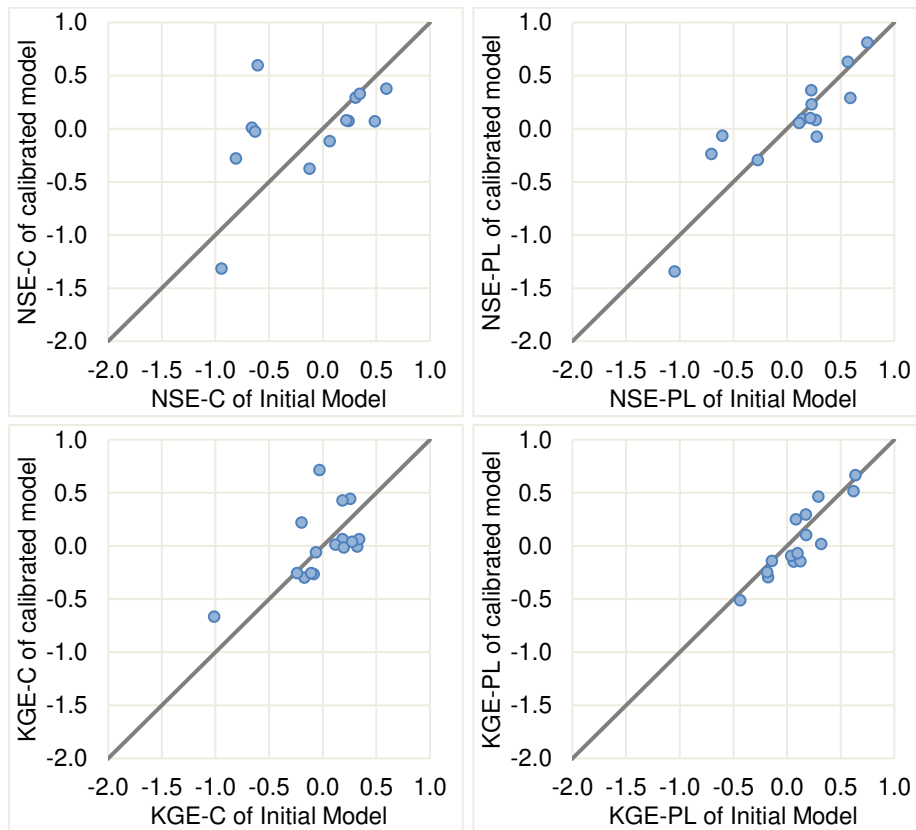


Figure 31: Scatterplots comparing BFC results of the initial model and the model with set 2 as input values.

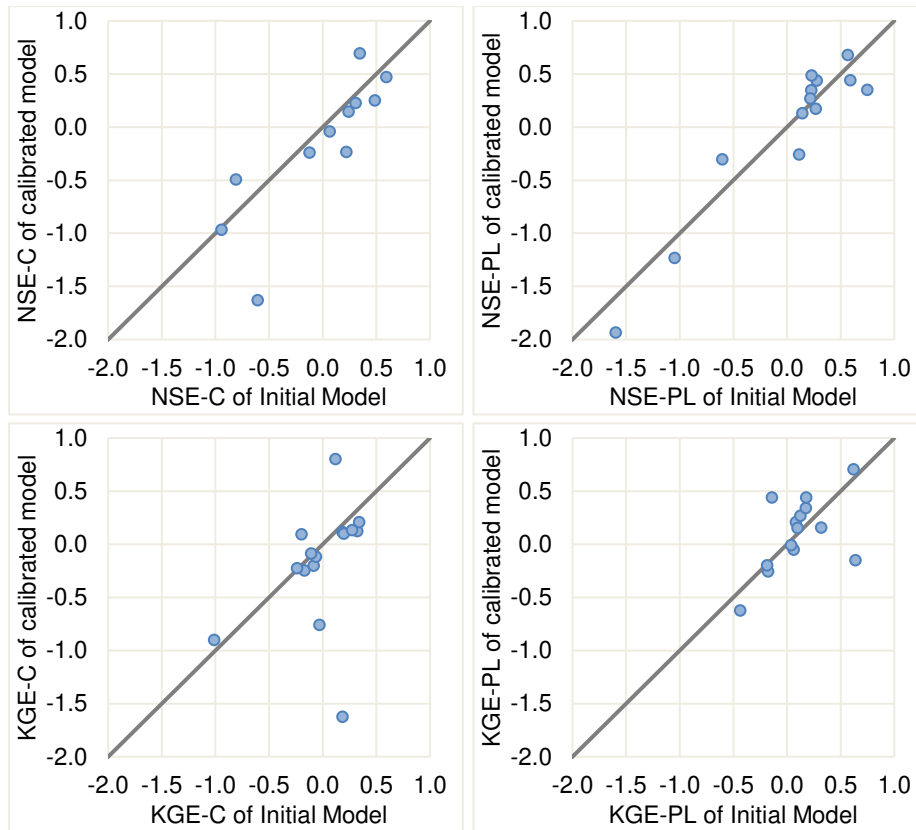


Figure 32: Scatterplots comparing BFC results of the initial model and the model with set 3 as input values.

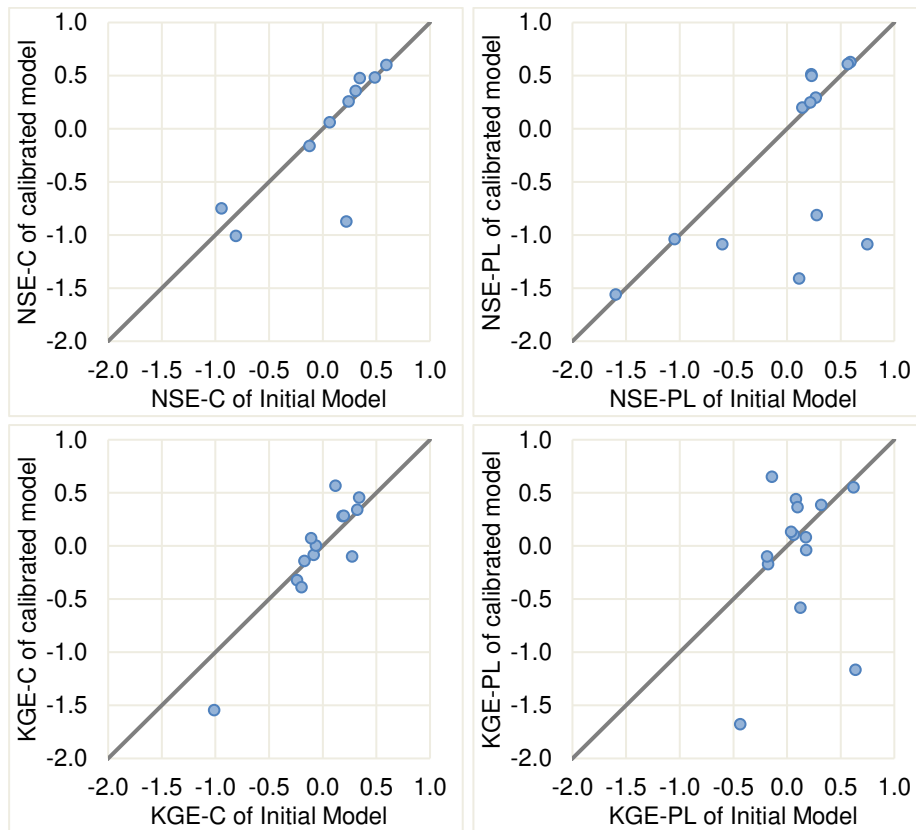


Figure 33: Scatterplots comparing BFC results of the initial model and the model with set 4 as input values.

The conclusion can be drawn, that the verification of the water quality calibration was not successful. There are several reasons for this outcome. NSE and KGE might not be suitable for this kind of analysis. They both compare absolute runoff values. This is not the objective of this work since a reliable correlation between observed turbidity and simulated TSS is missing. For this reason, only the qualitative reaction of the pollutograph was of bigger interest for the calibration of the water quality model. However, no other tool was found in literature to be more applicable for this kind of analysis. Other reasons might be found in the observations. On one hand the surface of the observed catchment is rather small so that slight disturbances of measurements or the runoff during events have a big impact on the results and are not buffered. In addition, a low frequency of recalibrating and maintaining the gauging station certainly result in a less accurate representation of real runoff processes. On the other hand, a bigger amount of observed data would improve the capacity of generalising runoff behaviour. However, it should not be disregarded that the model performances strongly vary from one event to another, making it difficult to generalise input and output values.

### 5.6 De-Sealing Modelling

The following results discuss the correlation between a de-sealing scenario applied by the percentage of reduced sealed surface and a subsequent reduction of runoff and washed-off pollution. Table 27 presents median values from all simulated events. The reduction effects are assessed by computing the percentage difference (PD) of the peak discharge  $Q_{max}$ , the total runoff volume  $V_{tot}$ , the peak concentration  $C_{max}$ , the total washed-off pollutant loads PL and the event mean concentration EMC. The results obtained by the initial model and the calibrated model can be compared. A deeper understanding is promoted by Figure 34 and Figure 35 where boxplots allow a distinct view of the results. In the appendix 2, Table 11 and Table 12 show the results of the simulations of every event separately and additionally mean and standard deviation values for each reduction indicator. A comparison of the reliability of the uncalibrated and the calibrated model was concluded by a normalised standard deviation, which is presented in Table 28.

Table 27: De-sealing results presented through the median of all events.

De-sealing of	PD $Q_{max}$	PD $V_{tot}$	PD $C_{max}$	PD PL	PD EMC
50% - Uncalibrated model	43	47	-8	43	-3
50% - Calibrated model	47	47	-2	47	-1
100% - Uncalibrated model	94	98	89	100	97
100% - Calibrated model	90	96	89	100	94

According to Table 27 a median runoff retention of 47% was obtained through both the uncalibrated and the calibrated model within a land de-sealing of 50% of the impervious surface. Considering a de-sealing of 100% the total runoff volume was reduced respectively by 98% and 96% with the uncalibrated and the calibrated model. It is not surprising that the obtained reduction is almost as high as the reduction of the impervious surface. Within 14 out of 17 events only the impervious surface contributes to the total runoff. Hence permeabilising this surface directly reduces the total runoff. Similar decreases were achieved for the peak discharge with a reduction of 43% and 47% for 50% less impervious surface cover and 94 and 90% for a total reduction of impervious surfaces, respectively for uncalibrated and calibrated simulations. The washed-off pollutant load is directly linked to the total runoff volume. For the uncalibrated model a decrease by 47% and 98% of  $V_{tot}$  reduces PL by 43% and 100%. The same behaviour was observed for the calibrated model where a decrease of 47% and 96% of the runoff volume led to a reduction of 47% and 100% of the exported TSS mass.

## Results and discussion

Considering a land de-sealing of 50% higher peak and mean concentrations are registered: increases of 8% and 2% were obtained for  $C_{max}$  while EMC raised by 3% and 1%. These elevated values are a direct consequence of  $V_{tot}$  reductions. Higher concentration values are registered because there is less runoff available to dilute the washed-off TSS. This outcome is of no further concern. No negative impact is expected from it since in total a high reduction of TSS loads is achieved and the concentrations are elevated only from a relative perspective. What can be derived from this outcome of a de-sealing of 50% is that the TSS load reduction does not equal the runoff reduction, but it rests slightly lower, leading to higher concentrations.

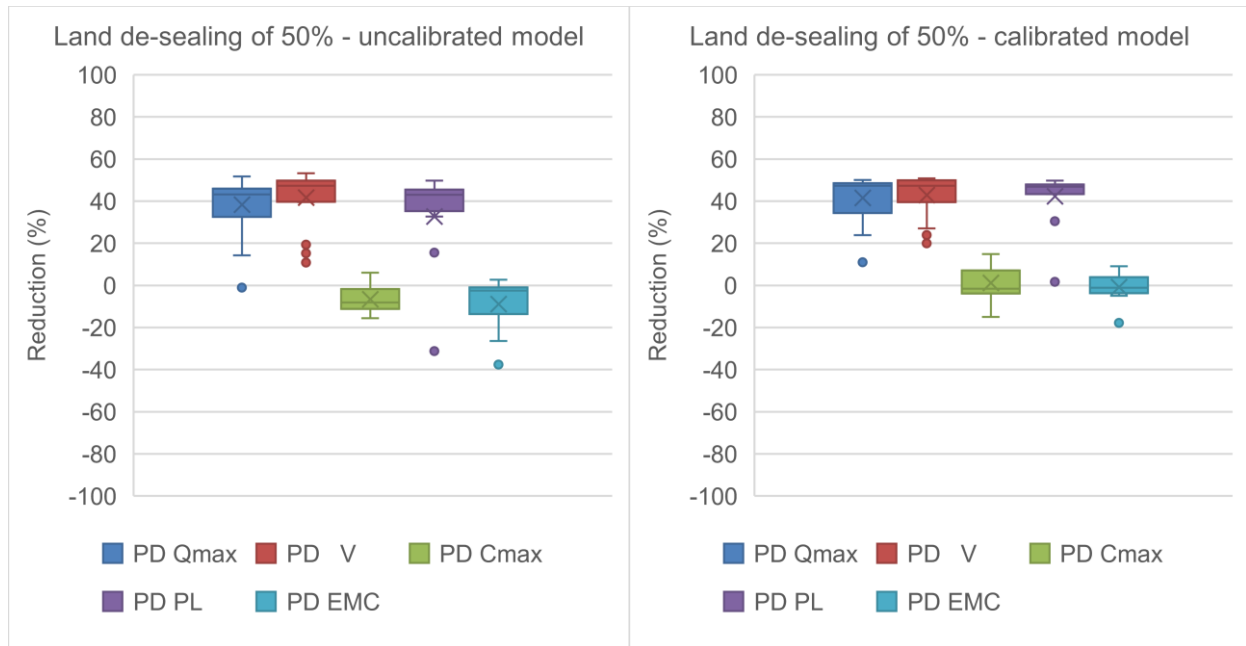


Figure 34: Relative reduction of runoff and TSS through a land de-sealing of 50%, simulated with the uncalibrated model (on the left side) and the calibrated model (on the right side).

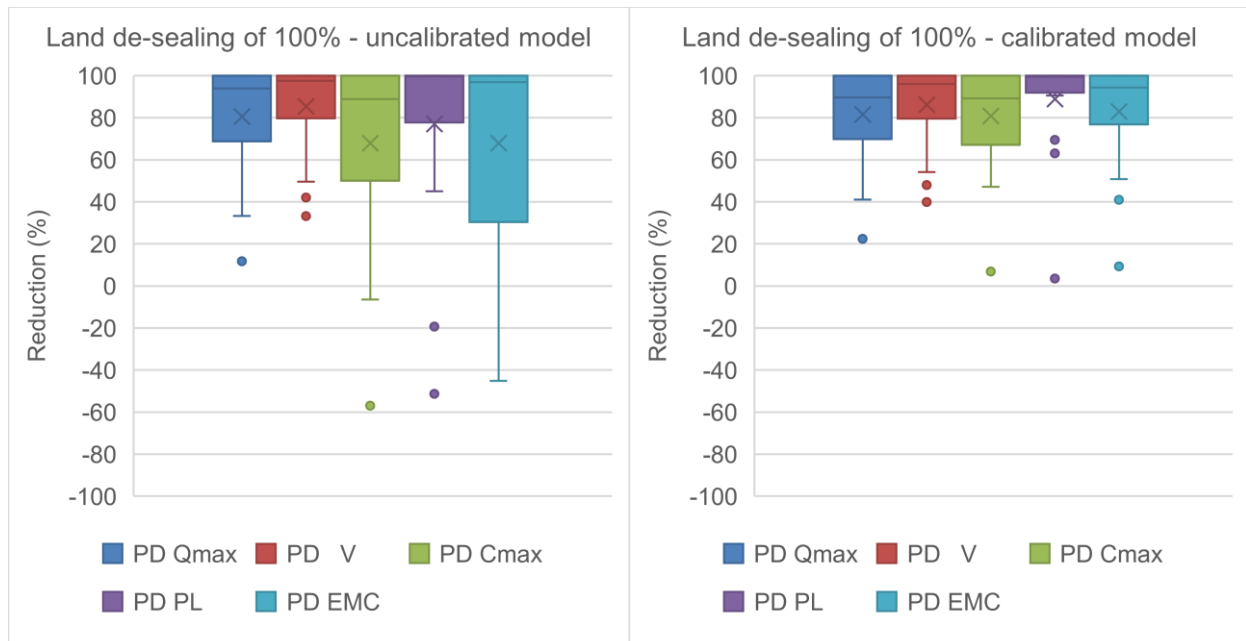


Figure 35: Relative reduction of runoff and TSS through land de-sealing of 100%, simulated with the uncalibrated model (on the left side) and the calibrated model (on the right side).

Comparing the input values of the water quality parameters of the uncalibrated and the calibrated model, the uncalibrated  $K_w$  is a power of ten higher, leading to a higher availability of TSS. In contrast the uncalibrated IB is 87% lower which causes that less TSS is available. Since the parameter values have undergone a big change, it can be expected that the two models react differently on the de-sealing scenarios. Figure 34 and Figure 35 suggest that more realistic results were obtained with the calibrated model. For every event  $Q_{max}$ ,  $V_{tot}$  and PL results above 0 were achieved, representing reduction effects of all simulations. Negative values occurred only for  $C_{max}$  and EMC for a 50% land de-sealing, raising the concentration up to 15% and 18% (in Figure 34 on the right side). Considering the beforehand explained reason for the increase of concentration, this outcome seems acceptable. In contrast, using the uncalibrated model negative  $C_{max}$  and EMC values occur for both the 50% and 100% de-sealing scenario. With the maximum concentration raising by up to 57% and the EMC until 45%, the magnitude surpasses the beforehand accepted elevation. In addition, negative values were also obtained for  $Q_{max}$  once within the 50% de-sealing scenario and for PL twice within each scenario. Much studied and nowadays commonly used the positive benefits of pervious pavements reducing runoff and pollution loads are proved. For this reason, negative results for PL reductions are not considered as well representing real life processes. Comparing the used parameter values of the PSC (elevated depression storage and a rougher manning coefficient) to the parameters of the initial subcatchment (0% de-sealing), the former theoretically leads to reduction and retardation effects. In worst case no reduction is expected when no infiltration can take place, but a raise would not be possible in any case.

Looking closer at the Figure 34 and Figure 35 and the corresponding results in the appendix 2, Table 11 and Table 12, these negative PL reduction values only occur for the tree events where the PSC contributes to the runoff. In theory the runoff which is generated from the PSC within the scenario of 0% de-sealing should be the same for the scenarios of 50% and 100% since the parameters of this subcatchment were not changed for simulating the different scenarios. To check whether the PSC produced an additional runoff all scenarios (0-50-100% de-sealing) were run for one of these 3 events (RG\_7-9-2h) for the uncalibrated and the calibrated model and the response of each subcatchment was observed separately. In this way it was proved that the PSC had the same contribution and no change of runoff and TSS occurred. Table 13 to Table 18 in the appendix 2 give an insight into the subcatchment contribution of the event RG\_7-9-2h.

Analysing the differences between the uncalibrated and the calibrated model, only two changes were carried out during the model optimisation process (see also Table 5 and Table 6 where the differences are marked with double crossbars (//) ):

- DS and n values of the ISC
- $K_w$  and IB values of all subcatchments

DS and n of ISC cannot lead to the questionable negative PL values since within the 100% de-sealing scenario the subcatchment ISC is completely replaced and would therefore have no influence. For this reason, the used DS and n values of ISC could only have impacted the 50% scenario but should not have led to an influence on the results of a 100% de-sealing. The latter parameters seem more applicable. Within the verification of the calibration of the water quality parameters it was already stated that the model response is very sensitive to the parameters IB and  $K_w$ .

## Results and discussion

---

Table 28: Mean standard deviation of all results of the uncalibrated and the calibrated simulations for both de-sealing scenarios.

	50% de-sealing	100% de-sealing
Uncalibrated	14	36
Calibrated	9	23
PD (%)	35	36

Table 28 resumes computations of mean standard deviations of each de-sealing scenario distinguishing between the two models. Comparing the two models de-sealing simulations with the uncalibrated model result in higher mean standard deviations by 35% and 36%. These findings propose a higher reliability on the calibrated model, whose reduction results of all events are in average located closer to each other.

### 6. Interpretation

The beneficial effects of pervious pavements are presented through the simulations with EPA SWMM. An implementation of PP by replacing 50% and 100% of the impervious surface led to significant reductions of the runoff and TSS inputs into receiving waters or draining networks. Considering the runoff volume of the observed catchment, the discharge tends to decrease approximately linearly as the de-sealing percentage increases. This decrease of runoff leads to a reduction of TSS, which is almost identical due to its direct relation to the runoff. As generally known and summarised as one of the first by the U.S. Environmental Protection Agency (1983) de-sealing reduction is closely linked to runoff reduction. The model used in this study seems applicable for simulating de-sealing scenarios due to its reasonable results.

However, these are not new findings and similar models were already created within various studies. A new outcome is, that the calibration of the model led to a better simulation performance. Comparing the uncalibrated and the calibrated model regarding the conducted de-sealing, more reliable results were obtained with the calibrated model. This finding was derived from the range of the reduction results and by a standard deviation which was 35% and 36% lower for the calibrated model. The de-sealing simulations of the calibrated model also appear more realistic considering the “negative reduction” of PL which was obtained for extreme stormwater events where the pervious subcatchment contributed to the surface runoff.

For a closer evaluation of the developed model its background including the used input data is further discussed to assess the impact they have and the reliability of the outcomes. Observed rainfall data is one of the most crucial input parameters for the carried-out modelling purposes. The recorded rainfall data needs to be as coherent as possible to the real rainfall arriving on the observed catchment to well reproduce observations. The comparison of the two RGs revealed continuous higher recordings for the primarily used RG. Being both relatively close to the catchment this finding suggests that proximity is not the only decisive factor to evaluate if a specific RG is representative. Both RGs consist of the same measuring apparatus but their exposition to meteorological influences differs. Considering the work of Habib et al. (1999), Nešpor and Sevruc (1999) and Blocken and Carmeliet (2006), it is assumed that wind is the cause for the recorded differences. Widely investigated, wind reduces rainfall recordings due to a decreased sampling surface of the RG and turbulences around the apparatus. In the case of Polytech, the RG is protected by wind without being affected by wind shading. With 14 out of 17 events RG Polytech is primarily used for simulations. Due to its proximity and its exposition, RG Polytech is considered to represent well the rain falling on the catchment and to be appropriate for this work. Simulations conducted with the secondary RG are expected to produce less reliable hydrographs and pollutographs. RG UM35 was used for the simulation of 3 out of 17 events. Using the data of both RGs leads to an uncertainty of the used model. What influence this outcome has on the computed reduction potentials was not further evaluated. Since similar projects might use RGs which are even further from the study site and are exposed to different environmental conditions, it is suggested to further analyse the impact of recorded rainfall inaccuracies on de-sealing results. When precise simulations of TSS loads or similar values are requested for specific applications it is suggested to apply RG correction methods as for example proposed by Hochedlinger et al. (2007).

Other than the calibration of the hydrological parameters, the calibration of the water quality parameters was not successful, which was reflected through the verification. A reason for this outcome is that the observed turbidity and the simulated TSS could not be correlated. For creating

## Interpretation

---

a reliable correlation with an accurate approximation, a large database is needed (Bertrand-Krajewski et al. 2010) which was not available for this study. However, this is not the only explanation for the unsuccessful calibration. Considering the small surface of the study site, water quality measurements are error prone. Already small unexpected and unconsidered activities or environmental effects on-site can have relatively big influences on observations. Such unrepresentative observations when implemented in a calibration could result in distorted calibrated parameter values. As reflected in all the carried out analyses (the sensitivity analysis, the calibration evaluation, and the de-sealing modelling) the model turned out to be sensitive to changes of the parameters IB and KW. This confirms the perception that unrepresentative measurements can directly lead to strong influences on the simulations.

In this work a comparison of different de-sealing scenarios (0-50-100%) is rather envisaged than to determine specific simulation results. It is evident that inaccurate input values affect simulation results. But within all carried-out scenarios, the same model approach and measurement inaccuracies were used. For example, the same RGs, runoff data and TSS correlation were applied for all scenarios. Hence, comparing responses of scenarios, it is not expected that the measurement errors, implemented in this study, have a significant influence on the obtained reduction potentials. Nonetheless, for successful model calibrations, observations which sufficiently represent real life processes are required. Unrepresentative observations could lead to poor model performances, impeding a model optimisation.

## 7. Conclusion and outlook

The conclusion is organised by responding to the research questions, formulated in chapter 2. The responses are based on the discussion and the interpretation of the results, from which further research activities can be derived.

### 1) Data Analysis

The rainfall data of the RG Polytech seems to be representative since it is located directly next to observed catchment and is affected by the same environmental influences. RG UM35 appears to be less representative according to a comparison to Polytech data. It reveals that significant lower values were continuously recorded for RG UM35. However, the objective of this work is to obtain an understanding of general reduction potentials of total suspended solids (TSS) loads. This task is addressed by comparing land-cover scenarios which implicate the same input data. Relying on the same input accuracies, it is expected that the results are not necessarily impacted by the presented RG differences.

Considering the observed runoff data, the recording time steps of 5 minutes and sensor errors can distort simulation results. A lack of maintenance of the gauging station can be another source of inaccuracy. However, in general the observed runoff events used in this work correlated well with the recorded rainfall in most cases. 17 runoff events from an observation period of 14 months were found to be exploitable. Representing an entire year, the data covers all seasons and annual meteorological phenomena. This suggests a good set up of input data for modelling purposes.

The acquisition of enough data was the major obstacle in this work. No correlation could be drawn between the observed turbidity and simulated TSS since not enough data could be sampled during the observation period. It is unclear what influence this lack of information has on the magnitude of computed TSS loads and the simulated TSS load reduction.

### 2) Model Set-Up:

Two subcatchments were defined by realising the representation of land cover regarding pollutant built-up/ wash-off processes, as proposed by Rio et al. (2020). The pervious subcatchment PSC combines pervious areas either covered with vegetation or gravel. The impervious subcatchment ISC implicates only an impervious area for pedestrian use, which is one coherent area comprising one pathway for pedestrian and a terrace with a ramp. The outlet of PSC flows on to the downstream part of ISC. This was not considered. Keeping the simplifications of Rio et al. (2020) each subcatchment was modelled to discharge directly into one common outlet. This simplification leaves hydraulic processes unconsidered. An underestimation of washed-off pollutants is expected from this simplification simulating less runoff over the ISC as in real life.

Boundaries of the catchment were difficult to determine even with a topographical survey. It cannot be specified in which direction the runoff from the upper boundaries goes due to different slope inclinations. Since catchments are defined by having only one outlet the surface of the modelled subcatchment is rather underestimated. In this way it can be assured that all the rain arriving on this surface goes to the same catchment outlet. However, the amount of additional run-on from the non-considered undefinable surface above cannot be determined. This might be a reason why the runoff coefficients from all events strongly vary as presented.

### 3) Model Optimisation and Simulations:

The hydrological performance of the model measured by the used best-fit criteria NSE, KGE and RPD is considered as satisfactory. Contrarily a verification of the calibration of the water quality parameters was not possible. The non-established correlation between TSS and turbidity is one possible reason for this outcome. It might also be questioned if the chosen BFC (NSE and KGE) are adequate tools for this study to reflect the performance of water quality simulations. Concerning this work the pollutograph is interesting mainly in terms of its responsivity, yet used BFC evaluated the approximation to observed values, which is not suitable due to the non-established correlation. The reproduction of observed pollutographs is additionally complicated due to the high sensitivity of the water quality parameters. Within all model set-up processes the model turned out to be very sensitive regarding the parameters initial built-up IB and wash-off coefficient  $K_w$ . Since the area of the observed catchment is rather small unconsidered activities or environmental effects can have a relatively high influence on the results in comparison to bigger study areas where such interferences are buffered. Implicating unrepresentative measurements for a model optimisation leads to a distortion of calibrated parameter values.

Further pursued land de-sealing simulations presented significant runoff and pollutant reductions. The TSS load reduction depends on and is concurrent with the discharge reduction.

### 4) Conclusion of calibration effects:

Regarding median reduction results no significant differences between the uncalibrated and the calibrated model were found, suggesting that a focus on the model calibration might not be necessary for simulating de-sealing scenarios. In contrast, the standard deviation of the results indicates a higher reliability of simulations with the calibrated model. This finding is supported by unreasonable negative results of PL reductions which were obtained with the uncalibrated model. Those outcomes suggest that the decision whether to focus on calibration in de-sealing modelling depends on the exact question or the objective of the modelling. When the approximate knowledge about the magnitude of runoff and pollutant reduction is sufficient, the modelling priority must not necessarily be a precise calibration. The higher the accuracy of the results is required, the more focus should be set on a model optimisation.

Within further research activities it would be interesting to test the model sensitivity regarding rainfall data with variations in recording quality. This could reveal information about the impact of RG representativity on simulation results.

In this study the hydrological sensitivity was tested only for parameters of the ISC, which was a priority task since the PSC contributed to the runoff only within 3 events. However, for gaining a better insight into the model one could test the sensitivity of hydrological parameters of PSC.

Using the same modelling approach as Rio et al. (2020) pollution was applied on all surfaces of the model through a simple initial built-up variable, which was the same value at the start of every rainfall event, regardless the time without rain before the event. The establishment of a built-up function would lead to more accurate pollutograph simulations. Additionally, the used simplification envisaged one set of water quality parameters (IB and  $K_w$ ) for all subcatchments. In further investigations a distinction of the parameter sets could be made for different surface occupations. In this study this distinction was not necessary since ISC dominated all runoff processes.

It is suggested to intensify sampling campaigns in further projects to establish a correlation between the observed turbidity and simulated washed-off pollutants or total suspended

## **Conclusion** and outlook

---

solids. This task requires a sufficiently large number of runoff events to achieve a sufficient level of representativity (Bertrand-Krajewski et al. 2010).

The gauging station is additionally equipped with a conductivity sensor, which works remotely from the other devices. Implicating conductivity data could help interpreting turbidity data. This could provide more information about the composition of pollutants and their sources.

The observed catchment covers a relatively small surface, which makes the observed data more susceptible to unexpected influences and disruptions. The monitoring of a bigger catchment could be beneficial for similar simulations. A catchment with different surface occupations, for example a street with motorised traffic is a good way to investigate specific pollutants.

### 8. Summary

In urban areas surface runoff of stormwater events produces high peak hydrographs due to a high percentage of impervious surfaces. Surface runoff simultaneously washes particles off surfaces and depending on the drainage system transports them into receiving waters. Widely investigated, urban surface pollution leads to a degradation of the quality of waterbodies and to an endangerment of the ecosystem. A reduction of surface runoff and, along with it, pollutant loads is therefore endeavoured. To evaluate the water and contaminant retention potential of urban surfaces at the scale of cities a doctoral thesis was realised by Rio (2020). Within the thesis a rainwater and contaminant runoff model was developed with the programme SWMM. Informing decision makers about the beneficial effects of green/blue infrastructure (GBI) the study outcomes support a sustainable urban planning, which is necessary to comply with the European Water Framework Directive (DIRECTIVE 2000/60/EC). In this empirical master thesis, the model of Rio (2020) was further investigated, by modelling an observed catchment which enabled an optimisation of model parameters.

The monitored catchment covers a pedestrian area which is located on the study site of Rio (2020) in the city of Montpellier, France. The observations of the catchment included rainfall data and runoff data comprising discharge as well as turbidity measurements. The observed data was recorded at the outlet of the monitored catchment within an interval of 5 minutes over a 14-month period. A rain gauge (RG) which is located next to the catchment was primarily used. For covering a data lack another RG, which is situated 168 m from the principal one, was implied. 17 runoff events were exploitable for simulations. As a first task of the study the data of the two RGs were compared in order to evaluate the representativity and reliability of them. A topographical survey was carried out to define the catchment surface. As a next task the SWMM model was created by distinguishing between surface covers as proposed by Rio et al. (2020). The catchment was therefore represented by a pervious (PSC) and an impervious (ISC) subcatchment and further input values were predefined by Rio. Simulations reproduce discharge and total suspended solids (TSS) concentration curves of each exploitable event. The third task comprised a sensitivity analysis and a parameter calibration comparing the observations with the model simulations. Within the verification it was tested whether the calibration improved the hydrological and the water quality responses. Finally de-sealing scenarios were computed to obtain the potentials of discharge and pollution reduction. The scenarios comprised a de-sealing of 50% and 100% of the impervious surface. Simulations were carried out twice, once for the uncalibrated and once the calibrated model. Their comparison allowed to draw a conclusion about the effect of a calibration on de-sealing results. This evaluation was part of the last task.

The comparison of the two RG revealed continuous higher recordings for the primarily used RG. Simulations conducted with the primary RG are expected to produce more reliable hydrographs and pollutographs. Despite differences, it is concluded that the rain data are suitable for the carried-out simulations. The sensitivity analysis suggested initial losses  $DS_{imp}$  and the Manning Coefficient  $n_{imp}$  of the ISC for a hydrological calibration. For the water quality calibration, the initial built-up IB and the wash-off coefficient  $K_w$  (both applied on the whole catchment) were the most interesting parameters. Through the hydrological calibration best-fit criteria (NSE, KGE and RPD) indicated an improvement of the model performance. On the contrary, a verification of the water quality calibration was not possible. A non-established correlation between the observed turbidity and the simulated TSS is considered as one reason for this outcome. Therefore, the chosen BFC for analysing the water quality response (NSE and KGE) did not seem suitable for this work.

## Summary

---

Additionally, the reproduction of observed pollutographs was complicated due to the revealed high sensitivity of the water quality parameters.

The de-sealing simulations proved that a runoff reduction led to a simultaneous reduction of pollutant loads. Their reduction percentage was approximately the same. The comparison between simulations with the uncalibrated and the calibrated model led to an interesting outcome. On one hand the reduction magnitude was similar, suggesting that a strong focus on a prior calibration is not necessary when a general estimation of reduction potentials is requested. On the other hand, results of the uncalibrated model were less reliable regarding particular unrealistic results and the standard deviation which was 35% to 36% higher. For tasks where a precise reduction potential of pollutants through de-sealing measures is required, a calibration is recommended.

The creation and investigation of the used model contributes to research about the application of GBI simulated with SWMM. The modelling approach of Rio (2020) was investigated and validated. The outcomes of this study allow a better comprehension of the considered parameters and gave more insights into the sensitivity and reliability of the de-sealing model. The findings can give directions to model simplifications and support an efficient model set-up for simulating de-sealing scenarios.

## 9. Literature and References

### 9.1 Bibliography

- Alves, A., Gersonius, B., Kapelan, Z., Vojinovic, Z., and Sanchez, A. (2019): Assessing the Co-Benefits of green-blue-grey infrastructure for sustainable urban flood risk management. *Journal of Environmental Management*, 239, 244–254.
- Azeez, N., Sabbar, A. (2012): Efficiency of Duckweed (*Lemna minor* L.) in Phytotreatment of Wastewater Pollutants from Basrah Oil Refinery. *Journal of Applied Phytotechnology in Environmental Sanitation*, 1(4), 163–172.
- Bertrand-Krajewski, J.-L., Joannis, C., Chebbo, G., Ruban, G., Métadier, M., Lacour, C. (2010): Comment utiliser la turbidité pour estimer en continu les concentrations en MES et/ou DCO - Une approche méthodologique pour les réseaux d'assainissement. (How to use turbidity to continuously estimate suspended solids and/or COD concentrations - A methodological approach for sewerage networks.) *Techniques Sciences Méthodes* 1/2 2010(2), 36-46.
- Bertrand-Krajewski, J.-L. (2004): TSS concentration in sewers estimated from turbidity measurements by means of linear regression accounting for uncertainties in both variables. *Water Science & Technology*, 50(11), 81–88.
- Bilotta, G. S. and Brazier, R. E. (2008): Understanding the influence of suspended solids on water quality and aquatic biota. *Water Research*, 42(12), 2849–2861.
- Blocken, B. and Carmeliet, J. (2006): On the accuracy of wind-driven rain measurements on buildings. *Building and Environment*, 41(12), 1798–1810.
- Bonhomme, C. and Petrucci, G. (2017): Should we trust build-up/wash-off water quality models at the scale of urban catchments? *Water Research*, 108, 422–431.
- Borris, M., Viklander, M., Gustafsson, A.-M., Marsalek, J. (2014): Modelling the effects of changes in rainfall event characteristics on TSS loads in urban runoff. *Hydrological Processes*, 28(4), 1787–1796.
- Brudler, S., Rygaard, M., Arnbjerg-Nielsen, K., Hauschild, M. Z., Ammitsøe, C., and Vezzaro, L. (2019): Pollution levels of stormwater discharges and resulting environmental impacts. *Science of The Total Environment*, 663, 754–763.
- Butler, D. and Davies, J. W. (2004): *Urban Drainage*. 2nd edition, Spon Press, London, United Kingdom.
- Charters, F. J., O'Sullivan, A. D., and Cochrane, T. A. (2022): Influences of zinc loads in urban catchment runoff: Roof type, land use type, climate and management strategies. *Journal of Environmental Management*, 322, 116076.
- Chow, V. T. (1959): *Open-Channel Hydraulics*. McGraw-Hill Book Company, Inc., New York, United States of America.
- Chowdhury, D., Melin, A., and Villez, K. (2021): Automatic Drift Correction through Nonlinear Sensing. In: Rieger, C. et al. (Eds.): 2021 Resilience Week (RWS), 18-21 Oct. 2021, Salt Lake City, UT, United States of America., pp.1–6.

- Egodawatta, P., Thomas, E., and Goonetilleke, A. (2007): Mathematical interpretation of pollutant wash-off from urban road surfaces using simulated rainfall. *Water Research*, 41(13), 3025–3031.
- Fraga, I., Charters, F. J., O'Sullivan, A. D., and Cochrane, T. A. (2016): A novel modelling framework to prioritize estimation of non-point source pollution parameters for quantifying pollutant origin and discharge in urban catchments. *Journal of Environmental Management*, 167, 75–84.
- Gasperi, J., Le Roux, J., Deshayes, S., Ayrault, S., Bordier, L., Boudahmane, L., Budzinski, H., Caupos, E., Caubrière, N., Flanagan, K., Guillon, M., Huynh, N., Labadie, P., Meffray, L., Neveu, P., Partibane, C., Paupardin, J., Saad, M., Varnede, L., and Gromaire, M.-C. (2022): Micropollutants in Urban Runoff from Traffic Areas: Target and Non-Target Screening on Four Contrasted Sites. *Water*, 14(3), 394.
- Habersack, H., Haimann, M., Kerschbaumsteiner, W., Lalk, P. (2017): SCHWEBSTOFFE IM FLIESSGEWÄSSER - LEITFADEN ZUR ERFASSUNG DES SCHWEBSTOFFTRANSPORTES (SUSPENDED SUBSTANCES IN WATERWAYS - GUIDELINES FOR DETECTING SUSPENDED SUBSTANCE TRANSPORT), 2nd Edition, Bundesministerium für Land- und Forstwirtschaft, Umwelt und Wasserwirtschaft, Vienna, Austria.
- Habib, E., Krajewski, W. F., Nesper, V., and Kruger, A. (1999): Numerical simulation studies of rain gage data correction due to wind effect. *Journal of Geophysical Research: Atmospheres*, 104(D16), 19723–19733.
- Hannouche, A., Chebbo, G., Ruban, G., Tassin, B., and Joannis, C. (2011): Relation entre la turbidité et les matières en suspension en réseau d'assainissement unitaire (Relationship between turbidity and suspended solids in a combined sewerage network). *Techniques Sciences Méthodes*, (10), 42–50.
- Herngren, L., Goonetilleke, A., and Ayoko, G. A. (2005): Understanding heavy metal and suspended solids relationships in urban stormwater using simulated rainfall. *Journal of Environmental Management*, 76(2), 149–158.
- Hochedlinger, M., Sprung, W., Kainz, H., König, K. (2007): CSO Modelling Considering Moving Storms and Tipping Bucket Gauge Failures. *Water Practice and Technology*, 2(1), wpt2007024.
- Inoue, T., Fukue, M., Mulligan, C. N., and Uehara, K. (2009): In situ removal of contaminated suspended solids from a pond by filtration. *Ecological Engineering*, 35(8), 1249–1254.
- Institut national de la statistique et des études économiques (INSEE) (2022a): Comparateur de territoires (Territory comparator), Intercommunalité-Métropole de 7344 Montpellier Méditerranée Métropole (243400017), Comparateur de territoires – Intercommunalité-Métropole de Montpellier Méditerranée Métropole (243400017) | Insee, (date of visit: 13/11/2022).
- Institut national de la statistique et des études économiques (INSEE) (2022b): Dossier complet Commune de Montpellier (34172) (Complete file Municipality of Montpellier), POP T2M - Indicateurs démographiques en historique depuis 1968, Dossier complet – Commune de Montpellier (34172) | Insee, (date of visit: 13/11/2022).

- Jeong, H., Choi, J. Y., Lee, J., Lim, J., and Ra, K. (2020): Heavy metal pollution by road-deposited sediments and its contribution to total suspended solids in rainfall runoff from intensive industrial areas. *Environmental Pollution*, 265, 115028.
- Lacour, C. et al. (2010): Évaluation de flux de polluants dans un réseau unitaire à partir de mesures en continu de turbidité (Evaluation of pollutant flows in a combined network from continuous turbidity measurements). *Techniques Sciences Méthodes* 1/2 2010(3), 47-53.
- Kajikawa, H. and Kobata, T. (2019): Evaluation and correction for long-term drift of hydraulic pressure gauges monitoring stable and constant pressures. *Measurement*, 134, 33–39.
- Lehtinen, S. (2014): Simulation of stormwater quality in an urban catchment using the Stormwater Management Model (SWMM). Master's thesis, Department of Civil and Environmental Engineering, Aalto University School of Engineering, Espoo, Finland [in English].
- Leutnant, D., Muschalla, D., Uhl, M. (2016): Stormwater Pollutant Process Analysis with Long-Term Online Monitoring Data at Micro-Scale Sites. *Water*, 8(7), 299.
- Li, R., Hua, P., Zhang, J., and Krebs, P. (2020): Effect of anthropogenic activities on the occurrence of polycyclic aromatic hydrocarbons in aquatic suspended particulate matter: Evidence from Rhine and Elbe Rivers. *Water Research*, 179, 115901.
- Liu, A., Goonetilleke, A., and Egodawatta, P. (2012): Inherent Errors in Pollutant Build-Up Estimation in Considering Urban Land Use as a Lumped Parameter. *Journal of Environmental Quality*, 41(5), 1690–1694.
- Mantonovic, Maxicannata (2022): istSOS2 - Sensor Observation Service Data Management System, <http://hydro-h2u.msem.univ-montp2.fr/istsos/admin/> (last date of visit: 24/02/2023).
- Marchioni, M. and Becciu, G. (2015): Experimental results on permeable pavements in Urban areas: A synthetic review. *International Journal of Sustainable Development and Planning*, 10(6), 806–817.
- Nassani, A. A., Yousaf, Z., Radulescu, M., Balsalobre-Lorente, D., Hussain, H., and Haffar, M. (2023): Green Innovation through Green and Blue Infrastructure Development: Investigation of Pollution Reduction and Green Technology in Emerging Economy. *Energies*, 16(4), 1944.
- Nešpor, V. and Sevruck, B. (1999): Estimation of Wind-Induced Error of Rainfall Gauge Measurements Using a Numerical Simulation. *Journal of Atmospheric and Oceanic Technology*, 16(4), 450–464.
- ÖNORM EN (2005): EN 872:2005. Water quality - Determination of suspended solids - Method by filtration through glass fibre filters, Austrian Standards Institute/ Österreichisches Normungsinstitut, Vienna, Austria.
- ÖNORM EN ISO (2016): EN ISO 7027-1:2016. Water quality - Determination of turbidity - Part 1: Quantitative methods, Austrian Standards Institute/ Österreichisches Normungsinstitut, Vienna, Austria.
- Petrucci, G. and Bonhomme, C. (2014): The dilemma of spatial representation for urban hydrology semi-distributed modelling: Trade-offs among complexity, calibration and geographical data. *Journal of Hydrology*, 517, 997–1007.

- Rammal, M., Berthier, E. (2020): Runoff Losses on Urban Surfaces during Frequent Rainfall Events: A Review of Observations and Modeling Attempts. *Water*, 12(10), 2777.
- El Gaouzi, A. (2021): *Métrologie de la turbidité et concentration des matières en suspension dans les cours d'eau urbain (Metrology of turbidity and concentration of suspended solids in urban waterways)*. Rapport de Stage, UMR HydroSciences Montpellier, Montpellier, France.
- Rio, M. (2020): Flux de contaminants dans un bassin versant côtier méditerranéen lors d'évènements pluvieux : quels bénéfices de la désimperméabilisation des espaces urbanisés ? : étude à différentes échelles sur la zone de Montpellier (Contaminant flows in a Mediterranean coastal watershed during rainfall events: what are the benefits of desealing urbanised areas? : study at different scales in the area of Montpellier), *École doctorale GAIA, Unité de recherche HydroSciences Montpellier [in French]*.
- Rio, M., Salles, C., Rodier, C., Cantet, F., Marchand, P., Mosser, T., Cernesson, F., Monfort, P., and Tournoud, M.-G. (2017): An empirical model to quantify fecal bacterial loadings to coastal areas: Application in a Mediterranean context. *Comptes Rendus Geoscience*, 349(6), 299–309.
- Rio, M., Salles, C., Cernesson, F., Marchand, P., and Tournoud, M.-G. (2020): An original urban land cover representation and its effects on rain event-based runoff and TSS modelling. *Journal of Hydrology* 586, 124865.
- Rio, M., Salles, C., and Tournoud, M.-G. (2021): Modelling the effects of stormwater control measures on runoff volume and particulate load in urban catchments. *Urban Water Journal*, 18(2), 79–90.
- Rossman, L. A. (2015): *Storm Water Management Model User's Manual*. Version 5.1, United States Environmental Protection Agency, Cincinnati, Ohio, United States of America.
- Rüdel, H., Fliedner, A., Herrchen, M. (2007): *Strategie für ein stoffangepasstes Gewässermonitoring (Machbarkeitsstudie) - Erfassung potentiell sorbierender oder akkumulierender Stoffe in den Kompartimenten Biota, Sedimenten und Schwebstoffen (Strategy for substance-adapted water body monitoring (feasibility study) - registration of potentially sorbing or accumulating substances in the compartments biota, sediments and suspended matter)*. Fraunhofer – Institut für Molekularbiologie und Angewandte Ökologie, Bundesministerium für Land- und Forstwirtschaft, Vienna, Austria.
- Rügner, H., Schwientek, M., Beckingham, B., Kuch, B., and Grathwohl, P. (2013): Turbidity as a proxy for total suspended solids (TSS) and particle facilitated pollutant transport in catchments. *Environmental Earth Sciences*, 69(2), 373–380.
- Schmutz, S. (2009): *Einfluss von Nasslagern auf den ökologischen Zustand und die Fischfauna von Fließgewässern (Influence of wet storage of logs on the ecological status and fish fauna of running waters)*. Gutachten, Fachabteilung 10C Forstwesen, Amt der Steiermärkischen Landesregierung, Graz, Austria.
- Soltaninia, S., Taghavi, L., Hosseini, S. A., Motamedvaziri, B., and Eslamian, S. (2022): The effect of land-use type and climatic conditions on heavy metal pollutants in urban runoff in a semi-arid region. *Journal of Water Reuse and Desalination*, 12(4), 384–402.
- Stangl, R., Minixhofer, P., Wulsch, T., Briefer, A., and Scharf, B. (2022): *Green-blue infrastructure in the built environment – sustainable and resource-saving designs for urban structures*

- and open spaces. IOP Conference Series: Earth and Environmental Science, 1078(1), 012132.
- Taghizadeh, S., Khani, S., and Rajaei, T. (2021): Hybrid SWMM and particle swarm optimization model for urban runoff water quality control by using green infrastructures (LID-BMPs). *Urban Forestry & Urban Greening*, 60, 127032.
- Urbaniak, M., Skowron, A., Frątczak, W., Zieliński, M., and Wesołowski, W. (2010): Transport of Polychlorinated Biphenyls in Urban Cascade Reservoirs: Levels, Sources and Correlation to Environmental Conditions, *Polish Journal of Environmental Studies*, 19, 201-211.
- U.S. Department of Agriculture (1986): *Urban Hydrology for Small Watersheds*. Technical Release 55, Conservation Engineering Division, U.S. Department of Agriculture, Washington, D.C., United States of America.
- U.S. Environmental Protection Agency (1983): *Results of the Nationwide Urban Runoff Program. Volume I, Water Planning Division*, United States Environmental Protection Agency, Washington, D.C., United States of America.
- Vrugt, J. A. and de Oliveira, D. Y. (2022): Confidence intervals of the Kling-Gupta efficiency. *Journal of Hydrology*, 612, 127968.
- Versini, P.-A., Joannis, C., Chebbo, G. (2015) : *Guide technique sur le mesurage de la turbidité dans les réseaux d'assainissement (Technical guide on the measurement of turbidity in sewer networks)*. Guides et protocoles, Onema, LEESU et IFSTTAR/LEE, Vincennes, France.

## 9.2 Legal Framework References

### 9.2.1 European Union

- DIRECTIVE 2000/60/EC OF THE EUROPEAN PARLIAMENT AND OF THE COUNCIL of 23 October 2000 establishing a framework for Community action in the field of water policy (2000). [EUR-Lex - 32000L0060 - EN - EUR-Lex \(europa.eu\)](#).
- DIRECTIVE 2006/7/EC OF THE EUROPEAN PARLIAMENT AND OF THE COUNCIL of 15 February 2006 concerning the management of bathing water quality and repealing Directive 76/160/EEC (2006). [EUR-Lex - 32006L0007 - EN - EUR-Lex \(europa.eu\)](#).
- DIRECTIVE 2006/11/EC OF THE EUROPEAN PARLIAMENT AND OF THE COUNCIL of 15 February 2006 on pollution caused by certain dangerous substances discharged into the aquatic environment of the Community (2006). [EUR-Lex - 32006L0011 - EN - EUR-Lex \(europa.eu\)](#).
- DIRECTIVE 2008/56/EC OF THE EUROPEAN PARLIAMENT AND OF THE COUNCIL of 17 June 2008 establishing a framework for community action in the field of marine environmental policy (2008). [EUR-Lex - 32008L0056 - EN - EUR-Lex \(europa.eu\)](#).
- DIRECTIVE 2008/105/EC OF THE EUROPEAN PARLIAMENT AND OF THE COUNCIL of 16 December 2008 on environmental quality standards in the field of water policy, amending and subsequently repealing Council Directives 82/176/EEC, 83/513/EEC, 84/156/EEC, 84/491/EEC, 86/280/EEC and amending Directive 2000/60/EC of the European Parliament and of the Council (2008). [EUR-Lex - 32008L0105 - EN - EUR-Lex \(europa.eu\)](#).
- COMMISSION DIRECTIVE 2009/90/EC of 31 July 2009 laying down, pursuant to Directive 2000/60/EC of the European Parliament and of the Council, technical specifications for

chemical analysis and monitoring of water status (2009). [EUR-Lex - 32009L0090 - EN - EUR-Lex \(europa.eu\)](#).

COMMUNICATION FROM THE COMMISSION TO THE EUROPEAN PARLIAMENT, THE COUNCIL, THE ECONOMIC AND SOCIAL COMMITTEE AND THE COMMITTEE OF THE REGIONS Our life insurance, our natural capital: an EU biodiversity strategy to 2020 COMMUNICATION FROM THE COMMISSION TO THE EUROPEAN PARLIAMENT, THE COUNCIL, THE ECONOMIC AND SOCIAL COMMITTEE AND THE COMMITTEE OF THE REGIONS Our life insurance, our natural capital: an EU biodiversity strategy to 2020 (2011). [EUR-Lex - 52011DC0244 - EN - EUR-Lex \(europa.eu\)](#).

DIRECTIVE 2013/39/EU OF THE EUROPEAN PARLIAMENT AND OF THE COUNCIL of 12 August 2013 amending Directives 2000/60/EC and 2008/105/EC as regards priority substances in the field of water policy (2013). [EUR-Lex - 32013L0039 - EN - EUR-Lex \(europa.eu\)](#).

COMMUNICATION FROM THE COMMISSION TO THE EUROPEAN PARLIAMENT, THE COUNCIL, THE EUROPEAN ECONOMIC AND SOCIAL COMMITTEE AND THE COMMITTEE OF THE REGIONS Green Infrastructure (GI) — Enhancing Europe's Natural Capital (2013). [EUR-Lex - 52013DC0249 - EN - EUR-Lex \(europa.eu\)](#)

COMMUNICATION FROM THE COMMISSION TO THE EUROPEAN PARLIAMENT, THE COUNCIL, THE EUROPEAN ECONOMIC AND SOCIAL COMMITTEE AND THE COMMITTEE OF THE REGIONS EU Biodiversity Strategy for 2030 Bringing nature back into our lives (2020). [EUR-Lex - 52020DC0380 - EN - EUR-Lex \(europa.eu\)](#).

Proposal for a REGULATION OF THE EUROPEAN PARLIAMENT AND OF THE COUNCIL on nature restoration (2022). [EUR-Lex - 52022PC0304 - EN - EUR-Lex \(europa.eu\)](#).

### 9.2.2 Austria

Verordnung des Bundesministers für Land- und Forstwirtschaft, Umwelt und Wasserwirtschaft über die Überwachung des Zustandes von Gewässern (Gewässerzustandsüberwachungsverordnung – GZÜV), §§ 59c bis 59f Wasserrechtsgesetz 1959 (WRG 1959), BGBl. Nr. 215, last amended by BGBl. I Nr. 123/2006.

Verordnung des Bundesministers für Land- und Forstwirtschaft, Umwelt und Wasserwirtschaft über die Festlegung des Zielzustandes für Oberflächengewässer (Qualitätszielverordnung Chemie Oberflächengewässer – QZV Chemie OG), § 30a Abs. 2 Z 2 Wasserrechtsgesetz 1959 (WRG 1959), BGBl. I Nr. 215, last amended by BGBl. I Nr. 87/2005.

Verordnung des Bundesministers für Land- und Forstwirtschaft, Umwelt und Wasserwirtschaft über die Festlegung des ökologischen Zustandes für Oberflächengewässer (Qualitätszielverordnung Ökologie Oberflächengewässer – QZV Ökologie OG), § 30a Abs. 2 Z 1 und 3 Wasserrechtsgesetz 1959 (WRG 1959), BGBl. Nr. 215, last amended by BGBl. I Nr. 123/2006 and Bundesministeriengesetznovelle 2009, BGBl. I Nr. 3.

### 9.2.3 France

A. 25 janvier 2010 relatif aux méthodes et critères d'évaluation de l'état écologique, de l'état chimique et du potentiel écologique des eaux de surface pris en application des articles R. 212-10, R. 212-11 et R. 212-18 du code de l'environnement, NOR : DEVO1001032A.

L. n° 92-3, 3 janvier 1992, sur l'eau (1), NOR : ENVX9100061L.

## Literature and References

---

- L. n° 2004-338, 21 avril 2004, portant transposition de la directive 2000/60/CE du Parlement européen et du Conseil du 23 octobre 2000 établissant un cadre pour une politique communautaire dans le domaine de l'eau (1), NOR : DEVX0200193L.
- L. n° 2006-1772, 30 décembre 2006, sur l'eau et les milieux aquatiques (1), NOR : DEVX0400302L.
- Bureau des milieux marins, et al. (2018): *Guide relatif aux règles d'évaluation de l'état des eaux littorales dans le cadre de la DCE*. Ministère de la Transition écologique et solidaire. <https://www.eaufrance.fr/sites/default/files/2019-04/guide-reeel-2018-3.pdf> (date of visit: 10 March 2023).
- Ministère de l'Environnement, de l'Énergie et de la Mer (2016): *Guide technique Relatif à l'évaluation de l'état des eaux de surface continentales (cours d'eau, canaux, plans d'eau)*. Ministère de la Transition écologique et de la Cohésion des territoires. [Guide REEE-ESC mise à jour 2016 V13 \(eaufrance.fr\)](#) (date of visit: 9 March 2023).
- Ministère de l'Environnement, de l'Énergie et de la Mer (2020): *Plan micropolluants 2016-2021 pour préserver la qualité des eaux et la biodiversité*. Ministère de la Transition écologique et de la Cohésion des territoires. [2021 011 EARM4 Mise à jour du plan micropolluants \(ecologie.gouv.fr\)](#) (date of visit: 10 March 2023).
- Montpellier Méditerranée Métropole (2022a): Milieux aquatiques et inondations. *ZOOM SUR LES PAPI, LES PROGRAMMES D'ACTION DE PRÉVENTION DES INONDATIONS, Milieux aquatiques et inondations | Montpellier Méditerranée Métropole (montpellier3m.fr)* (date of visit: 13 March 2023).
- Montpellier Méditerranée Métropole (2022b): Le Schéma de Cohérence Territoriale (SCoT). *LES 4 OBJECTIFS DE LA RÉVISION DU SCOT, Le Schéma de Cohérence Territoriale (SCoT) | Montpellier Méditerranée Métropole (montpellier3m.fr)* (date of visit: 13 March 2023).
- Montpellier Méditerranée Métropole (2022c): Assainissement. *3 MISSIONS INDISPENSABLES AU SERVICE DES HABITANTS, Assainissement | Montpellier Méditerranée Métropole (montpellier3m.fr)* (date of visit: 13 March 2023).

## 10. List of abbreviations

BFC	Best-fit Criteria
$C_{\max}$	Maximum Concentration
CN	Curve Number
COD	Chemical Oxygen Demand
Cu	Copper
DS	Depression Storage
DSC	De-sealed Sub-Catchment
$E_w$	Wash-off Exponent
FNU	Formazine Nephelometric Unit
GBI	Green/Blue Infrastructures
HSM	HydroSciences Montpellier
IB	Initial Built-up
ISC	Impervious Sub-Catchment
KGE	Kling–Gupta Efficiency
$K_w$	Wash-off Coefficient
$n$	Manning Coefficient
NSE	Nash-Sutcliffe Efficiency
PAHs	Polycyclic Aromatic Hydrocarbons
Pb	Lead
PCBs	Polychlorinated Biphenyls
PD	Percentage Difference error
PL	Pollutant Load
PP	Pervious Pavements
PSC	Pervious Sub-Catchment
$Q_{\max}$	Maximum Discharge
RG	Rain Gauge
RPD	Relative Percentage Difference
SWMM	Storm Water Management Model
TSS	Total Suspended Solids
$V_{\text{tot}}$	Total Discharged Volume
WQRU	Water Quality Response Units
Zn	Zinc

## 11. List of Tables and Figures

### 11.1 Tables

Table 1: Input Parameter values of the initial model .....	19
Table 2: Parameter values for the sensitivity analysis of hydrological parameters.....	20
Table 3: Parameter values for the sensitivity analysis of water quality parameters.....	21
Table 4: List of events chosen for calibration.....	22
Table 5: Input parameter values of the SWMM model with a de-sealing of 50%. For parameters, where it was necessary to distinguish between the uncalibrated and the calibrated values a double crossbar ( // ) separates the uncalibrated (before the crossbars) from the calibrated value (after the crossbars). .....	24
Table 6: Input parameter values of the SWMM model with a de-sealing of 100%. For parameters, where it was necessary to distinguish between the uncalibrated and the calibrated values a double crossbar ( // ) separates the uncalibrated (before the crossbars) from the calibrated value (after the crossbars). .....	25
Table 7: Comparison of absolute rainfall values registered at RG Polytech and UM35.....	26
Table 8: Observed rainfall events with a total rainfall sum $\geq 3,0\text{mm}$ .....	28
Table 9: Runoff events correlated with observed runoff.....	29
Table 10: Simulation results of all runoff events, modelled with the uncalibrated model and opposed to the runoff observations.....	31
Table 11: Results of event chosen for sensitivity analysis simulated with initial model.....	32
Table 12: Results of the sensitivity analysis of the hydrological input parameters.....	33
Table 13: NSE results of the sensitivity analysis of the water quality input parameters.....	33
Table 14: Median values of each tested parameter combination calculated separately for all 4 best-fit criteria.....	35
Table 15: Median of all calculated events and all criteria combined for every parameter combination.....	37
Table 16: Comparison of median results of each best-fit criteria of uncalibrated and calibrated model .....	37
Table 17: Median values of all parameter value combinations considering all 5 calibration events, tested for NSE-C, NSE-PL, KGE-C and KGE-PL.....	41
Table 18: Median of all calculated events and all criteria combined for every parameter combination.....	42
Table 19: Mean difference of the combination of all best-fit criteria.....	43
Table 20: Median result considering only the variable concentration by coupling NSE-C and KGE-C. ....	43
Table 21: Median result considering only the variable pollutant load by coupling NSE-PL and KGE-PL.....	43

## List of Tables and Figures

---

Table 22: Comparison of the median and the mean best-fit criteria results of the initial and the best parameter sets.....	44
Table 23: Comparison of NSE and KGE results of the uncalibrated (left) and the calibrated (right) model. ....	48
Table 24: Comparison of NSE and KGE results of the uncalibrated model (on the left side) and the parameter sets 1 and 2 from calibrated model (on the right side). ....	49
Table 25: Comparison of NSE and KGE results of the uncalibrated model (on the left side) and the parameter sets 3 and 4 from calibrated model (on the right side). ....	49
Table 26: Number of improved events considering each tested BFC separately. ....	50
Table 27: De-sealing results presented through the median of all events. ....	53
Table 28: Mean standard deviation of all results of the uncalibrated and the calibrated simulations for both de- sealing scenarios.....	56

## 11.2 Figures

Figure 1: The methodology followed in this work. ....	12
Figure 2: Study site “Polytech”, pervious surfaces are hatched in green, impervious surfaces are hatched in red. ....	13
Figure 3: Overview of the exact positions of the rain gauges and the runoff gauging station. ...	14
Figure 4: Outfall of the observation catchment with a rain channel and a catchpit. ....	15
Figure 5: Surface runoff gauging station, covered with a protection rake. ....	16
Figure 6: Surface runoff gauging station consisting of a sampling bucket with 3 sensors. ....	16
Figure 7a and b: Comparison of the rain gauges “Polytech” and “UM35” for the observation period from 01.11.2021 to 01.11.2022. ....	26
Figure 8: Combination of cumulative rainfall & rain intensity for both rain gauges (RG Polytech and RG UM35). ....	27
Figure 9: Runoff observation periods. ....	29
Figure 10: Results of two observed runoff events with sensor errors: 1) on the right side the event RG_17-8-18h, 2) on the left side the event RG_2-1-23h. ....	30
Figure 11: Comparison of observed and simulated hydrograph. ....	32
Figure 12: Comparison of observed and simulated pollutograph. ....	32
Figure 13: Range of Nash-Sutcliffe Efficiency regarding an alteration of parameter values. ....	34
Figure 14: Hydrograph simulation with alterations of Depression Storage and fixed Manning Coefficient at 0.025. ....	34
Figure 15: Hydrograph simulation with alterations of Manning coefficient and fixed Depression Storage at 0.5 mm. ....	35
Figure 16: Boxplots which present the hydrological calibration results by combining all BFC efficiencies for different DS and a fixed n of 0.01. ....	36
Figure 17: Boxplots which present the hydrological calibration results by combining all BFC efficiencies for different DS and a fixed n of 0.0125. ....	36
Figure 18: Boxplots which present the hydrological calibration results by combining all BFC efficiencies for different DS and a fixed n of 0.025. ....	37
Figure 19: Comparison of the uncalibrated model on the left side and the hydrologically calibrated model on the right side with the events (from the top to the bottom): 1) RG_24-11-23h, 2) RG_6-9-12h, 3) RG_24-09-1h and 4) RG_14-11-9h. ....	38
Figure 20: Comparison of the uncalibrated model on the left side and the hydrologically calibrated model on the right side with the event RG_4-12-9h. ....	39
Figure 21: TSS Concentration for a Wash-off Coefficient of 0.001 and an alteration of the initial built-up between 10 and 200kg/ha. ....	39
Figure 22: TSS Concentration for an initial built-up of 100 kg/ha and an alteration of the wash-off coefficient between 0.0001 and 0.01. ....	40
Figure 23: All BFC results presented with boxplots with all parameter value combinations. ....	42

## List of Tables and Figures

---

Figure 24: Event RG_24-11-23h simulated with the initial model (on top) and the calibrated model (on the bottom) presented with pollutographs of the concentration (left) and of the pollution load (right).....	45
Figure 25: Event RG_6-9-12h simulated with the initial model (on top) and the calibrated model (on the bottom) presented with pollutographs of the concentration (left) and of the pollution load (right).....	45
Figure 26: Event RG_24-9-1h simulated with the initial model (on top) and the calibrated model (on the bottom) presented with pollutographs of the concentration (left) and of the pollution load (right).....	46
Figure 27: Event RG_14-11-10h simulated with the initial model (on top) and the calibrated model (on the bottom) presented with pollutographs of the concentration (left) and of the pollution load (right).....	46
Figure 28: Event RG_4-12-10h simulated with the initial model (on top) and the calibrated model (on the bottom) presented with pollutographs of the concentration (left) and of the pollution load (right).....	47
Figure 29: NSE-Q results (left side) and KGE-Q results (right side) of the initial model (horizontal axis) and the calibrated model (vertical axis).....	48
Figure 30: Scatterplots comparing BFC results of the initial model and the model with set 1 as input values.....	51
Figure 31: Scatterplots comparing BFC results of the initial model and the model with set 2 as input values.....	51
Figure 32: Scatterplots comparing BFC results of the initial model and the model with set 3 as input values.....	52
Figure 33: Scatterplots comparing BFC results of the initial model and the model with set 4 as input values.....	52
Figure 34: Relative reduction of runoff and TSS through a land de-sealing of 50%, simulated with the uncalibrated model (on the left side) and the calibrated model (on the right side).....	54
Figure 35: Relative reduction of runoff and TSS through land de-sealing of 100%, simulated with the uncalibrated model (on the left side) and the calibrated model (on the right side).....	54

## 12. Appendix

### Table of contents of the Appendix

<b>1.</b>	<b><i>Model Calibration</i></b>	<b>1</b>
1.1	Hydrological Calibration	1
1.2	Calibration of the Water Quality Response	4
<b>2.</b>	<b><i>De-sealing Modelling</i></b>	<b>7</b>
<b>3.</b>	<b><i>Curriculum Vitae</i></b>	<b>12</b>

# 1. Model Calibration

## 1.1 Hydrological Calibration

Results of the 4 tested best-fit-criteria (Nash-Sutcliffe-Efficiency of the runoff, Kling-Gupta-Efficiency of the runoff and the Relative Percentage Difference of the maximum runoff  $Q_{max}$  and the total discharged volume  $V_{tot}$ ) for all parameter value combinations, analysed for every calibration event.

Table 1: Stormwater event 24/11/2021, evaluation of the results with each parameter value set.

NSE Q	n						
DepStore		0	0.25	0.5	0.75	1	1.25
	0.01	0.78	0.79	0.80	0.81	0.81	0.80
	0.0125	0.80	0.81	0.83	0.83	0.83	0.81
	0.025	0.86	0.87	0.86	0.86	0.84	0.80
KGE Q							
DepStore		0	0.25	0.5	0.75	1	1.25
	0.01	0.75	0.76	0.77	0.77	0.76	0.75
	0.0125	0.77	0.78	0.78	0.78	0.78	0.77
	0.025	0.78	0.79	0.79	0.78	0.77	0.75
RPD Qmax							
DepStore		0	0.25	0.5	0.75	1	1.25
	0.01	0.72	0.72	0.72	0.72	0.72	0.72
	0.0125	0.70	0.70	0.70	0.70	0.70	0.70
	0.025	0.62	0.62	0.62	0.62	0.62	0.62
RPD V							
DepStore		0	0.25	0.5	0.75	1	1.25
	0.01	0.39	0.39	0.39	0.39	0.39	0.39
	0.0125	0.42	0.42	0.42	0.42	0.42	0.42
	0.025	0.45	0.45	0.45	0.45	0.45	0.45

## Model Calibration

Table 2: Stormwater event 06/09/2022, evaluation of the results with each parameter value set.

NSE Q		n						
DepStore			0	0.25	0.5	0.75	1	1.25
	0.01		0.79	0.78	0.77	0.77	0.76	0.76
	0.0125		0.78	0.77	0.76	0.76	0.75	0.74
	0.025		0.72	0.71	0.70	0.69	0.68	0.67
KGE Q		n						
DepStore			0	0.25	0.5	0.75	1	1.25
	0.01		0.72	0.71	0.71	0.71	0.69	0.69
	0.0125		0.71	0.70	0.69	0.69	0.68	0.67
	0.025		0.65	0.64	0.63	0.62	0.61	0.60
RPD Qmax		n						
DepStore			0	0.25	0.5	0.75	1	1.25
	0.01		0.72	0.72	0.72	0.72	0.72	0.72
	0.0125		0.71	0.71	0.71	0.71	0.71	0.71
	0.025		0.65	0.65	0.65	0.65	0.65	0.65
RPD V		n						
DepStore			0	0.25	0.5	0.75	1	1.25
	0.01		0.88	0.88	0.87	0.86	0.86	0.85
	0.0125		0.88	0.88	0.87	0.86	0.86	0.85
	0.025		0.88	0.88	0.87	0.86	0.86	0.85

Table 3: Stormwater event 24/09/2022, evaluation of the results with each parameter value set.

NSE Q		n						
DepStore			0	0.25	0.5	0.75	1	1.25
	0.01		0.53	0.53	0.53	0.53	0.53	0.53
	0.0125		0.62	0.53	0.53	0.53	0.53	0.53
	0.025		0.53	0.52	0.52	0.52	0.52	0.52
KGE Q		n						
DepStore			0	0.25	0.5	0.75	1	1.25
	0.01		0.31	0.31	0.31	0.31	0.31	0.31
	0.0125		0.55	0.31	0.31	0.31	0.31	0.31
	0.025		0.30	0.30	0.30	0.30	0.30	0.30
RPD Qmax		n						
DepStore			0	0.25	0.5	0.75	1	1.25
	0.01		0.19	0.19	0.19	0.19	0.19	0.19
	0.0125		0.19	0.19	0.19	0.19	0.19	0.19
	0.025		0.17	0.17	0.17	0.17	0.17	0.17
RPD V		n						
DepStore			0	0.25	0.5	0.75	1	1.25
	0.01		-0.98	-0.98	-0.98	-0.98	-0.98	-0.98
	0.0125		-0.98	-0.98	-0.98	-0.98	-0.98	-0.98
	0.025		-0.98	-0.98	-0.98	-0.98	-0.98	-0.98

## Model Calibration

Table 4: Stormwater event 14/11/2022, evaluation of the results with each parameter value set.

NSE Q	n						
DepStore		0	0.25	0.5	0.75	1	1.25
	0.01	0.56	0.56	0.56	0.56	0.56	0.56
	0.0125	0.55	0.55	0.55	0.55	0.56	0.56
	0.025	0.54	0.54	0.54	0.54	0.54	0.54
KGE Q							
DepStore		0	0.25	0.5	0.75	1	1.25
	0.01	0.40	0.40	0.41	0.42	0.42	0.42
	0.0125	0.40	0.41	0.41	0.42	0.42	0.43
	0.025	0.41	0.41	0.42	0.42	0.42	0.43
RPD Qmax							
DepStore		0.00	0.25	0.50	0.75	1.00	1.25
	0.01	0.89	0.89	0.89	0.89	0.89	0.89
	0.0125	0.90	0.90	0.90	0.90	0.90	0.90
	0.025	0.96	0.96	0.96	0.96	0.96	0.96
RPD V							
DepStore		0	0.25	0.5	0.75	1	1.25
	0.01	0.56	0.56	0.56	0.57	0.57	0.58
	0.0125	0.56	0.56	0.57	0.57	0.57	0.58
	0.025	0.56	0.56	0.57	0.57	0.57	0.58

Table 5: Stormwater event 04/12/2022, evaluation of the results with each parameter value set.

NSE Q	n						
DepStore		0	0.25	0.5	0.75	1	1.25
	0.01	0.65	0.67	0.70	0.71	0.70	0.63
	0.0125	0.64	0.67	0.68	0.70	0.67	0.60
	0.025	0.61	0.62	0.62	0.60	0.55	0.46
KGE Q							
DepStore		0	0.25	0.5	0.75	1	1.25
	0.01	0.31	0.42	0.54	0.65	0.73	0.73
	0.0125	0.31	0.43	0.54	0.66	0.72	0.71
	0.025	0.33	0.43	0.55	0.63	0.63	0.57
RPD Qmax							
DepStore		0	0.25	0.5	0.75	1	1.25
	0.01	0.79	0.79	0.79	0.79	0.74	0.61
	0.0125	0.76	0.76	0.76	0.74	0.69	0.55
	0.025	0.59	0.59	0.57	0.53	0.48	0.41
RPD V							
DepStore		0	0.25	0.5	0.75	1	1.25
	0.01	0.50	0.52	0.56	0.64	0.72	0.80
	0.0125	0.50	0.52	0.57	0.64	0.73	0.81
	0.025	0.51	0.53	0.58	0.66	0.75	0.83

## 1.2 Calibration of the Water Quality Response

Results of the 4 tested best-fit-criteria (Nash-Sutcliffe-Efficiency of the concentration and of the pollution load as well as Kling-Gupta-Efficiency of the concentration and of the pollution load) for all parameter value combinations, analysed for every calibration event.

Table 6: Stormwater event 24/11/2021, results for each BFC.

NSE C		KW									
IB		10	30	50	75	100	125	150	175	200	
	0.0001	-0.74	-0.69	-0.65	-0.60	-0.55	-0.51	-0.46	-0.41	-0.37	
	0.0005	-0.65	-0.46	-0.28	-0.08	0.10	0.25	0.38	0.48	0.56	
	0.001	-0.56	-0.20	0.09	0.38	0.56	0.65	0.65	0.54	0.35	
	0.005	0.07	<b>0.68</b>	-0.09	-3.00	-8.06	-15	-25	-36	-50	
NSE PL											
IB		10	30	50	75	100	125	150	175	200	
	0.0001	-0.31	-0.28	-0.25	-0.21	-0.18	-0.14	-0.11	-0.07	-0.04	
	0.0005	-0.25	-0.11	0.03	0.18	0.32	0.44	0.54	0.63	0.70	
	0.001	-0.18	0.09	0.31	0.54	0.69	0.79	0.81	0.77	0.67	
	0.005	0.29	<b>0.82</b>	0.42	-1.41	-4.69	-9.44	-16	-23	-32	
KGE C											
IB		10	30	50	75	100	125	150	175	200	
	0.0001	-0.42	-0.40	-0.38	-0.36	-0.34	-0.32	-0.29	-0.27	-0.25	
	0.0005	-0.38	-0.29	-0.21	-0.10	0.01	0.12	0.23	0.34	0.44	
	0.001	-0.34	-0.16	0.01	0.23	0.44	0.64	<b>0.79</b>	0.77	0.60	
	0.005	-0.01	0.77	0.29	-0.75	-1.79	-2.84	-3.89	-4.94	-5.99	
KGE PL											
IB		10	30	50	75	100	125	150	175	200	
	0.0001	-0.41	-0.39	-0.37	-0.35	-0.33	-0.30	-0.28	-0.26	-0.23	
	0.0005	-0.37	-0.28	-0.19	-0.07	0.04	0.16	0.27	0.38	0.50	
	0.001	-0.33	-0.14	0.04	0.26	0.49	0.70	<b>0.86</b>	0.77	0.56	
	0.005	0.01	0.83	0.23	-0.85	-1.94	-3.02	-4.11	-5.19	-6.28	

## Model Calibration

Table 7: Stormwater event 06/09/2022, results for each BFC.

NSE C	KW									
IB		10	30	50	75	100	125	150	175	200
	0.0001	-0.21	-0.14	-0.08	0.00	0.07	0.14	0.20	0.26	0.32
	0.0005	-0.09	0.18	0.39	0.57	0.67	0.69	0.63	0.48	0.24
	0.001	0.03	0.43	0.66	<b>0.71</b>	0.50	0.02	-0.73	-1.74	-3.02
	0.005	0.33	0.28	-1.35	-5.61	-12	-22	0.63	-47	0.24
NSE PL										
IB		10	30	50	75	100	125	150	175	200
	0.0001	-0.06	-0.03	0.00	0.04	0.08	0.11	0.14	0.17	0.20
	0.0005	0.00	0.13	0.24	0.35	0.43	0.49	0.51	0.50	0.46
	0.001	0.05	0.27	0.42	0.52	<b>0.53</b>	0.44	0.25	-0.03	-0.41
	0.005	0.23	0.51	0.36	-0.44	-1.92	-4.07	0.51	-10	0.46
KGE C										
IB		10	30	50	75	100	125	150	175	200
	0.0001	-0.40	-0.36	-0.31	-0.25	-0.20	-0.14	-0.08	-0.02	0.03
	0.0005	-0.32	-0.11	0.09	0.34	0.59	0.80	0.78	0.56	0.31
	0.001	-0.24	0.12	0.48	<b>0.84</b>	0.57	0.12	-0.33	-0.78	-1.24
	0.005	0.01	0.50	-0.18	-1.34	-2.54	-3.75	0.78	-6.16	0.31
KGE PL										
IB		10	30	50	75	100	125	150	175	200
	0.0001	-0.43	-0.40	-0.36	-0.32	-0.28	-0.24	-0.20	-0.16	-0.12
	0.0005	-0.37	-0.22	-0.07	0.10	0.28	0.44	0.57	0.65	0.63
	0.001	-0.31	-0.05	0.20	0.49	0.67	0.57	0.30	-0.01	-0.34
	0.005	-0.14	0.43	<b>0.69</b>	0.08	-0.67	-1.42	0.57	-2.94	0.63

Table 8: Stormwater event 24/09/2022, results for each BFC

NSE C	KW									
IB		10	30	50	75	100	125	150	175	200
	0.0001	-0.47	-0.42	-0.37	-0.32	-0.27	-0.23	-0.19	-0.15	-0.12
	0.0005	-0.38	-0.19	-0.07	-0.02	-0.08	-0.24	-0.50	-0.87	-1.35
	0.001	-0.28	-0.03	-0.01	-0.29	-0.93	-1.93	-3.28	-4.99	-7.05
	0.005	0.08	-0.38	-2.97	-9.22	-19	-32	-48	-68	-91
NSE PL										
IB		10	30	50	75	100	125	150	175	200
	0.0001	-0.67	-0.57	-0.49	-0.39	-0.30	-0.22	-0.15	-0.08	-0.03
	0.0005	-0.50	-0.17	0.04	<b>0.13</b>	0.03	-0.26	-0.74	-1.41	-2.27
	0.001	-0.35	0.08	0.11	-0.42	-1.58	-3.37	-5.78	-8.82	-12.49
	0.005	0.06	-0.54	-3.98	-12	-25	-42	-64	-90	-121
KGE C										
IB		10	30	50	75	100	125	150	175	200
	0.0001	-0.61	-0.57	-0.53	-0.48	-0.43	-0.38	-0.33	-0.28	-0.24
	0.0005	-0.52	-0.33	-0.16	0.01	0.12	0.14	0.06	-0.10	-0.30
	0.001	-0.41	-0.09	0.13	0.15	-0.12	-0.53	-1.00	-1.50	-2.01
	0.005	0.04	<b>0.28</b>	-0.79	-2.30	-3.84	-5.38	-6.93	-8.48	-10
KGE										
IB		10	30	50	75	100	125	150	175	200
	0.0001	-0.48	-0.42	-0.37	-0.30	-0.24	-0.17	-0.11	-0.05	0.01
	0.0005	-0.38	-0.13	0.10	0.34	<b>0.49</b>	0.44	0.23	-0.04	-0.34
	0.001	-0.27	0.15	0.47	0.37	-0.11	-0.67	-1.26	-1.85	-2.45
	0.005	0.10	0.32	-0.83	-2.40	-3.98	-5.57	-7.16	-8.75	-10

## Model Calibration

Table 9: Stormwater event 14/11/2022, results for each BFC.

NSE C	KW									
IB		10	30	50	75	100	125	150	175	200
	0.0001	-1.26	-0.98	-0.76	-0.56	-0.45	-0.43	-0.49	-0.65	-0.89
	0.0005	-0.82	-0.28	-0.63	-2.33	-5.42	-9.91	-16	-23	-32
	0.001	-0.50	-0.36	-2.50	-8.40	-18	-31	-48	-68	-92
	0.005	<b>-0.03</b>	-8.32	-31	-81	-154	-250	-368	-510	-676
NSE PL										
IB		10	30	50	75	100	125	150	175	200
	0.0001	-0.03	0.23	0.33	0.25	-0.06	-0.62	-1.41	-2.44	-3.71
	0.0005	0.33	-0.26	-3.09	-9.76	-20	-34	-51	-71	-96
	0.001	<b>0.42</b>	-2.11	-9.73	-26	-51	-84	-124	-173	-229
	0.005	-0.24	-12	-38	-92	-169	-270	-395	-542	-714
KGE C										
IB		10	30	50	75	100	125	150	175	200
	0.0001	-0.50	-0.36	-0.23	-0.08	0.06	0.17	0.25	0.27	0.25
	0.0005	-0.25	0.22	0.33	-0.17	-0.88	-1.63	-2.40	-3.18	-3.96
	0.001	-0.04	0.41	-0.29	-1.49	-2.73	-3.98	-5.24	-6.50	-7.76
	0.005	<b>0.42</b>	-1.68	-4.27	-7.54	-11	-14	-17	-21	-24
KGE PL										
IB		10	30	50	75	100	125	150	175	200
	0.0001	-0.30	0.03	0.33	<b>0.59</b>	0.48	0.13	-0.27	-0.69	-1.12
	0.0005	0.17	0.31	-0.96	-2.62	-4.28	-5.95	-7.62	-9.29	-11
	0.001	0.47	-0.61	-2.59	-5.08	-7.57	-10	-13	-15	-18
	0.005	0.46	-2.44	-5.63	-9.63	-14	-18	-22	-26	-30

Table 10: Stormwater event 04/12/2022, results for each BFC.

NSE C	KW									
IB		10	30	50	75	100	125	150	175	200
	0.0001	-7.30	-7.02	-6.76	-6.45	-6.14	-5.85	-5.58	-5.31	-5.06
	0.0005	-6.76	-5.58	-4.61	-3.68	-3.07	<b>-2.79</b>	-2.83	-3.20	-3.88
	0.001	-6.15	-4.21	-3.08	-2.84	-3.88	-6.20	-9.81	-15	-21
	0.005	-3.16	-9.40	-35	-96	-186	-308	-461	-644	-858
NSE PL										
IB		10	30	50	75	100	125	150	175	200
	0.0001	-0.05	-0.01	0.03	0.09	0.13	0.18	0.23	0.27	0.31
	0.0005	0.03	0.23	0.38	0.53	0.63	<b>0.68</b>	0.67	0.61	0.50
	0.001	0.13	0.45	0.63	0.67	0.50	0.12	-0.46	-1.26	-2.26
	0.005	0.63	-0.39	-4.63	-14	-29	-49	-74	-104	-139
KGE C										
IB		10	30	50	75	100	125	150	175	200
	0.0001	-0.42	-0.37	-0.33	-0.27	-0.22	-0.17	-0.12	-0.07	-0.02
	0.0005	-0.33	-0.12	0.06	0.20	<b>0.22</b>	0.09	-0.12	-0.39	-0.68
	0.001	-0.22	0.13	0.22	-0.12	-0.68	-1.30	-1.95	-2.61	-3.27
	0.005	0.22	-1.89	-4.50	-7.81	-11	-14	-18	-21	-24
KGE PL										
IB		10	30	50	75	100	125	150	175	200
	0.0001	-0.41	-0.37	-0.33	-0.28	-0.23	-0.18	-0.13	-0.08	-0.03
	0.0005	-0.33	-0.13	0.07	0.31	0.53	0.70	0.71	0.55	0.33
	0.001	-0.23	0.16	0.53	<b>0.72</b>	0.33	-0.15	-0.64	-1.14	-1.64
	0.005	0.51	-0.58	-2.54	-5.00	-7.47	-9.93	-12	-15	-17

## 2. De-sealing Modelling

Table 11: De-sealing results for every event with the uncalibrated model.

	50% desealing					100% desealing				
	PD Q <sub>max</sub>	PD V <sub>tot</sub>	PD C <sub>max</sub>	PD PL	PD EMC	PD Q <sub>max</sub>	PD V <sub>tot</sub>	PD C <sub>max</sub>	PD PL	PD EMC
RG_24-11-4h	45	53	-11	46	-3	100	100	100	100	100
RG_24-11-13h	45	47	-6	46	0	100	100	100	100	100
RG_24-11-22h	45	51	-8	45	-2	100	100	100	100	100
RG_11-3-17h	32	15	-6	16	-12	47	42	49	45	17
RG_13-3-9h	33	40	6	38	-5	68	79	-6	78	61
RG_20-3-16h	52	49	0	50	0	90	98	89	100	97
RG_20-4-14h	46	50	-10	42	2	100	100	100	100	100
RG_24-6-8h	47	50	-11	38	-14	100	100	100	100	100
RG_6-9-all	39	43	-13	33	-26	83	87	79	86	22
RG_7-9-2h	-1	11	-3	-31	-38	12	33	-57	-51	-45
RG_7-9-22h	47	47	6	48	-2	94	96	83	99	82
RG_14-9-4h	45	49	-8	43	-3	100	100	100	100	100
RG_24-9-1h	43	40	-14	38	-13	73	80	52	78	39
RG_14-11-9h	14	19	3	-31	-35	33	50	15	-19	1
RG_28-11-7h	43	50	-16	45	-2	100	100	100	100	100
RG_4-12-9h	43	50	-11	44	-2	100	100	100	100	100
RG_15-12-4h	32	43	-8	45	3	70	88	51	94	82
<b>mean results</b>	38	42	-7	33	-9	81	85	68	77	68
<b>median results</b>	43	47	-8	43	-3	94	98	89	100	97
<b>Std. Deviation</b>	13	13	6	24	12	26	22	45	44	44

Table 12: De-sealing results for every event with the calibrated model.

	50% desealing					100% desealing				
	PD Q <sub>max</sub>	PD V <sub>tot</sub>	PD C <sub>max</sub>	PD PL	PD EMC	PD Q <sub>max</sub>	PD V <sub>tot</sub>	PD C <sub>max</sub>	PD PL	PD EMC
RG_24-11-4h	48	51	-2	48	-3	100	100	100	100	100
RG_24-11-13h	49	47	-2	48	1	89	95	89	99	94
RG_24-11-22h	50	49	-2	48	-4	100	100	100	100	100
RG_11-3-17h	33	24	13	34	9	52	48	66	70	51
RG_13-3-9h	34	39	15	45	7	69	79	65	91	77
RG_20-3-16h	48	50	0	50	0	90	98	90	100	97
RG_20-4-14h	50	50	-2	47	-1	100	100	100	100	100
RG_24-6-8h	50	51	-3	47	-3	100	100	100	100	100
RG_6-9-all	42	43	-4	47	3	84	87	83	97	83
RG_7-9-2h	11	20	8	2	-18	22	40	7	3	9
RG_7-9-22h	49	47	3	49	1	94	96	89	100	92
RG_14-9-4h	47	49	-5	43	-5	100	100	100	100	100
RG_24-9-1h	44	40	4	46	5	74	80	69	93	77
RG_14-11-9h	24	27	6	30	-4	41	54	47	63	41
RG_28-11-7h	46	49	-15	43	-5	100	100	100	100	100
RG_4-12-9h	47	51	-6	47	-2	100	100	100	100	100
RG_15-12-4h	34	43	11	46	4	71	88	68	96	87
<b>mean results</b>	41	43	1	42	-1	81	86	81	89	83
<b>median results</b>	47	47	-2	47	-1	90	96	89	100	94
<b>Std. Deviation</b>	11	10	8	11	6	23	19	24	24	25

## De-sealing Modelling

The tables below present the simulations of all scenarios (0-50-100% de-sealing) for the event RG\_7-9-2h which prove that PSC produced no additional runoff at a de-sealing of 50% and 100%. The uncalibrated and the calibrated model are compared by observing the runoff contribution of each subcatchment separately.

Table 13: Scenario of a 50% de-sealing with the uncalibrated model.

PSC - 50%			ISC - 50%- uncalib			DSC - 50%- uncalib		
-uncalib	Q	C		Q	C		Q	C
	(l/s)	(mg/l)		(l/s)	(mg/l)		(l/s)	(mg/l)
00:50:00	0	0	00:50:00	0	0	00:50:00	0	0
00:55:00	0	0	00:55:00	0	0	00:55:00	0	0
01:00:00	0	0	01:00:00	0	0	01:00:00	0	0
01:05:00	0	0	01:05:00	0.04	12	01:05:00	0	0
01:10:00	0	0	01:10:00	0.62	204	01:10:00	0	0
01:15:00	0	0	01:15:00	0.74	160	01:15:00	0	0
01:20:00	0	0	01:20:00	1.25	134	01:20:00	0	0
01:25:00	0	0	01:25:00	1.3	0	01:25:00	0.01	2
01:30:00	0	0	01:30:00	2.66	0	01:30:00	0.5	165
01:35:00	0	0	01:35:00	1.03	0	01:35:00	0.38	98
01:40:00	0	0	01:40:00	0.3	0	01:40:00	0.18	39
01:45:00	0	0	01:45:00	0.14	0	01:45:00	0.1	21
01:50:00	0	0	01:50:00	0.1	0	01:50:00	0.07	14
01:55:00	0	0	01:55:00	1.67	0	01:55:00	0.54	114
02:00:00	1.14	418	02:00:00	3.9	0	02:00:00	1.77	277
02:05:00	1.46	0	02:05:00	2.96	0	02:05:00	1.7	0
02:10:00	1.6	0	02:10:00	2.87	0	02:10:00	1.79	0
02:15:00	1.77	0	02:15:00	2.97	0	02:15:00	1.97	0
02:20:00	1.87	0	02:20:00	2.98	0	02:20:00	2.08	0
02:25:00	2.65	0	02:25:00	4.08	0	02:25:00	2.96	0
02:30:00	1.83	0	02:30:00	2.55	0	02:30:00	2.02	0
02:35:00	0.85	0	02:35:00	1.03	0	02:35:00	0.91	0
02:40:00	0.29	0	02:40:00	0.25	0	02:40:00	0.29	0
02:45:00	0.12	0	02:45:00	0.09	0	02:45:00	0.11	0
02:50:00	0.06	0	02:50:00	0.04	0	02:50:00	0.05	0
02:55:00	0.03	0	02:55:00	0.02	0	02:55:00	0.03	0

## De-sealing Modelling

Table 14: Scenario of a 50% de-sealing with the calibrated model.

PSC - 50%			ISC - 50%-calib			DSC - 50%-calib		
-calib	Q	C		Q	C		Q	C
	(l/s)	(mg/l)		(l/s)	(mg/l)		(l/s)	(mg/l)
00:50:00	0	0	00:50:00	0	0	00:50:00	0	0
00:55:00	0	0	00:55:00	0	0	00:55:00	0	0
01:00:00	0	0	01:00:00	0	0	01:00:00	0	0
01:05:00	0	0	01:05:00	0.01	1	01:05:00	0	0
01:10:00	0	0	01:10:00	0.75	186	01:10:00	0	0
01:15:00	0	0	01:15:00	0.76	179	01:15:00	0	0
01:20:00	0	0	01:20:00	1.3	289	01:20:00	0	0
01:25:00	0	0	01:25:00	1.31	246	01:25:00	0.01	2
01:30:00	0	0	01:30:00	2.72	433	01:30:00	0.5	124
01:35:00	0	0	01:35:00	0.93	49	01:35:00	0.38	93
01:40:00	0	0	01:40:00	0.2	10	01:40:00	0.18	42
01:45:00	0	0	01:45:00	0.09	5	01:45:00	0.1	23
01:50:00	0	0	01:50:00	0.08	4	01:50:00	0.07	16
01:55:00	0	0	01:55:00	1.83	87	01:55:00	0.54	128
02:00:00	1.14	313	02:00:00	3.95	131	02:00:00	1.77	410
02:05:00	1.46	345	02:05:00	2.94	0	02:05:00	1.7	282
02:10:00	1.6	285	02:10:00	2.87	0	02:10:00	1.79	218
02:15:00	1.77	225	02:15:00	2.98	0	02:15:00	1.97	170
02:20:00	1.87	155	02:20:00	2.98	0	02:20:00	2.08	117
02:25:00	2.65	133	02:25:00	4.1	0	02:25:00	2.96	100
02:30:00	1.83	20	02:30:00	2.51	0	02:30:00	2.02	14
02:35:00	0.85	6	02:35:00	0.93	0	02:35:00	0.91	4
02:40:00	0.29	2	02:40:00	0.14	0	02:40:00	0.29	1
02:45:00	0.12	1	02:45:00	0.04	0	02:45:00	0.11	0
02:50:00	0.06	0	02:50:00	0.02	0	02:50:00	0.05	0
02:55:00	0.03	0	02:55:00	0.01	0	02:55:00	0.03	0

Table 15: Scenario of a 100% de-sealing with the calibrated model

PSC - 100% - calib		DSC - 100% - calib	
Q (l/s)	C (mg/l)	Q (l/s)	C (mg/l)
00:50:00	0	00:50:00	0
00:55:00	0	00:55:00	0
01:00:00	0	01:00:00	0
01:05:00	0	01:05:00	0
01:10:00	0	01:10:00	0
01:15:00	0	01:15:00	0
01:20:00	0	01:20:00	0
01:25:00	0	01:25:00	0.01
01:30:00	0	01:30:00	0.81
01:35:00	0	01:35:00	0.73
01:40:00	0	01:40:00	0.38
01:45:00	0	01:45:00	0.23
01:50:00	0	01:50:00	0.16
01:55:00	0	01:55:00	0.95
02:00:00	1.14	02:00:00	3.28
02:05:00	1.46	02:05:00	3.37
02:10:00	1.6	02:10:00	3.56
02:15:00	1.77	02:15:00	3.91
02:20:00	1.87	02:20:00	4.15
02:25:00	2.65	02:25:00	5.82
02:30:00	1.83	02:30:00	4.12
02:35:00	0.85	02:35:00	1.97
02:40:00	0.29	02:40:00	0.72
02:45:00	0.12	02:45:00	0.31
02:50:00	0.06	02:50:00	0.16
02:55:00	0.03	02:55:00	0.09

Table 16: Scenario of a 100% de-sealing with the uncalibrated model.

PSC - 100% - uncalib		DS - 100% - uncalib	
Q (l/s)	C (mg/l)	Q (l/s)	C (mg/l)
00:50:00	0	00:50:00	0
00:55:00	0	00:55:00	0
01:00:00	0	01:00:00	0
01:05:00	0	01:05:00	0
01:10:00	0	01:10:00	0
01:15:00	0	01:15:00	0
01:20:00	0	01:20:00	0
01:25:00	0	01:25:00	0.01
01:30:00	0	01:30:00	0.81
01:35:00	0	01:35:00	0.73
01:40:00	0	01:40:00	0.38
01:45:00	0	01:45:00	0.23
01:50:00	0	01:50:00	0.16
01:55:00	0	01:55:00	0.95
02:00:00	1.14	02:00:00	3.28
02:05:00	1.46	02:05:00	3.37
02:10:00	1.6	02:10:00	3.56
02:15:00	1.77	02:15:00	3.91
02:20:00	1.87	02:20:00	4.15
02:25:00	2.65	02:25:00	5.82
02:30:00	1.83	02:30:00	4.12
02:35:00	0.85	02:35:00	1.97
02:40:00	0.29	02:40:00	0.72
02:45:00	0.12	02:45:00	0.31
02:50:00	0.06	02:50:00	0.16
02:55:00	0.03	02:55:00	0.09

Table 17: Scenario of a 0% de-sealing (initial parameter values) with the calibrated model.

PSC - 0% -calib		ISC - 0% -calib	
Q (l/s)	C (mg/l)	Q (l/s)	C (mg/l)
00:50:00	0	00:50:00	0
00:55:00	0	00:55:00	0
01:00:00	0	01:00:00	0
01:05:00	0	01:05:00	0.01
01:10:00	0	01:10:00	1.4
01:15:00	0	01:15:00	1.52
01:20:00	0	01:20:00	2.58
01:25:00	0	01:25:00	2.61
01:30:00	0	01:30:00	5.41
01:35:00	0	01:35:00	1.91
01:40:00	0	01:40:00	0.46
01:45:00	0	01:45:00	0.21
01:50:00	0	01:50:00	0.17
01:55:00	0	01:55:00	3.58
02:00:00	1.14	02:00:00	7.89
02:05:00	1.46	02:05:00	5.89
02:10:00	1.6	02:10:00	5.73
02:15:00	1.77	02:15:00	5.95
02:20:00	1.87	02:20:00	5.95
02:25:00	2.65	02:25:00	8.19
02:30:00	1.83	02:30:00	5.03
02:35:00	0.85	02:35:00	1.91
02:40:00	0.29	02:40:00	0.35
02:45:00	0.12	02:45:00	0.1
02:50:00	0.06	02:50:00	0.04
02:55:00	0.03	02:55:00	0.02

Table 18: Scenario of a 0% de-sealing (initial parameter values) with the uncalibrated model.

PSC - 0% -uncalib		ISC - 0% -uncalib	
Q (l/s)	C (mg/l)	Q (l/s)	C (mg/l)
00:50:00	0	00:50:00	0
00:55:00	0	00:55:00	0
01:00:00	0	01:00:00	0
01:05:00	0	01:05:00	0.05
01:10:00	0	01:10:00	1.07
01:15:00	0	01:15:00	1.43
01:20:00	0	01:20:00	2.43
01:25:00	0	01:25:00	2.59
01:30:00	0	01:30:00	5.22
01:35:00	0	01:35:00	2.19
01:40:00	0	01:40:00	0.71
01:45:00	0	01:45:00	0.34
01:50:00	0	01:50:00	0.23
01:55:00	0	01:55:00	3.09
02:00:00	1.14	02:00:00	7.65
02:05:00	1.46	02:05:00	5.97
02:10:00	1.6	02:10:00	5.75
02:15:00	1.77	02:15:00	5.94
02:20:00	1.87	02:20:00	5.95
02:25:00	2.65	02:25:00	8.1
02:30:00	1.83	02:30:00	5.18
02:35:00	0.85	02:35:00	2.19
02:40:00	0.29	02:40:00	0.62
02:45:00	0.12	02:45:00	0.24
02:50:00	0.06	02:50:00	0.12
02:55:00	0.03	02:55:00	0.07

### 3. Curriculum Vitae

CORNELIA FÜRNKRANZ



#### Personal information

Name	Cornelia Fürnkranz
Address	Montevideogasse 10, 1130 Vienna, Austria
Phone	+43 650 6912913
E-mail	c.fuernkranz@outlook.at
Date of Birth	17/11/1996
Nationality	Austrian

#### Education

2020 – present	<b>Master programme: Civil Engineering and Water Management</b>
2016 – 2020	<b>Bachelor's degree: Civil Engineering and Water Management</b> University of Natural Resources and Life Sciences (BOKU), Vienna, Austria
	<b>Erasmus – Exchange Semesters:</b>
01 – 07 2021	Water Sciences and Technologies – Polytech Montpellier, France
01 – 07 2018	Groundwater Hydrology & Coastal Engineering – Polytechnic University of Valencia, Spain
2006 – 2014	<b>Secondary School GRG13 Wenzgasse, Vienna, Austria</b> Graduation June 2014
01 – 07 2012	<b>Wellington High School, New Zealand</b> Exchange semester

#### Work experience

10 2022 – 02 2023	<b>HydroSciences Montpellier, France</b>
Research Traineeship	Research Group: Urban Hydrology and Hydraulics <ul style="list-style-type: none"><li>- Master thesis cooperation: "Experimental Stormwater Runoff Modelling to Simulate the Reduction Potential of Pollutant Loads Through Land De-Sealing Measures".</li></ul>
08 – 09 2022	<b>Engineers Without Borders, Democratic Republic of the Congo</b>
	Voluntary work on site for the project "TshuWa" <ul style="list-style-type: none"><li>- Rainwater management planning &amp; building supervision</li><li>- Educational campaign on water hygiene</li></ul>
2020 – 2022	<b>University of Natural Resources and Life Sciences, Vienna</b>
Student assistant	Institute for Soil Physics and Rural Water Management <ul style="list-style-type: none"><li>- Teaching positions: "Soil Conservation and Soil Protection (in English)" and "Practical Field Works"</li></ul>
2019 – 2022	<b>Fürnkranz Geoconsulting Umwelttechnik GmbH, Vienna</b>
Marginal employment	<ul style="list-style-type: none"><li>- Soil exploration, groundwater monitoring, surveying, contaminant investigations</li><li>- Dimensioning of water infiltration basins</li><li>- Bachelor thesis cooperation: "Soil physical investigations for the realisation of a water infiltration system"</li></ul>

08 – 09 2019 & 2021 Internships	<b>Dipl.-Ing. Schattovits Ziviltechniker GmbH, Vienna</b> <ul style="list-style-type: none"> <li>- Dimensioning of hydrological &amp; hydraulic constructions</li> <li>- Creation of technical plans and technical reports in the fields of urban water management</li> </ul>
08 2020 Internship	<b>PORR Umwelttechnik GmbH, Vienna</b> <ul style="list-style-type: none"> <li>- Research and planning of geophysical depollution of contaminated sites</li> </ul>
08 2018 Internship	<b>AEP Planung und Beratung GmbH, Tyrol</b> <ul style="list-style-type: none"> <li>- Creation of technical plans in the fields of urban water management and road engineering</li> </ul>
07 2018 Internship	<b>Team Kernstock Ziviltechniker GmbH, Vienna</b> <ul style="list-style-type: none"> <li>- Calculations and creation of technical plans in the fields of urban water management and landfill construction</li> </ul>

## Professional skills

Electronic data processing	MS Office Auto CAD MathCAD
Additional courses	ArcGIS: "GIS simulations of soil erosion and sediment transport", within the transnational cooperation project Aktion82p3 at the Faculty of Civil Engineering, CTU Prague, Czech Republic, 2021  Project Leadership: "Fieldworks on sustainable water management on a remote island", within an Erasmus Short Term Mobility on Samothraki, Greece, 2022
Language skills	German – native language English – level C2 (exchange semester in New Zealand) French – level C2 (exchange semesters in France; work in DR Congo) Spanish – level C1 (exchange semester in Spain; work in Ecuador)

## Volunteer activities

2017 – 2020	<b>Student association "ÖH-BOKU Kraftwerk"</b> <ul style="list-style-type: none"> <li>- Committee for improving study conditions &amp; event planning</li> <li>- Organisation of the "Hydrology and Water Management Conference 2020"</li> </ul>
2016 – 2022	<b>University "Freshers" Mentor &amp; Erasmus Mentor</b> <ul style="list-style-type: none"> <li>- Supporting first year and Erasmus students</li> <li>- Training on group dynamics, teamwork, and mediation</li> </ul>
2015 – 2018	<b>Scout Leader, Group 39 Vienna</b>
2014 – 2015	<b>Voluntary Service Year, Pedro Carbo, Ecuador</b> <ul style="list-style-type: none"> <li>- at the school UEEA: language teacher &amp; accounting assistance</li> <li>- at the cooperative for small agricultural landowners CAAM: Reforestation projects &amp; construction of rainwater harvesting systems in rural areas</li> </ul>

## Interests

Hiking, artistic gymnastics, winter sports, climbing, playing music (piano, ukulele, guitar), travelling

Vienna, 20.03.2023